SCIENCE • TECHNOLOGY • RESEARCH HIGHLIGHTS • VISIONS

Dissertation
82

Improving the performance of solid oxide fuel cell systems

Matias Halinen

VTT

VTT SCIENCE 82

Improving the performance of solid oxide fuel cell systems

Matias Halinen

Thesis for the degree of Doctor of Science in Technology to be presented with due permission of the Aalto University School of Science for public examination and criticism in Auditorium K216 at Aalto University School of Science (Espoo, Finland), on the 8th of May, 2015 at 12 noon.

ISBN 978-951-38-8237-2 (Soft back ed.)
ISBN 978-951-38-8238-9 (URL: http://www.vtt.fi/publications/index.jsp)

VTT Science 82

ISSN-L 2242-119X
ISSN 2242-119X (Print)
ISSN 2242-1203 (Online)

JULKAISIJA – UTGIVARE – PUBLISHER

Teknologian tutkimuskeskus VTT Oy
PL 1000 (Tekniikantie 4 A, Espoo)
02044 VTT
Puh. 020 722 111, faksi 020 722 7001

Teknologiska forskningscentralen VTT Ab
PB 1000 (Teknikvägen 4 A, Esbo)
FI-02044 VTT
Tfn +358 20 722 111, telefax +358 20 722 7001

VTT Technical Research Centre of Finland Ltd
P.O. Box 1000 (Tekniikantie 4 A, Espoo)
FI-02044 VTT, Finland
Tel. +358 20 722 111, fax +358 20 722 7001

Grano Oy, Kuopio 2015

Preface

The publications of this thesis work were produced in several research projects (RealDemo, SofcPower, FINSOFC, Large-SOFC and ASSENT) at the VTT Technical Research Centre of Finland. Financial support of the projects is gratefully acknowledged. The grant from Gasum Gas Fund is gratefully acknowledged as it enabled the finalization of this thesis after my career at VTT.

I thank my supervisor Professor Peter Lund of Aalto University for guidance during the final stages of this thesis. Rolf Rosenberg and Jari Kiviaho are thanked for the opportunity to work in the VTT Fuel Cell Team.

An SOFC system is an aggregate of different materials and components and its operation is based on several physical phenomena, making the research highly cross-technical by nature. I am grateful to many professionals who provided their advice to me over the years.

I thank my co-authors and former colleagues at VTT, Matti Noponen, Jari Pennanen, Antti Pohjoranta, Jaakko Saarinen, Markus Rautanen and Olivier Thomann, for their contributions to the publications. I am indebted to M. Noponen for clarifying many aspects of fuel cells in the early stages of the research process and for always having time for a discussion. Likewise, J. Pennanen is thanked for many in-depth discussions and for proving constructive criticism on the relevance of the research topics. I had priceless support from A. Pohjoranta during the final stages of the thesis work: thank you for reviewing the manuscript and providing excellent comments.

Without the skills and experience of Kari Koskela, Kai Nurminen, Pekka Simell, Pekka Ståhlberg, Jouko Kukkonen and Jorma Stick the experimental setups would not have been realized. Timo Lehtinen and Mikko Kotisaari provided help with the actual experiments while Kaija Luomanperä and Päivi Jokimies rigorously analysed the gas samples.

Forschungzentrum Jülich provided several stacks for the experiments with the 5 kW test rig. Ico Vinke, Bert deHaart and Reinhard Erben are all gratefully acknowledged for their contribution to getting the stacks up and running at VTT.

The design process of the 10 kW system included intensive collaboration between different research teams at VTT and other organizations. Michael Pastula, Brian Borglum, Ben Nuttall, Todd Machacek, Cam Rankin, and Olivier Grande from Versa Power Systems are thanked for their contribution to the system design,

smoothly executed stack assemblies and input during the experimental activities. Pauli Salminen, Esa Ahlgren and Petri Seppänen from Aalto University are thanked for their work with the mechanical design of the BoP module. Vesa Väisänen, Tomi Riipinen and Jani Hiltunen from Lappeenranta University of Technology developed a robust and working power conversion unit for the experiments. It was great working with you.

Cooperation with the Finnish SOFC system integrators Wärtsilä and Convion worked well for me. Especially Erkko Fontell, Tero Hottinen, Kim Åström, Tuomas Hakala, Jukka Göös, Miika Jussila, Anna Nummela and Kimmo Keränen are thanked for providing help, support and ideas during the research process.

I have gained much from my friends and family, and I am extremely lucky to know such a bunch of nice and fun people. Especially I would like to thank my mother Sirkka and brother Samuli for always supporting me.

Finally, my greatest and warmest gratitude is to my wife Taru, daughter Pihla and son Oiva. You make my life complete and a happy one. Thank you for your support and love.

Helsinki, 16th of March, 2015

Matias Halinen

Academic dissertation

Supervising professor

Professor, Dr. Peter Lund
Department of Applied Physics
Aalto University School of Science
Espoo, Finland

Preliminary examiners

Professor, Dr. Mohsen Assadi
Department of Petroleum Engineering
University of Stavanger
Stavanger, Norway

Associate Professor, Dr. Masoud Rokni
Department of Mechanical Engineering
Thermal Energy
Technical University of Denmark
Lyngby, Denmark

Opponent

Professor, Dr. Robert Steinberger-Wilckens
School of Chemical Engineering
University of Birmingham
United Kingdom

List of publications

This thesis is based on seven original publications which are referred to in the text as [P1–P7].The publications are reproduced with kind permission from the publishers

[P1] M. Halinen, J. Saarinen, M. Noponen, I. C. Vinke, J. Kiviaho. Experimental analysis on performance and durability of SOFC demonstration unit. Fuel Cells. (2010) Vol. 10 (3), 440–452. doi: 10.1002/fuce.200900152

[P2] M. Halinen, M. Rautanen, J. Saarinen, J. Pennanen, A. Pohjoranta, J. Kiviaho, M. Pastula, B. Nuttall, C. Rankin, B. Borglum. Performance of a 10 kW SOFC Demonstration Unit, ECS Transactions. (2011), Vol. 35 (1), 113–120. doi: 10.1149/1.3569985

[P3] M. Halinen, O. Thomann, J. Kiviaho. Effect of anode off-gas recycling on reforming of natural gas for solid oxide fuel cell systems, Fuel Cells. (2012) Vol. 12 (5), 754–760, doi: 10.1002/fuce.201200047

[P4] M. Halinen, J. Pennanen. Analysis of leakages in a solid oxide fuel cell stack in a system environment. Fuel Cells. (2015). In press. 18 pages. doi: 10.1002/fuce.201400072

[P5] M. Halinen, O. Thomann, J. Kiviaho. Experimental study of SOFC system heat-up without safety gases. International Journal of Hydrogen Energy. (2014), Vol. 39 (1), 552–561 doi: 10.1016/j.ijhydene.2013.10.043

[P6] M. Halinen, A. Pohjoranta, J. Pennanen, J. Kiviaho. Stack temperature estimation in system environment by utilizing the design of experiments methodology. ECS Transactions. (2013) Vol. 57 (1), 205–214, doi: 10.1149/05701.0205ecst

[P7] M. Halinen, A. Pohjoranta, J. Pennanen, J. Kiviaho. Application of Multivariable Regression Model for SOFC Stack Temperature Estimation in System Environment, Proceedings of 11th SOFC & SOE Forum 2014, Chapter 15 – Sessions B12/A13, 183–190

Additionally, the following publications are related to the work but are not included in the thesis

i. M. Noponen, M. Halinen, J. Kiviaho, J. Saarinen. Feasibility of Autothermally Reformed Natural Gas on Anode Supported Solid Oxide Fuel Cells, Journal of Fuel Cell Science and Technology, (2006) Vol. 3 (4), 438–444 doi: 10.1115/1.2349526

ii. M. Noponen, M. Halinen, J. Saarinen, J. Kiviaho. Experimental Study of Anode Gas Recycling on Efficiency of SOFC, ECS Transactions, (2007) Vol. 5 (1), 545–551, doi: 10.1149/1.2729034

iii. J. Saarinen, M. Halinen, J. Ylijoki, M. Noponen, P. Simell, J. Kiviaho. Dynamic Model of 5 kW SOFC CHP Test Station, Journal of Fuel Cell Science and Technology, (2007) Vol. 4 (4), 397–405, doi: 10.1115/1.2759502

iv. M. Halinen, J. Pennanen, O. Himanen, J. Kiviaho, P. Silventoinen, J. Backman, P. Salminen. SofcPower 2007–2012 Project – The Finnish SOFC System Research Flagship. The Journal of Fuel Cell Technology, (2013), Vol. 13 (1), 32–39

v. M. Rautanen, M. Halinen, M. Noponen, J. Kiviaho. Experimental Study of a SOFC Stack Operated with Autothermally Reformed Diesel Fuel. Fuel Cells, (2012), Vol. 13 (2), 304–308. doi: 10.1002/fuce.201200115

vi. A. Pohjoranta, M. Halinen, J. Pennanen, J. Kiviaho. Multivariable linear regression for SOFC stack temperature estimation under degradation effects. Journal of the Electrochemical Society. (2014), Vol. 161 (4), F425–F433, doi: 10.1149/2.029404jes

vii. A. Pohjoranta, M. Halinen, J. Pennanen, J. Kiviaho, Solid oxide fuel cell stack temperature estimation with data-based modeling – Designed experiments and parameter identification, Journal of Power Sources, (2015), Vol. 277, 464–473, doi: 10.1016/j.jpowsour.2014.08.130

viii. A. Pohjoranta, M. Halinen, J. Pennanen, J. Kiviaho, Model predictive control of the solid oxide fuel cell stack temperature with models based on experimental data, Journal of Power Sources, (2015), Vol. 277, 238–250, doi: 10.1016/j.jpowsour.2014.11.126

Author's contributions

In [P1], the author was mainly responsible for the implementation of the 5 kW test rig at VTT, while the stack design and assembly were carried out by FZJ. The author was mainly responsible for carrying out the experimental work and related data analysis, and for writing the manuscript.

In [P2], the author was mainly responsible for the design of the 10 kW system, while the stack module was built by a team of VPS. In particular, the author carried out the process layout design as well as the design and implementation of the control system. The author was mainly responsible for carrying out the experimental work and related data analysis, and for writing the manuscript.

In [P3], the author had the main responsibility for design of the experiments and the setup, carrying out the experimental work and related data analysis, and for writing the manuscript.

In [P4], the author was mainly responsible for design of the experimental setup, carrying out the experimental work and the related data analysis, and for writing the manuscript. J. Pennanen contributed by defining the model for diffusive leakage.

In [P5], the author had the main responsibility for writing the manuscript, design of the experiments and the experimental setups, as well as for carrying out the experimental work in the SOFC system and related data analysis. O. Thomann was responsible for the *ex-situ* experiments.

In [P6], the author was mainly responsible for design of the experimental setup and for carrying out the experiments. Detailed design of the experiments, data analysis, and writing the manuscript were a collaborative effort between A. Pohjoranta and the author.

In [P7], the author contributed to the design of the experiments and data analysis. The author was mainly responsible for design of the experimental setup, carrying out the experiments and writing the manuscript.

Contents

List of abbreviations and symbols

AC	Alternating Current
AOGR	Anode Off-Gas Recycling
BoP	Balance of Plant
CPOx	Catalytic partial oxidation
DC	Direct Current
FZJ	Forschungzentrum Jülich, Germany
MLR	Multivariable Linear Regression
PCU	Power Conversion Unit
SOFC	Solid Oxide Fuel Cell
SR	Steam Reforming
VOC	Volatile Organic Compounds
VPS	Versa Power Systems Ltd, Canada
VTT	VTT Technical Research Centre of Finland
WR	Water Recycling

FU	Fuel utilization, -
O/C	Oxygen-to-carbon ratio, -
H/C	Hydrogen-to-carbon ratio, -
FU_{SOFC}	Fuel utilization of an SOFC stack, -
FU_{sys}	Fuel utilization of the system, -
$\dot{n}_{air}$	Flow rate of inlet air, mol s^{-1}
$\dot{n}_{fuel}$	Flow rate of inlet fuel, mol s^{-1}

$\dot{n}_{rec}$	Flow rate of anode recycle gas, mol s^{-1}
$\dot{n}_{Aout}$	Flow rate of stack anode outlet gas, mol s^{-1}
$\dot{n}_{Ain}$	Flow rate of stack anode inlet gas, mol s^{-1}
RR	Recycling ratio, -
$\dot{n}_{leak,O_2}$	Oxygen leakage from air to the fuel side of the stack, mol s^{-1}
$\dot{n}_{leak,fuel}$	Fuel leakage from fuel to the air side of the stack, mol s^{-1}
GHSV	Gas Hourly Space Velocity, h^{-1}
AU	Air utilization, $AU = I / (4\,F\,0.21\,\dot{n}_{air})$, -
U_{sofc}	SOFC voltage, V
I	Current, A
ASR	Area Specific resistance, Ω m^{-2}
G	Gibbs' energy, J mol^{-1}
H	enthalpy, J mol^{-1}
P	power, W
LHV	Lower Heating Value, J mol^{-1}

1. Introduction

1.1 Background

Climate change, induced by global warming due to the extensive emissions of greenhouse gases from mankind's modern industrial activities, is often presented as the greatest challenge of our time. The majority of the greenhouse gases causing climate change originate from the utilization of fossil fuels for energy production and transportation. Thus the significant reduction of these emissions is a key element in mitigating climate change before irreversible damage is done to our planet.

The reduction of greenhouse gas emissions poses a severe challenge, as the modern energy production ecosystem is mostly based on the utilization of fossil fuels, such as coal and oil, both for transportation and for stationary applications. Changing this on a global scale is a challenge in the political, the economic as well as the technological sense.

However, certain changes in the paradigms for energy production and use are emerging. The utilization of non-fossil, renewable sources, such as solar and wind energy, has gained ground and enables energy production without any net greenhouse gas emissions. It is clear that with novel technologies the greenhouse gas emissions can be reduced significantly. The need for such technologies is urgent.

Fuel cells are power sources which convert the chemical energy of the inlet fuel electrochemically to electricity and heat. They are one promising energy technology that could mitigate global warming by significantly increasing the efficiency of electrical power production: even 60% net electric efficiency has been demonstrated [1]. Other advantages include minimal local emissions, low noise and scalability to different ranges of output power while maintaining high efficiency. Fuel cells can be used in a wide range of applications as portable power sources and auxiliary or main power units for vehicles, as back-up or uninterrupted power supply units, and in distributed or central heat and power production.

Solid oxide fuel cells (SOFCs), the topic of this thesis, are well suited for stationary applications, i.e. to produce combined heat and power (CHP) for residential households [1] [2] [3] and in medium-scale distributed generation [4] [5]. In addition to CHP applications, stationary SOFC systems are used in premium power applications to provide an uninterrupted power supply e.g. for data centres [6].

Besides stationary applications, SOFC-based auxiliary power units for heavy-duty vehicles are also being developed [7] [8]. The first SOFC-based products are currently entering the market: in 2012 ca. 23,000 systems were shipped worldwide to customers, mainly in Japan [9].

The SOFCs provide greater fuel flexibility than most other fuel cells types. As well as hydrogen, which is the primary fuel for most fuel cell types, SOFCs are able to utilize fossil or renewable hydrocarbon fuels, such as natural gas. This simplifies the required fuel processing equipment. The fuel flexibility is enabled by internal fuel reforming, i.e. the capability to convert conventional hydrocarbon fuels such as methane to syngas containing hydrogen. Thus deployment of SOFCs is potentially simpler and less expensive compared to other fuel cell types which use hydrogen as a fuel.

An SOFC system operates at a high temperature, typically above 700 °C. Figure 1 illustrates the fundamental design and the operating principles of an SOFC system. In addition to fuel, air is fed to the system to enable the electrochemical reactions and also for thermal management purposes. The heart of the system is the energy-producing SOFC stack assembly. Due to the high operating temperature of SOFCs, the inlet air must be preheated in the Balance-of-plant (BoP) section by recuperating heat from the stack off-gases and by burning unspent fuel. Fuel pre-reforming equipment is needed to safely process the inlet hydrocarbon fuels before supplying them to the SOFC stack.

Direct current (DC) produced in the SOFC must be treated with power conversion equipment to convert it to grid-compliant alternating current (AC) of suitable voltage and frequency. The heat in the exhaust gases can be utilized e.g. for district heating. A control system and relevant process measurements are needed to monitor and regulate the entire system in order to realize its safe, reliable and efficient operation. Additionally, safety and start-up equipment are required to heat up the system and the stack to the operating temperature, and to protect the system and its surroundings from damage in the case of failures.

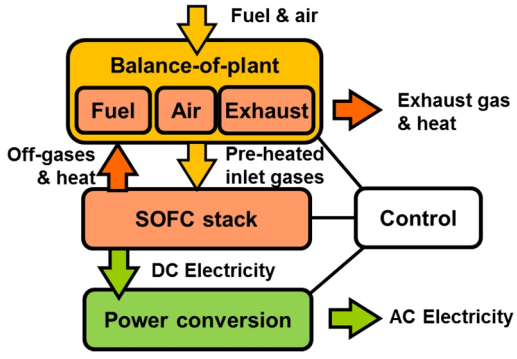

Figure 1. The basic structure of a stationary SOFC power plant.

Even though SOFC systems are gradually entering the market, their wide-spread use is still hindered by a combination of several issues, primarily their cost, lifetime, reliability and robustness.

The cost of SOFC systems is still high: ca. 6,000 €/kW is a widely declared [10] (but unverified) value for Bloom's 200 kW larger stationary systems in the USA. CLFC's residential units are sold for ca. 13,500 €/kW in the U.K. [11]. It has been estimated that the economically feasible investment cost for the system is ca. 1500 €/kW and the early markets must be supported by subsidies and incentives in order to build up the industry to a commercially competitive level [12].

The main cost element in the stationary SOFC power plants is the stack module containing the SOFC stack aggregate and the related peripherals. It has been presented that 21–75% of the systems' total cost can be due to the stack module. Of the other system components, fuel processing, control and air equipment have been all deemed as the most substantial contributors to the final system cost. [13] [14] [15]. The discrepancy of the results demonstrates well that the final cost of systems is dependent not only on the stack module, but also on the overall system design and the chosen components.

Due to their high cost, a sufficiently long lifetime for the SOFC stacks is the prime requirement for commercialisation of SOFC power plants. The SOFC exhibits inherent performance degradation during its active operation and a lifetime of 5 years with a performance degradation of less than 0.25% kh^{-1} is typically presented as a prerequisite for commercial viability [14] [16]. Currently the research efforts in the field of planar SOFC stack technology are reaching these targets [17] [18]. However, these accomplishments still remain to be transferred from laboratories to commercial mass production and to the systems.

As opposed to e.g. combustion engines, fuel cell stacks have no moving parts. Therefore they have a potential for extended periods of reliable and robust, uninterrupted operation. Currently, however, with low production numbers of the systems and limited operating experience of their BoP components, unexpected component failures are a common reason for operation interruptions, which may also cause damage to the costly SOFC stack [1] [19] [20] [21].

1.2 Thesis objectives and scope

The research work covered by this thesis stemmed from Finnish SOFC R&D projects initiated in 2002, which targeted to realize a commercially viable stationary SOFC CHP system utilizing the planar stack technology [14] [22].

Research on system design and components was required to discover feasible technical solutions which would enable reaching the targeted electrical efficiency of 45% for the final products [14]. Moreover, the degradation rate and other characteristics of planar SOFC stacks in a system environment were to be investigated in order to understand their suitability for commercial deployment. The reliability, durability and characteristic performance of most BoP components in their actual working environment were also insufficiently established at that time. Research

was needed to identify suitable commercially available products or to develop them in-house if no such components were available.

In various fuel system design approaches, the focus of the research was on the so-called anode off-gas recycling (AOGR) concept. AOGR was selected to eliminate the need for external water supply during active operation of the systems, improving their self-sufficiency and robustness towards external disturbances.

It was realized that during active system operation, the operating environment of the costly SOFC stack must be controlled rigorously. Overheating, fuel starvation and carbon formation were identified as major operational concerns as they might lead to accelerated performance degradation or irreversible damage. Simplification of the instrumentation arrangements and the peripheral equipment needed for stack control and protection was identified as one of the necessary research topics.

Two tangible objectives were formulated for this thesis work:

1) *Design an SOFC system concept having a high electrical efficiency and self-sustained operational capability. Prove the feasibility of the design and its components by building and operating a proof-of-concept system prototype.*
2) *Develop solutions which improve the operation of SOFC systems by preventing fuel starvation, carbon formation or overheating. Validate them experimentally using the constructed proof-of-concept system*.

The first objective of building an actual proof-of-concept system was motivated by the fact that even though there are several simulation works available in the literature [15] [23] [24] [25] [26] [27] [28], there are fewer actual implementations of such proof-of-concept prototypes. Moreover, such actual implementations of SOFC systems are typically developed by industrial companies, and the component information, detailed design and controls are not available for public research. Thus designing and building complete system hardware was considered to provide novel information on the selection of BoP components and overall layout design.

A similar motivation is present for the second objective of improving the operation of SOFC systems. Research conducted with complete system hardware instead of computer simulation tools would inherently steer the work to face real, previously unsolved or unreported challenges. Additionally, the objective of validating the developed methods in actual system conditions was considered beneficial to promote the exploitation potential of the results by the industrial companies developing the SOFC stacks and systems.

2. Research questions

The contribution of this thesis work to the design and operation of SOFC systems is presented by answering five specific research questions, described in the following.

2.1 Design and components for an SOFC system [P1, P2]

To date, several prototype and pre-commercial systems have been produced and tested. However, the design concepts of these systems differ with respect to the system layout, stack design, fuel processing techniques and BoP components. A difficult situation arises for system developers when trying to select the system design and components: there is no single prevailing design or set of components to realize a feasible SOFC system. Thus the first research question of this thesis project was:

1. *What is a feasible design and set of components for an SOFC system?*

Furthermore, according to the previously mentioned objectives, the system design should realize high electrical efficiency, above 45%, and use anode off-gas recycling to enable self-sufficient operation without an external water supply.

Question 1 is addressed in Section 4.1 based on [P1] and [P2]. In [P1], the feasibility of basic BoP components that are needed to build SOFC systems is investigated by experiments in their operational environment. In [P2], the design and implementation of a complete 10 kW proof-of-concept SOFC system incorporating an anode off-gas recycle loop is described. The validity of the design is investigated by long-term experiments.

2.2 Operation of a pre-reformer with anode off-gas recycling [P3]

In all SOFC systems employing a catalytic fuel processing system, it is important to establish correct dimensioning and a safe operating envelope for the fuel pro-

cessing catalyst. These issues are emphasised in systems with anode off-gas recycling, since the flow rates are higher compared to systems without gas recycling and the operating conditions favour carbon formation. Thus the relevant research question when assessing the design and operation of the fuel pre-reformer in a system with AOGR is:

2. *What are the conditions for efficient and carbon-free operation of a fuel pre-reformer with anode off-gas recycling?*

This research question is addressed in Section 4.2, in which the results of [P3] provide specific information on the feasible operating conditions enabling carbon-free and efficient operation when using a specific precious metal catalyst.

2.3 Leakages of an SOFC stack in the system environment [P4]

SOFC stacks require sufficient gas-tightness for successful operation. Leakages between the fuel and air streams flowing through the stack mean that less fuel is left available for the electrochemical reactions, and if the leakages are high enough they may lead to fuel starvation and permanent damage to the SOFC anode. Therefore, quantification of the stack leakages is relevant for efficient and safe design and operation of SOFC systems, which leads us to the third question of this dissertation:

3. *How is it possible to detect and quantify stack leakages and their effects in SOFC systems?*

This question is addressed in Section 4.3, in which [P4] describes a method to detect and quantify the stack leakages in an SOFC system.

2.4 Protection of the SOFC stack during heat-up [P5]

Fuel starvation can lead to re-oxidation of the nickel on the SOFC anode, which can lead to irreversible damage to the whole stack. Fuel starvation and anode re-oxidation must be prevented not only during normal system operation, but also during the system heat-up and cool-down cycles. A conventional method for anode protection is to supply a reducing, pre-mixed protection gas from pressurized gas storage. However, the use of a pre-mixed gas storage is not desirable due to the consequent servicing requirements, leading to the fourth research question of this thesis:

4. *How is it possible to protect the SOFC anode from re-oxidation without using a pre-mixed safety gas during system heat-up?*

This question is addressed in Section 4.4, where an operational strategy to heat-up an SOFC system without a pre-mixed safety gas is presented based on [P5].

2.5 Thermal management of an SOFC stack [P6, P7]

The temperature inside an SOFC stack affects both its performance and its lifetime. Therefore, monitoring and regulating the internal temperature of the stack is important for system operation, but the required sensor arrangements can be both costly and complex. Estimating the stack temperature indirectly from other readily available process measurements is therefore motivated, leading to the fifth and final research question of this dissertation:

5. *How is it possible to estimate and regulate the internal temperature of an SOFC stack during system operation?*

This question is addressed in Section 4.5 based on [P6, P7]. In [P6] an approach is described to realize a stack temperature estimate based on designed experiments, experimental data and multivariable regression (MLR) models. In [P7], the approach is validated by applying an MLR-estimate in closed-loop temperature control of an SOFC stack in an actual system environment.

2.6 Research process and article relations

The research process and the primary relations between the articles and the research questions are depicted in Figure 2. The research questions are interlinked as they all address issues related to the design and operation of stationary SOFC systems. The extent of the research questions varies: the first question addresses the components, design and operation of entire systems, whereas the latter four questions focus on a specific topic related to the design and operation of SOFC systems.

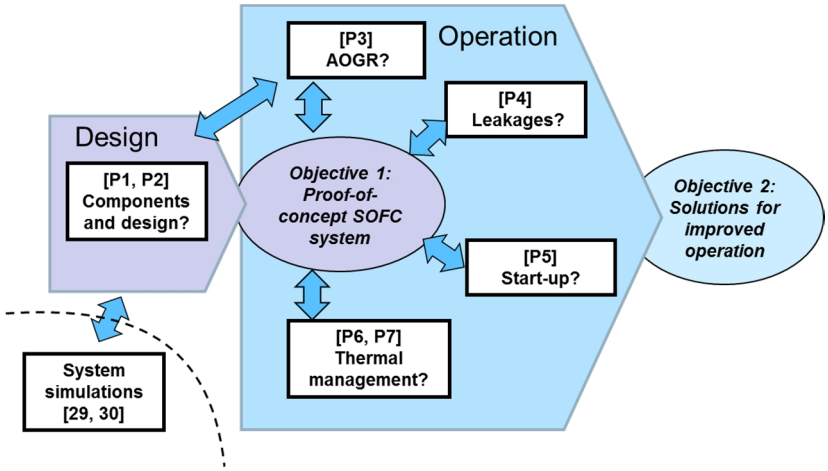

Figure 2. Relations between the objectives of the thesis work, the articles and the research questions.

The first phase of the research work was focused mainly on system design issues. The starting point was identification and development of the necessary BoP components suitable for SOFC systems [P1]. These BoP components were adopted and used to realize a feasible SOFC system design [P2], enabling the construction of the 10 kW proof-of-concept stationary SOFC system. It should be noted that the system design described in [P2] also included important research and development efforts outside the scope of this thesis. In particular, the various components used in the 10 kW system were dimensioned by utilizing the ProSofc simulation tools [29] [30] developed in-house at VTT. The simulation work was closely coupled to the thesis work, as the results of [P1] and [P3] were used to formulate the functionality of models.

In the second phase, the research was focused more on the operational aspects of the SOFC systems. Here, the existing hardware – a 10 kW SOFC system – was utilized as a research platform to develop, test and validate solutions which can improve the systems' operation as described in [P4–P7].

3. Solid oxide fuel cell technology

3.1 Operating principle of an SOFC

In principle a fuel cell is a simple device. An SOFC consists of two electrodes and a gas-tight ceramic electrolyte [31] [32] [33]. Figure 3 depicts the operating principle of an SOFC. The dense ceramic electrolyte becomes an ion conductor at high temperature. Decomposition and reduction of oxygen occurs at the cathode by electrons and the resulting oxygen ions are transported through the electrolyte. At the anode, the oxygen ions react with the inlet fuel generating oxidation products, heat and electrons. The electrons are freed through an external circuit enabling electricity production, while the heat is vented from the cell with the oxidation products and other gases.

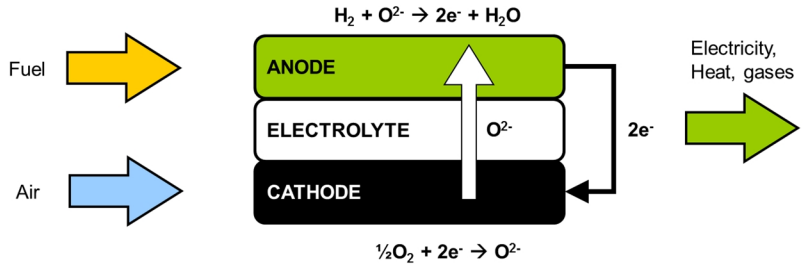

Figure 3. The operating principle of a solid-oxide fuel cell.

The half-cell reactions occurring at anode and cathode, and the total reaction in an SOFC operated with hydrogen, are given in Eqs. (1)–(3), respectively.

$$H_2 + O^{2-} \rightarrow H_2O + 2e^- \quad (1)$$

$$½O_2 + 2e^- \rightarrow O^{2-} \quad (2)$$

$$H_2 + ½O_2 \rightarrow H_2O + 2e^- \quad \Delta G(800°C) = -189\,\mathrm{kJ\,mol^{-1}} \quad (3)$$

3.2 Current-voltage behaviour

The thermodynamic potential difference between the anode and cathode results in a voltage difference over the SOFC. The reversible cell voltage for the system in Eqs. (1)–(3) can be calculated by using the Nernst equation Eq. (4).

$$E_0 = -\frac{\Delta G}{2F} + \frac{RT}{2F} \cdot \ln\left(\frac{p_{H_2}\sqrt{p_{O_2}}}{p_{H_2O}}\right) \quad (4)$$

where E_0 is the reversible voltage of an SOFC, ΔG is the Gibbs free energy of the total fuel cell reaction Eq. (3), F is the Faraday constant, R is the ideal gas constant, T is the temperature, p_{H_2} and p_{O_2} are the partial pressures of the reactants and p_{H_2O} is the partial pressure of the product.

The voltage of a fuel cell decreases due to non-ideal losses. The losses are descriptively denoted by an *overpotential* which is required or a *polarization* which arises, respectively, when current is drawn from the cell. The losses are categorized as activation, ohmic and mass-transfer losses. Figure 4 depicts the cumulative effect of the losses on the fuel cell voltage and the dominating loss mechanism with respect to the magnitude of the current.

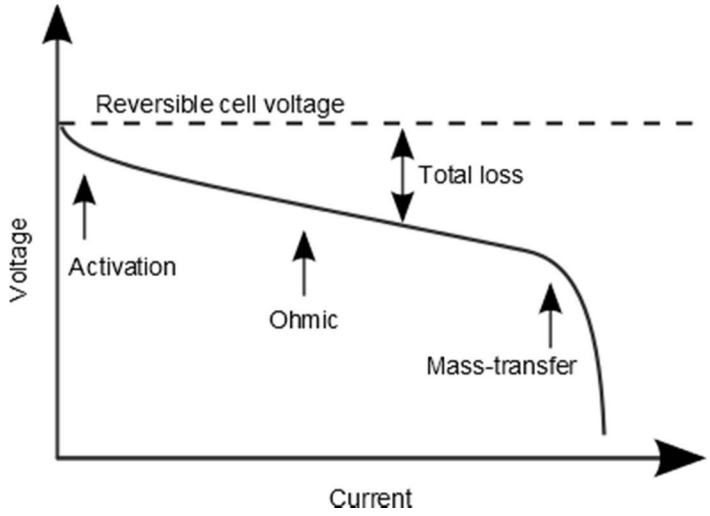

Figure 4. Losses in a fuel cell during electrical loading

Activation losses are dominant at low current and are associated with electrode reaction kinetics. Ohmic losses exhibit a linear relationship with the current and are due to the electrical resistance of the various components of the fuel cell. Finally, the mass-transfer losses occur at high current due to limited transport of reactants to (or products from) the reaction sites at the electrodes. An SOFC is rarely operated in the region of mass-transfer losses, due to risks associated with fuel starvation and the subsequent risk of damaging the anode, as discussed in more detail in the next sections.

3.3 SOFC systems

Figure 5 illustrates a general design for a stationary, natural gas fuelled SOFC system with its basic components. The system components can be divided on the basis of their functionality into different subsystems, which are briefly described in the following. For more information on the different parts of the systems the reader can consider the following comprehensive textbooks written on fuel cells and SOFCs in particular [33] [34] [35] [36].

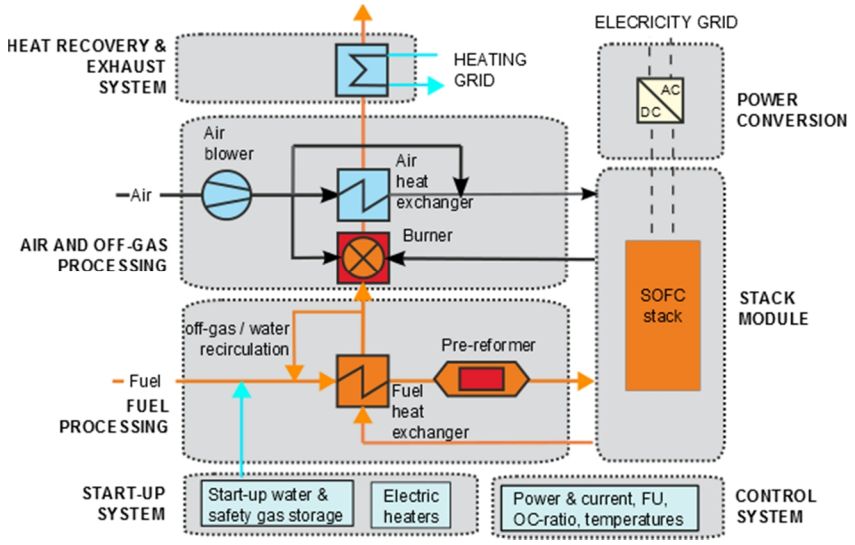

Figure 5. An example of a stationary SOFC system design with its basic components

3.3.1 Solid oxide fuel cell stack

The normal operating voltage of a single SOFC is less than 1 V, typically in the range of 0.7–0.9 V in the system environment. Therefore, to realize higher and more practical voltage levels, the cells are connected electrically in series and assembled together into stacks. Stacking is also needed to deliver the reactants to the cells. SOFCs come in different geometries and designs, and can be divided into tubular, micro-tubular and planar stack designs. Planar anode-supported stack designs were used in this thesis work [37] [38].

Figure 6 depicts the basic structure of a planar SOFC stack design. Anode-supported SOFCs have a thick nickel-ceramic anode electrode acting as a mechanical support for the cell. Metallic interconnect plates are employed to deliver the gases to the electrodes and to connect the cells electrically in series [39] [40] [41]. As discussed in Section 3.7, the gas-tightness of the stack is an important characteristic which can affect the design and operation of the entire system. Gas-tight seals are used at the interfaces between the cells and interconnect plates in order to prevent mixing and oxidation of inlet fuel and air [42] [43]. Typically, a compressive force is needed over a planar stack to achieve good electrical contacts as well as sufficient gas-tightness between the different parts of the stack assembly.

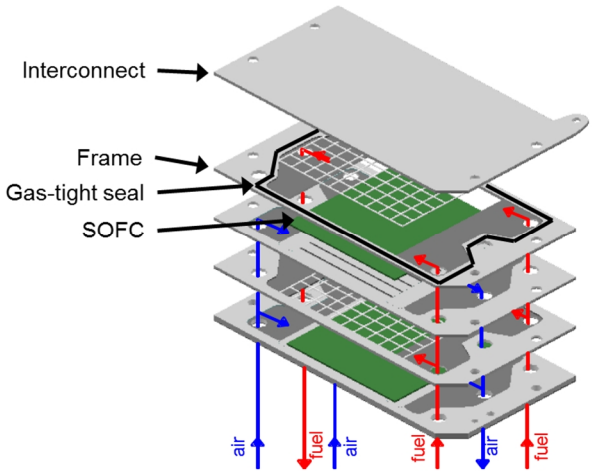

Figure 6. Basic structure of an SOFC stack. Adapted from [44].

3.3.2 Air and gas supply

The oxygen needed in the electrochemical reactions taking place in an SOFC is taken from the ambient air. The motive force for the air and fuel gas can be provided by various commercially available electric motor-driven blowers and compressors, accompanied by filtering of airborne dust and particles [33]. The efficiency of the air blower is an important parameter as it typically contributes significantly to the system's internal power consumption and the resulting net electric efficiency [15] [24], Eq. (10). Commercially available side-channel blowers such as that used for the 10 kW system in [P2] can achieve an efficiency of 35%.

3.3.3 Air pre-heating

The most significant design issue of the air processing subsystem is typically related to air preheating [23] [34]. The inlet air must be heated close to the operating temperature of an SOFC stack in order to prevent excessive thermal gradients and stresses. This leads to the requirement of a small temperature difference between the air inlet and outlet of the stack, which in turn promotes the use of high air stoichiometry (i.e. higher than the electrochemically necessary air flow) in order to absorb the heat generated in the SOFC. The high air stoichiometry, the great temperature difference from the ambient to the SOFC operating temperature and the temperature difference over the stack necessitate a high heat transfer coefficient for the air system heat exchanger. Concurrently, the pressure drop of the air system heat exchanger must be low enough to maintain the power consumption of

the air blower at a tolerable level. Thus, an important design constraint for the air side heat-exchangers is the maximum permissible temperature difference between the stack cathode inlet and outlet air [15]. Plate-type heat-exchangers are typically employed in SOFC systems for their compact size, and were used in the 10 kW system described in [P2].

3.3.4 SOFC off-gas burning

Since the fuel is never fully utilized in the electrochemical reactions within the stack during its normal operation, the SOFC anode off-gas contains unoxidized fuel components, namely H_2 and CO. The unspent fuel must be burned before venting it to the exhaust, for safety reasons and to limit the system's emissions, especially the CO as well as NOx- and VOC-compounds, to permissible levels. Burning the unspent fuel can be carried out e.g. in an adjacent chamber integrated into the stack module, or by a separate burner component located downstream from the stack exhaust [2] [19] [21] [45]. Catalysts are often employed to ensure complete oxidation of fuel at temperatures below 900°C, where the formation of NOx -emissions is still negligible.

The off-gas burner can also be utilized to alleviate the heavy pre-heat duty of the air side heat-exchanger. The unspent fuel and the stack outlet air are mixed and oxidized in a burner before supplying the flue gas to the hot side of the air system heat-exchanger. This approach is considered beneficial in modelling studies and has been implemented in several SOFC systems in practice [2] [15] [20] [21] [24] [45]. However, alternative approaches, in which the burner is located after the air side heat exchanger, do also exist [19] [46]. The 10 kW system described in [P2] used a catalytic burner located after the stack upstream from the air heat exchanger.

3.3.5 Fuel processing

The fuel processing subsystem includes typically two steps: cleaning and fuel preprocessing. Fuel cleaning is required to remove any sulphur compounds or other impurities which could deactivate the catalysts in the system. The main function of the fuel processing subsystem is to prevent carbon formation in the SOFC and other system components, which is accomplished by reforming the fuel in a prereformer before heating.

Heating the fuel directly to the operating temperature of the stack without preprocessing it first at lower temperatures increases the probability of carbon formation in the heat exchangers, the pre-reformer and especially in the SOFC stack itself due to cracking of heavier hydrocarbons than methane [47]. Carbon formation must be prevented since it can render parts of the fuel system nonfunctional by e.g. blocking gas passage and deactivating catalysts. In addition, heavier hydrocarbons can cause deactivation of the SOFC anode reforming reactions [48], leading to decreased operating voltage and performance loss.

Carbon formation is avoided with a fuel pre-reformer, the purpose of which is to convert part or all of the inlet methane and all the heavier hydrocarbons into hydrogen-containing syngas. The selected pre-reforming technique has implications for the design and operation of the SOFC system, affecting e.g. the pre-heating requirements of the inlet gases and the attainable overall electrical efficiency.

There are two primary reforming techniques employed in SOFC systems: Catalytic partial oxidation (CPOx), Eq. (5), and steam reforming (SR), Eq. (6). CPOx is preferred for its simpler system design and SR for its high efficiency. Catalysts are typically used to decrease the operating temperature and size of the pre-reformer [35].

$$\mathrm{CH_4} + \tfrac{1}{2}\mathrm{O_2} \rightarrow \mathrm{CO} + 2\mathrm{H_2} \quad \Delta H(25°C) = -37\ \mathrm{kJ\ mol^{-1}} \tag{5}$$

$$\mathrm{CH_4} + \mathrm{H_2O} \leftrightarrow \mathrm{CO} + 3\mathrm{H_2} \quad \Delta H(25°C) = 206\ \mathrm{kJ\ mol^{-1}} \tag{6}$$

CPOx reforming utilizes the oxygen in the ambient air to oxidize a part of the inlet fuel according to Eq. (5). Additionally, the reaction in Eq. (5) is highly exothermic, which assists in the preheating of the inlet fuel close to the stack temperature. The major drawback of CPOx is a significant penalty to the net electric efficiency, as ca. 25% of the inlet fuel is oxidized already in the reformer and thus does not contribute to the electricity production.

Steam reforming as such does not decrease the electric efficiency, as the hydrocarbon fuel is reformed to carbon monoxide and hydrogen by using steam instead of oxygen. However, it requires a higher pre-heating duty of the inlet gases and/or of the pre-reformer itself due to the reforming reaction Eq. (6) being highly endothermic. Full conversion of inlet methane by SR in the pre-reformer would impose stringent heat transfer requirements for the fuel system's heat recuperation equipment. Fortunately, the nickel-cermet anode used in SOFCs is an effective SR catalyst, and therefore it is able to convert the inlet methane to hydrogen internally. The heat absorbed by the endothermic SR reaction enables a significant reduction of the cooling air flow, which typically has a further positive effect on the system's electrical efficiency [15] [24]. Thus full conversion of inlet methane in the pre-reformer is not a required or even a preferred design approach, and adiabatic steam reforming can be used to partially convert the inlet methane within the SOFC stack [49]. Arguably, a pre-reformer is not necessarily needed at all in the system if no higher hydrocarbons are present in the inlet fuel and if the stack is capable of complete internal reforming.

Uninterrupted supply of steam is required in steam reforming, which can be accomplished either by using an external water supply or by recirculating the wa-

ter/steam generated by the electrochemical reactions of the SOFC, as discussed in more detail in Section 3.6.

3.3.6 Start-up & safety system

A start-up system is needed to heat up the stack and system components to their designated operating temperatures [36]. System heat-up can be accomplished e.g. by electrical heaters and start-up burners. During shut-down, system cool-down occurs automatically when the power production in the system is discontinued, and can be actively hastened with the air blower. A steam generator is needed during the start-up of systems relying on steam reforming.

A safety system is required for cases of fuel supply failures or critical system faults, such as gas leakages or component failures, which necessitate shutting down the system completely. A special requirement for the safety system is the protection of the stack's anode from re-oxidation during thermal cycling of the system [50] . Development work has been carried out to develop cells and stacks capable of multiple reduction-oxidation (RedOx) cycles, but especially anode-supported cell designs are still susceptible to RedOx and require protection systems: volumetric change of the thick anode support during the RedOx cycle can create cracks in the electrolyte leading to leakages and detrimental combustion of fuel and air. The most straightforward way to realize an anode protection system and prevent re-oxidation is to supply a reducing atmosphere to the anode from a gas storage [36].

3.3.7 Power conversion

A power conversion unit (PCU) is needed to convert the DC current produced by the SOFC stack to grid-compatible AC current. The efficiency of the PCU contributes directly to the resulting net electrical efficiency of the system, see Eq. (10). The DC-AC conversion is made using an inverter typically having an efficiency in the range of 94–98% [36]. The inverter requires an input voltage of 410–1000 VDC [14]. Since the output voltage of an individual fuel cell stack is usually below 100 V, a boosting DC-DC converter can be used to generate an adequate inverter input voltage as well as to provide galvanic isolation from the grid [51]. A DC-DC converter will lower the total efficiency of the PCU, and the lower the stack voltage and the higher the magnitude of the voltage boost, the higher is the penalty to the efficiency. Alternatively, the inverter's DC input voltage can be increased by connecting single stacks electrically in series, which increases the PCU's efficiency [14] and ultimately can eliminate the need for a DC-DC booster. However, a high DC bus voltage will demand better electrical isolation at the high operating temperatures of the SOFC, which may complicate system design or diminish system reliability.

3.3.8 System control

System control is needed to provide the desired electric and thermal power output and to maintain the fuel utilization of the stack (to prevent fuel starvation), the O/C-ratio of fuel system gases (to prevent carbon formation) and the temperature of the components within safe boundaries.

Typically, the stacks are operated galvanostatically and thus the electric power of the system is adjusted by regulating the DC-current drawn for the stacks [51]. The maximum rate of change of the DC-current must be limited to match the slower transient response of other actuators of the system [28] used to supply gases and regulate the temperature.

Generally, the inlet fuel flow rate is adjusted so that *fuel utilization*, defined in Eq. (7), is kept close to but below a pre-defined maximum value. As discussed in Section 3.5, the maximum permissible fuel utilization rate is dependent on the used stack design. Too high fuel utilization may lead to non-optimal performance of even to fuel starvation and anode re-oxidation.

$$FU = \frac{I\, N_{cells}}{z_{fuel}\, F\, \dot{n}_{fuel}} \tag{7}$$

where FU is the fuel utilization, I is the stack current, N_{cells} is the number of cells in the stack, z_{fuel} is number of electrons in a mole of fuel that participate in the reaction and F is the Faraday constant and $\dot{n}_{fuel}$ is the inlet fuel flow rate.

The O/C*-ratio* is discussed in-depth in Section 3.6 but in brief, a sufficient oxygen-to-carbon (O/C) ratio must be maintained in the fuel system gases in order to avoid carbon formation. Carbon formation can occur e.g. by the Boudouard reaction via disassociation of carbon monoxide (Eq. (8)) or due to hydrocarbon cracking (Eq. (9)).

$$2\mathrm{CO} \rightarrow \mathrm{C} + \mathrm{CO_2} \qquad \Delta H(25°C) = -172\ \mathrm{kJ\ mol^{-1}} \tag{8}$$

$$\mathrm{CH_4} \rightarrow \mathrm{C} + 2\mathrm{H_2} \qquad \Delta \mathrm{H}(25°C) = 76\ \mathrm{kJ\ mol^{-1}} \tag{9}$$

The O/C-ratio can be maintained by external water supply and/or by recycling of oxidation products of the electrochemical reactions back to the system inlet. O/C-ratios of 2 are typically used for conventional steam reformers with external water supply [34], and the required amount of water can be calculated directly when fuel composition and flow rate are known.

The temperatures of the system components, e.g. the stack and the burner must be maintained within pre-defined values in order to prevent structural damage or performance degradation. Temperature management can be accomplished by adjusting the flow rates of the inlet air and fuel gases and by implementing adjustable by-passes and splitters to change the temperature and/or flow rate of the gases. Figure 5 illustrates such by-pass lines to regulate burner and stack module inlet temperatures. A feedback value of the internal stack temperature is required for system control as discussed in Section 3.9.

3.4 Efficiency and output power

The electrical output power and the efficiency of the SOFC system depend mainly on the electrochemical performance of the stack, but also on the internal, *parasitic*, power consumption of the BoP components, such as blowers, and the losses related to power conversion from DC to AC. The output power of an SOFC system is determined by Eq. (10)

$$P_{AC} = P_{DC,sofc}\,\eta_{PCU} - P_{blowers,aux} \tag{10}$$

where P_{AC} is the output power of the SOFC system, $P_{DC,sofc}$ is the output power of the SOFC stack, η_{PCU} is the total efficiency of the power conversion unit and $P_{blowers,aux}$ is the parasitic power consumption of blowers and auxiliary equipment of the system.

The net electric AC efficiency is determined by the system's AC electric output power and the reaction enthalpy of the inlet fuel flow according to Eq. (11).

$$\eta_{AC} = \frac{P_{AC}}{\dot{n}_{fuel}\,\Delta H_{fuel}} \tag{11}$$

where η_{AC} is the net electrical efficiency of the system, P_{AC} is the output power of the system, $\dot{n}_{fuel}$ is the inlet fuel flow rate and ΔH_{fuel} is the lower heating value of the fuel.

The electrochemical performance of the SOFC stack has the most significant impact on the achievable electrical efficiency of a complete system. Low area specific resistance (ASR) is required from the stack in order to achieve a sufficiently high power density, enabling compact stack size and high operating voltage, beneficial for the electrical efficiency of the system.

The maximum permissible fuel utilization rate, Eq. (7), is also a crucial characteristic affecting the electrical efficiency of the system and so it has to be considered during system design and operation. The relationship between the DC elec-

trical efficiency of the stack, the stack operating voltage and the fuel utilization rate is given by Eq. (12).

$$\eta_{\mathrm{DC}} = \frac{z\,F\,U_{sofc}}{\Delta H_{fuel}\,N_{cells}} FU \tag{12}$$

where η_{DC} is the DC electric efficiency of the stack, z is the number of electrons that participate in the reaction, F is the Faraday constant, U_{sofc} is the SOFC voltage, ΔH_{fuel} is the lower heating value of the inlet fuel, N_{cells} is the number of cells in the stack and FU is the fuel utilization.

The system's net electrical efficiency relates to stack DC efficiency according to Eq. (13).

$$\eta_{\mathrm{AC}} = \eta_{\mathrm{DC}}\,\eta_{\mathrm{PCU}} - \frac{P_{blowers,aux}}{\dot{n}_{fuel}\,\Delta H_{fuel}} \tag{13}$$

3.5 SOFC system designs

3.5.1 System efficiency

Table 1 summarizes results from recent stationary SOFC system demonstrations. Most results are from systems targeted for residential applications and having an output power of less than 2 kW. Of these systems CFCL's system [52] and the Japanese Ene-Farm systems [3] are already available on the market. Bloom Energy has installed several 200 kW systems [6] which claim higher than 50% efficiencies [4], but no detailed information has been published on the system layout, durability or efficiency. Apart from Bloom's system, the results for other larger stationary systems [19] [20] [P2] [45], have been obtained by using unique proof-of-concept prototypes. Results for some of these systems are reported based on the DC-efficiency, excluding the internal power consumption of the BoP components.

The electrical efficiency of the systems in Table 1 ranges from 32% to 60%, and is mainly determined by the used stack design and the choice of fuel processing technique. Systems utilizing CPOx have efficiency below 35%, whereas systems with SR achieve higher efficiencies. SR systems utilize different approaches to retain carbon-free operation: external water supply (ext), water recycling (WR) and anode off-gas recycling (AOGR). The rationale of selecting between different fuel processing approaches is described in the following sections.

Table 1. Overview of recent results for stationary SOFC systems. Adapted from [20]

System developer	Output power	η_{AC}	η_{DC}	Fuel processing system	Degra-dation	Test period	Ref.
	kW	%	%		% kh^{-1}	kh	
Bloom	200 / AC	>50	-	-	-	-	[4]
Wärtsilä	24 / DC	47	-	SR / AOGR	0.7–0.9	2	[19]
FZJ	20 / DC	41	54	SR / ext	-	5	[20]
AVL	6 / DC	-	55	SR / AOGR	-	1	[45]
NTT	6 / DC	44	56	SR / ext	-	1	
VTT (2010)	7 / AC	43	60	SR / AOGR	0.7	2	[P2]
VTT (2011)	8 / AC	49	-	SR / AOGR	-	2	[29] [30]
CFCL	1.5 / AC	60	-	SR / WR	0.5	8	[52]
ENE-farm	0.7 / AC	41–47	-	SR / WR	0.7	20–37	[3] [53]
Hexis	1 / AC	35	-	CPOx	<1	14	[2]
SOFCpower	1 / AC	32	-	CPOx	-	-	[54]

All the systems presented in Table 1 employ different stack and stack module designs. The output power of a single planar SOFC stack is usually in the range of 0.5–3 kW [1] [54] [55] [56] [57]. By using larger area cells the power output of a single stack can be increased and up to 16 kW of electric power has been demonstrated for a single stack [58]. The performance of recent stack designs is presented in the following sections. Smaller residential units incorporate a single-stack module [1] [2] which can be tightly integrated to hot BoP components in order to minimize thermal losses [52].

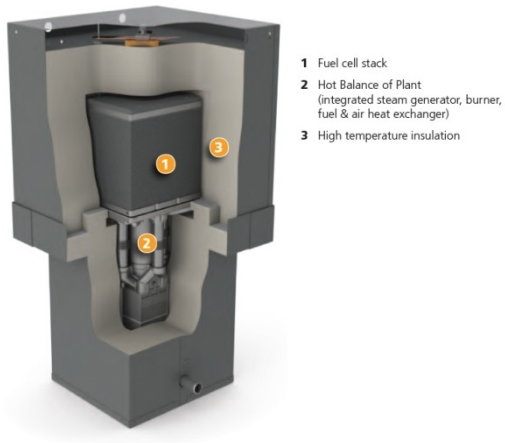

Figure 7. The single-stack Gennex™ SOFC module by CFCL [59]

In larger power systems, the output power of the complete system exceeds the nominal output power of a single stack. Therefore multi-stack assemblies are used for larger stationary systems [18] [19] [46] [56] [60]. In multi-stack systems, the components are not as closely integrated due to the larger physical size of the assembly, but the stacks and the BoP components are typically located in separate modules (Figure 8). A modular design approach was also used in the proof-of-concept system presented in [P2].

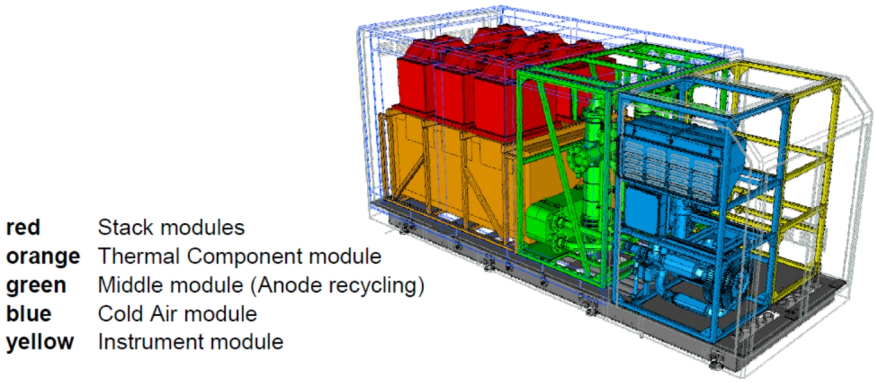

Figure 8. Modular multi-stack SOFC system concept by Wärtsilä [61]

3.5.2 Stack efficiency

The maximum permissible fuel utilization rate of the SOFC stack limits the attainable electrical efficiency of the system. The fuel utilization rate of the stack may be restricted within a specified range if the flow distribution in the stack or between the stacks in a multi-stack system is not uniform [20]. A non-uniform fuel flow distribution increases the risk of local fuel starvation and subsequent anode re-oxidation in the stacks; this phenomenon is practically unavoidable in multi-stack systems, in which the flow distribution changes depending on the quality of the stacks [62].

Table 2 illustrates the efficiency of several planar SOFC stack designs based on their recently reported nominal fuel utilizations and average cell voltages. The attainable DC efficiencies for these stacks are calculated using Eq. (12) and the values should be treated as indicative because the results for stacks are measured with differing inlet fuel mixtures.

Table 2. Fuel utilization, operating voltage and calculated DC efficiency for recent planar stack designs.

Stack developer	Electric power kW	Fuel utilization %	Avg. cell voltage mV	Fuel gas in test	DC efficiency %	Ref
CFCL	1.7	85	839	natural gas	69[1]	[52]
VPS (2013)	16.0	68	840	synth. reformate	55[1]	[60]
TOFC	1.5	65	800	-	50[1]	[63]
VPS (2009)	10.5	62	820	synth. reformate	48[1]	[64]
IKTS	1.1	80	721	H_2-N_2 mix	46[2]	[56]
sunfire	1.0	75	737	H_2-N_2 mix	44[2]	[46]

[1]LHV of methane (803 kJ mol^{-1}) [2]LHV of hydrogen (242 kJ mol^{-1})

As seen in Table 2, most planar stack developers use fuel utilizations between 65 and 80%. The stacks with a higher operating voltage (>800 mV) require relatively low fuel utilization levels (<70%) and vice versa. Except for the CFLC stack, which is capable of both high fuel utilization and a high operating voltage and, consequently, a high efficiency of 69%, the DC-efficiency of planar SOFC stacks remains at 55% or below. For these stack designs, the stack fuel utilization and voltage will set the practically attainable AC efficiency below the same value.

The stack used in the 10 kW system [P2] corresponded to the VPS stack technology of 2009 [64] in Table 2. A typical fuel utilization rate of the stack was

61.5%, restricting its DC efficiency to below 50% without the use of anode off-gas recycling, as discussed in the next sections.

3.5.3 Water recycling

The FZJ and NTT systems, in Table 1, utilize steam reforming with external water supply. The systems are reported to achieve efficiencies above 40%. The use of a continuous external water supply during active operation renders the systems vulnerable to disturbances in the water supply, increases the servicing needs and increases the cost of the systems due to the required inlet water purification subsystem (filtered and ion-exchanged water is needed). Thus the use of an external water supply is not a preferred approach for SOFC system design.

The water demand for steam reforming systems can be fulfilled without any external supply by water recycling (WR), and this approach has been used in CFLCs and the ENE-Farm systems (Table 1). These systems can achieve a net AC efficiency of 60% and 45%, respectively.

Water recycling is obtained in practice by condensing the water from the exhaust gases and then pumping the liquid water to and evaporating it at the fuel system inlet by using the system's excess heat. The WR method is therefore an alluring option to realize an SOFC system's fuel processing due to its potential simplicity: low-cost equipment is available to pump the liquid water, to clean the water (de-ionizer) and to evaporate it.

The WR method will, however, require a period of external water supply during system heat-up when no steam is generated in the SOFC. Furthermore, the system's water self-sufficiency is related to the amount of condensate recovered from the exhaust, and prolonged independent system operation may not be possible without an external water supply [1]. The exhaust gas must be cooled below the dew point temperature in order to collect enough water for recycling. Higher air stoichiometries will increase the cooling duty of the exhaust gas condenser since the partial pressure of the steam is decreased at the exhaust. With an air utilization of 20%, the exhaust gases must be condensed close to 30°C in order to achieve steam-to-carbon ratios of 2 for the inlet fuel gas mixture, a commonly used value for carbon-free operation.

3.5.4 Anode off-gas recycling

The anode off-gas recycling (AOGR) concept, one main topic of this thesis work, provides an alternative approach to eliminating the need for an external water supply during active operation of the SOFC system. AOGR enables increasing the electrical efficiency of the stack while still maintaining the fuel utilization rate of the stack at a permissible level.

In AOGR, a part of the anode exhaust gas, which contains primarily steam, carbon dioxide and unoxidized fuel, is recycled back to the system inlet. The temperature of the recycled gas should preferably be as high as possible. A high

AOGR flow temperature will pre-heat the inlet gas, thus decreasing the heating duty of the fuel heat-exchanger before the pre-reformer. Compared to WR, AOGR requires more complex equipment due to the higher temperature of the recirculated fluid. An ejector or a special purpose high-speed blower is required to provide motive force to the recycle flow. Generally, the higher the AOGR temperature is, the more challenging it is to realize it in practice. However, modelling studies indicate that AOGR can provide higher electrical efficiencies compared to the WR approach [27] in a complete system.

The most distinct benefit of AOGR over WR materializes when a system design pursues electrical efficiencies above the DC efficiency limits set by the stack's fuel utilization: by recycling the unspent fuel the inlet fuel flow rate can be decreased and the *system fuel utilization* can be increased while still maintaining the *stack fuel utilization* at a desired level according to Eq. (14) [27].

$$FU_{sys} = \frac{FU_{sofc}}{1-RR\cdot\left(1-FU_{sofc}\right)} \tag{14}$$

where FU_{sys} is the system fuel utilization, FU_{sofc} is the stack fuel utilization and RR is the recycling ratio.

Recycling ratio is calculated according to Eq. (15).

$$RR = \frac{\dot{n}_{rec}}{\dot{n}_{out}} \tag{15}$$

where $\dot{n}_{rec}$ is the recycle gas flow rate and $\dot{n}_{out}$ is the stack anode side outlet flow rate.

In addition to the unspent fuel, the anode off-gas contains the oxidation products of the electrochemical reactions, which dilute the inlet fuel. Therefore use of AOGR can decrease the attainable cell voltage, and the higher the recycling ratio is the higher is the voltage decrease. In [65], experimental work with single cells indicates that the benefits of decreased inlet fuel flow outweigh the penalties of decreased cell voltage, resulting in significantly increased DC-efficiency, but only up to a certain maximum RR limit. The authors observed that with a given FU_{sofc}, there was an optimal RR value at which the DC-efficiency of a SOFC was maximal.

Clearly, the AOGR concept is necessary if a system is intended to have a higher electrical efficiency than is dictated by the allowable FU_{sofc}. Otherwise the FU_{sofc} restriction will limit the system's electric efficiency below 50% for most of the planar stack designs presented in Table 2. There are several modelling works available assessing the design of atmospheric SOFC systems with gas recycling,

but fewer experimental works are available which deal with or report the feasibility of actual implementations of such systems [23] [24] [27] [66] [67].

In [P2], a proof-of-concept design is presented for an SOFC system using a blower-based AOGR concept. Prior to [P2], there is only one reported study known to this author in which a blower-based AOGR concept was used successfully in a complete system: Wärtsilä achieved a net AC efficiency of 47% with a multi-stack assembly using lean landfill site gas as a fuel [19]. After [P2], AVL and FCE have presented blower-based system concepts reporting DC-efficiencies of 56% and 64%, respectively [45] [60]. Additionally, in [68] DC-efficiencies up to 63% were achieved with a laboratory prototype system using a blower-based AOGR concept, but certain fundamental system components e.g. an exhaust burner were not used in the experiments.

3.6 Fuel pre-reforming with AOGR

One of the major operational concerns in an SOFC system is the risk of forming solid carbon in the stack or other system components such as the fuel pre-reformer. The thermodynamic equilibrium is often used to assess the risk of carbon formation by calculating a *carbon limit temperature* below which there is a thermodynamic potential to form carbon [27] [67] [47]. At equilibrium, the carbon limit temperature depends only on the atomic C/H/O-ratios and the pressure of the fuel system gas (see e.g. [35] for a more detailed description).

In a system with AOGR and no external steam supply, the only source of carbon and hydrogen is the primary inlet fuel. Furthermore, oxygen may enter the fuel system only through the SOFC electrolyte. Considering that the system operates at a nearly constant pressure and that the H/C-ratio in the primary fuel is rather constant and known, the limit temperature for carbon formation in the fuel subsystem can be estimated based only on the ratio of oxygen to carbon. The O/C-ratio is defined according to Eq. (16).

$$O/C = \frac{\mathrm{x_{CO}} + 2\mathrm{x_{CO_2}} + \mathrm{x_{H_2O}}}{\mathrm{x_{CH_4}} + \mathrm{x_{CO}} + \mathrm{x_{CO_2}} + \cdots + \mathrm{n x_{C_nH_m}}} \tag{16}$$

where x is the molar fraction of the oxygen or carbon-containing component in the gas.

A higher O/C–ratio will mitigate the risk of carbon formation, since the carbon limit temperature decreases with increasing O/C-ratio. For example, according to the equilibrium, with an O/C-ratio of 1.5 or higher, carbon formation is not possible at temperatures above 650°C. Since planar SOFC stacks typically operate at higher temperatures, the O/C-ratio of 1.5 can be considered as a minimum practical safety limit during normal operation of an SOFC stack.

In an AOGR system, increasing the recycling ratio will increase the O/C-ratio of the fuel system gases, thus lowering the carbon limit temperature. Figure 9 depicts the carbon limit temperature with a varying recycling ratio. It can be seen that an RR of ca. 50% is needed to maintain carbon-free conditions above 650 °C i.e. at typical SOFC operating temperatures.

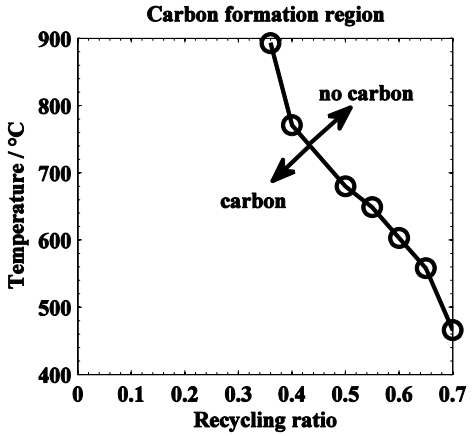

Figure 9. Carbon formation limit as a function of recycling ratio. Fuel: methane, FU_{sofc}: 60%. [69]

In addition to the stack, carbon formation in the pre-reformer must also be considered. This is especially relevant when using planar SOFC stack designs capable of achieving a high degree of internal reforming. For such stacks, adiabatic steam reforming is the preferred fuel-processing solution [14] [35] [52]. In adiabatic steam reforming, the inlet fuel gas is pre-heated, typically to 500–650 °C, and converted to its equilibrium composition and temperature in a pre-reformer reactor upstream from the SOFC stack. According to the equilibrium, and with typical SOFC system gas compositions, 10–25% of the inlet methane and all heavier hydrocarbons are converted and a temperature of 450–550 °C is reached at the reformer outlet. Catalysts are employed in pre-reformers to ensure that the equilibrium conversion is reached.

Using Figure 9 it can be seen that with a pre-reformer temperature of 450 °C, a higher RR of ca. 70% is needed to reach carbon-free conditions, compared to the minimum RR of 50% dictated by the stack temperature. When RR and the recycle flow rate are increased, the parasitic power consumption of the recirculation equipment, as well as size and cost of the fuel processing systems' components to maintain their pressure losses at a tolerable level, will also increase. Additionally, as shown in [65], the DC-efficiency of the SOFC can decrease rapidly when the RR is increased above a critical limit. Thus information concerning the carbon-free

operating conditions of the pre-reformer catalyst with respect to the minimum permissible RR and O/C-ratios is relevant for SOFC system design and operation.

The reformer catalysts can be divided into nickel and precious metal catalysts, based on the catalytically active material. Conventional Ni-based pellet catalysts have been utilized widely for adiabatic pre-reforming of natural gas and other feedstocks in the petrochemical industry. The industrial-scale use of Ni-based catalysts provides a good understanding of their capabilities and operational restrictions (see e.g. [35]). Ni-catalyst can be operated at conditions in which carbon formation is predicted to occur at equilibrium [47]. It has been shown that O/C-ratios as low as 1.0 (corresponding to RR below 40%) are usable for an SOFC pre-reformer employing a Ni-based catalyst [70]. Moreover, since the Ni-based catalysts offer sufficient reforming activity with low cost and high availability, there are several SOFC systems and pre-reformers known to use Ni-based reforming catalysts for natural gas reforming [14] [71] [72] [73] [74].

Precious metal catalysts have been less investigated due to their higher price. However, precious-metal catalysts, based on e.g. Rh, Ru or Pt, can offer several advantages over Ni-based catalysts [35] [75]:

- Precious metals have higher activity
- Risk of carbon formation is lower over precious metals
- Precious metal catalysts are typically non-pyrophoric at elevated temperatures and retain their activity under oxidizing conditions, making them easier to handle and dispose. By comparison, the Ni-based catalysts lose activity in contact with gas-phase oxygen, after which they require pre-treatment in a reducing atmosphere before re-use.
- Precious metal catalysts are suitable for both steam as well as CPOx reforming.

The use of precious metal catalysts enables smaller and more compact reactors as well as safer, simpler and more robust design and operation of the fuel pre-reformer. However, feasible sizing, wider carbon-free operating conditions as well as the durability of the precious metal catalysts should be established before using them in stationary SOFC systems.

There are only a few studies known to the author in which precious metal catalysts have been used for steam reforming in an SOFC system with anode off-gas recycling. In [68] and [76] a precious metal catalyst was used in a prototype system with an AOGR loop. In [65] a precious metal catalyst was used in a single-cell test stand. The authors used high operating and/or inlet gas temperatures, above 700°C, for the pre-reformer, in which more than 50% of the inlet methane was converted. To retain the potential benefits of the internal reforming capability of the SOFC stack, the operation of precious metal catalysts should also be assessed at lower temperatures. The work described in [P1] is the first publication known to the author in which a precious metal catalyst was used for adiabatic steam pre-reforming in an SOFC system. The investigation was continued in [P3], in which the carbon-free operation and feasible dimensioning of a precious metal catalyst using AOGR gas was resolved.

3.7 Stack leakages

The planar anode-supported SOFC designs require gas-tight seals between the cells and interconnect plates in order to prevent mixing and subsequent oxidation of the inlet fuel and air [42] [43]. Leakages have been reported to lead to operation restrictions [45], performance loss [54] [68], anode re-oxidation [21] or higher degradation rates [56] of the stacks. Additionally, seal failure can cause leakage of flammable gas to the ambient, which necessitates shutting down the system [20]. To improve gas-tightness, a compressive force is applied on the stack. Nevertheless, perfect gas-tightness is never achieved and experimental work has shown that as well as the seals, the cells themselves can exhibit intrinsic leakages during operation [77]. Thus the effects of intrinsic leakages, i.e. specific for the given cell and stack type, as well as the possibility of seal failure and resulting gas leak, must be taken into account in the design and operation of the systems.

The leakages can be considered in the design of a stack module. Naturally, a stack module requires efficient thermal insulation to minimize thermal losses. Additionally, a compression system is required for gas-tightness as well as well-defined interfaces for gases, current collection and instrumentation. Stack leakages can be accounted for in the design of the stack modules by employing an enclosure around the stack, which provides sufficient gas-tightness in the prevailing over-pressure of the system [8] [57] [58] [78]. Fuel leakages can then be ventilated from inside the gas-tight enclosure in a controlled manner preventing generation of explosive mixtures. The ventilation can be arranged e.g. by so-called internal air flush, in which the inlet or exhaust cathode air is used to ventilate the leakages from the module enclosure [8] [58] [78].

The leakages should also be taken into account in the system operation. Stack leakages cause uncontrolled burning of fuel and thus dilute the fuel gas, which lowers the stack voltage and the DC-efficiency as well as increasing the fuel utilization. Ultimately, leakages can cause local fuel starvation at the anode, again leading to re-oxidation of the nickel and so to irreversible damage [79].

On the system level, the effect of leakages on the fuel utilization of the stack can be estimated using Eqs. (17)–(19), in which it is assumed that both air and fuel leakages occur at the fuel inlet of the stack.

$$FU_{sofc} = \frac{FU_{sys}(1+L_{air})\left(1-RR(1-L_{fuel})\right)}{\left(1-FU_{sys}(1+L_{air})RR\right)(1-L_{fuel})}, \quad (17)$$

where L_{air}, calculated according to Eq. (18), is a coefficient describing the fraction of the electrochemically convertible fuel which is burned due to the air leakage to the stack inlet, i.e. the increase in the system's fuel utilization. L_{fuel}, calculated using Eq. (19), is a coefficient describing the fraction of fuel gas leaking from the stack inlet.

$$L_{air} = \frac{4\,\dot{n}_{leak,O_2}}{z\,\dot{n}_{fuel}} \quad (18)$$

$$L_{fuel} = \frac{\dot{n}_{Ain}}{\dot{n}_{leak,fuel}} \quad (19)$$

In Eq. (18), $\dot{n}_{leak,O_2}$ is the flow rate of oxygen leaking from air to the fuel side of the stack. In Eq. (19) $\dot{n}_{Ain}$ is the flow rate of stack inlet fuel gas and $\dot{n}_{leak,fuel}$ is the flow rate of fuel leaking to the air side of the stack.

Figure 10 illustrates the effects of leakages to the fuel utilization of the SOFC stack with and without AOGR. Systems utilizing AOGR suffer a relatively larger penalty for the stack fuel utilization. This is due to the effect of the leakages on the stack exhaust gas: less fuel is present in the recirculated exhaust gases compared to the no-leak case. According to Eq. (17), the effects of leakages on the stack fuel utilization can be compensated by decreasing the fuel utilization of the system or by increasing the recirculation ratio.

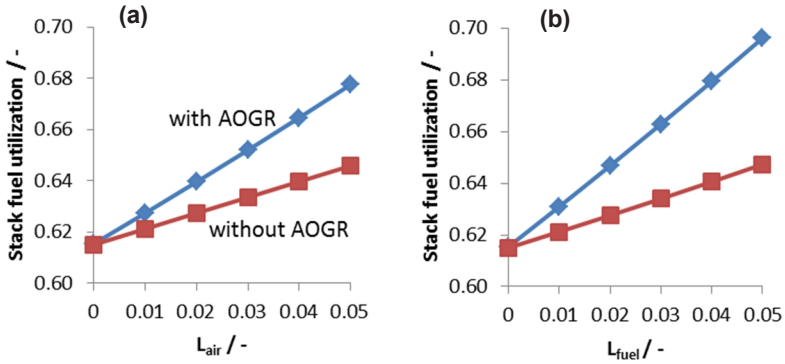

Figure 10. Effect of (a) air and (b) fuel leakage on the fuel utilization of the SOFC stack in a system with (◊) and without (□)AOGR.

Quantification of the stack leakages after the stack manufacturing process can be made in a relatively straightforward manner e.g. by pressurizing the stack with air and measuring the leak rates by flow or pressure sensors. However, the actual leak rates for the stacks may differ greatly when the same stack is operated at elevated temperatures and with different gas compositions. An eight-fold increase in the leak rate has been observed when the test gas is changed from air to an H_2-N_2 mixture [80]. Thus it is relevant to quantify the leakages of stacks in their actual operating conditions.

Quantification of SOFC leakages during their active operation is not a widely reported subject. In [77] the internal and external leakages of a single cell were measured and in [80] the internal leakages of a stack operated in a furnace were evaluated. Both studies reported that the stack leakages were dependent on the composition of the test gases, which means that the system-relevant leakage quantification should be made using actual, realistic fuel compositions.

Previously, when a stack has been operated in a system environment, the leakages have been assessed qualitatively by observing changes e.g. in stack temperature (leaking will increase stack temperature), open-circuit voltage (leaking will decrease stack voltage) or gas composition (leaking will change the gas composition of both air and fuel systems) [17] [21] [68] [81]. Apart from [P4], no other studies are known to this author which evaluate and quantify stack leakages in a system-relevant operating environment using actual fuels or realistic fuel compositions.

3.8 Start-up systems for anode protection

The performance and lifetime of an SOFC stack can decrease dramatically due to re-oxidation of the anode at elevated temperatures, and a safety system is needed to remove the oxygen entering the anode compartment. Currently the most commonly used anode protection method is to supply a pre-mixed reducing purge gas from a gas storage tank [50] [81]. Other methods, such as applying a reverse potential to the stack from an external power source [82] [83], reducing hydrogen from steam by oxidizing part of the pre-reformer catalyst to produce the reducing gas [50], or the use of additional external devices, such as a separate CPOx reformer, to generate the reducing gases [50] [81]. The methods published for anode protection appear to focus on situations in which stagnant gases are present in the system and a relatively low flow of oxygen enters the anode compartment. Stagnant gases are present in an SOFC system only during emergency shutdowns caused by a critical failure such as fuel supply interruption or air blower malfunction. However, in addition to the emergency shutdown situations, the anode should be protected from re-oxidation during normal thermal cycling when an active supply of gases is used to either heat up or cool down the stack. In the case of a non-hermetically sealed stack, the active supply of air and the resulting pressure and concentration differentials will increase the flow of oxygen entering the anode compared to emergency shutdowns with stagnant gases. AOGR can further complicate thermal cycling of SOFC systems, since any air leaking to the fuel system will be supplied to the stack inlet by the AOGR loop. If the air leakage becomes higher than anticipated, then protective measures such as the flow of purge gas may not be sufficient to prevent anode re-oxidation. For example, George reported that an air leakage caused oxidation of all nickel components in an AOGR system's fuel side during thermal cycling [21].

The anode protection equipment for emergency situations can potentially be dimensioned to handle the increased amount of oxygen entering the anode during

the system's normal thermal cycling. However, this may not result in an optimal solution for system design and operation. Higher capacity of the safety system can result in an unnecessary burden to the already high servicing and investment costs of the SOFC systems, especially when safety gas storage is used. Thus, to avoid additional costs, the generation of reducing safety gases for normal thermal cycles by using existing BoP components is required. There are several patents, e.g. [84] [85], in which potentially usable arrangements are described. Apart from [P5], the author is not aware of any other studies in the open literature in which the generation of reducing safety gases during SOFC system start-up has been investigated experimentally using a complete system.

3.9 Thermal management of the SOFC stack

The temperature inside a planar SOFC stack is interesting for several reasons. The stack temperature affects the stack performance as well as its degradation rate [32] [86]. Moreover, the stack characteristics do not remain identical over its lifetime due to voltage degradation. With constant control inputs, e.g. for stack current and air flow rate, the stack temperature will increase as the stack degrades and the heat production in the stack increases. Furthermore, excessive internal temperatures and thermal gradients during transient operation may lead to mechanical failure of the SOFC [87]. Therefore, it is highly desirable to monitor the internal stack temperature for control and diagnosis purposes.

The stack temperature is not a singular value, but a temperature distribution is present within a planar SOFC stack. The use of a single indirect measurement, i.e. a measurement placed outside the stack such as the outlet gas flow temperature measurement, may lead to significant underestimation of the actual internal temperature of the stack [88]. Especially for stack designs which utilize internal reforming using cross- and counter-flow configurations, the temperature maximum is located more towards the centre than the outlet of the active area of the cell [87]. Moreover, the temperature distribution and thus the magnitude and location of the temperature maximum changes according to the prevailing operating conditions. It is clear that single indirect measurements are as such not sufficient to achieve accurate control of the stack temperature.

The internal temperature distribution of an SOFC stack can be measured directly by installing measurement probes, such as thermocouples, inside the stack [17] [88] [89] [90] [91] [92]. A high number of thermocouples are needed to achieve a sufficient resolution for quantifying the stack's internal temperature profile and the temperature maximum. Clearly, a high number of internal sensors can be both technically difficult to implement as well as costly and so it is not the preferred approach for commercial systems, especially when multi-stack assemblies are used. The internal temperature sensors may also compromise the stack's durability and reliability by increasing the risk of gas leaks and short-circuits.

There are several control studies in which the regulation of stack internal temperature is accomplished by feedback control [25] [26] [93] [94] [95]. In most stud-

ies, air inlet flow rate and/or air inlet temperature are used as the controlled input. All studies assume that either a direct measurement of the stack temperature is available or an indirect measurement, e.g. the cathode outlet gas temperature measurement, can be used as a feedback signal for the stack temperature controller.

In principle, it would be possible to utilize a dynamic first-principles model in an embedded control system to estimate the stack temperature. The equations of the first-principles model could be formulated so that the estimate for the stack temperature could be found by using the model with indirect measurements, e.g. gas temperature, stack current or ambient temperature, as model inputs. Such a model could be run parallel with the actual system and the estimate provided by the model could serve as a feedback value for plant controllers. Several studies are available related to model-based stack temperature control [25] [94] [95]. However, no studies are known to this author in which such a model is implemented to a control system and applied to the temperature regulation of an SOFC stack. Arguably, the complexity, large number of non-measurable variables, computational burden and need for experimental data for validation purposes of the first-principles models can make them cumbersome and unreliable for practical control purposes.

The work in [P6] and [P7] was carried out in order to obtain a simple, robust and accurate estimate for the internal temperature of the SOFC stack, since the available models as well as physical measurements were either inaccurate or unsuitable for practical control purposes. Multi-variable linear regression (MLR) models and the design of experiments (DoE) methodology [96] were used. MLR enables simple, easily implementable and explicit tools for variable estimation. DoE is especially suitable for obtaining the data needed to calculate the parameters for the MLR models.

There are only a few publications available in which MLR and DoE have been utilized to estimate the internal temperature of an SOFC. These studies have been carried out in order to advance tubular SOFC stack technology. In [26] a simple MLR model is proposed, in which the stack mean temperature is calculated by several simple process measurements. The data is generated by a physical first-principles model instead of an actual system. MLR models and DoE have been utilized to estimate several properties, including the stack operating temperature, of a 100 kW SOFC system using tubular SOFCs [97] [98]. [P6] and [P7] are the only publications known to this author in which an MLR-based estimator has been used to estimate and regulate the internal temperature of an SOFC stack in an actual system environment.

4. Results and discussion

This section addresses the research questions formulated in Section 2 based on the results of Publications [P1]–[P7].

4.1 Design and components for a SOFC system [P1, P2]

Publications [P1] and [P2] address the research question 1: What is a feasible design and set of components for an SOFC system?

Suitable BoP components for an SOFC system are identified in [P1] and a feasible design for an SOFC system incorporating an AOGR loop is described in [P2]. The main results of the publications can be summarized as follows:

(i) A system design and a set of components providing water self-sufficient, thermally self-sustained system operation with a high electrical efficiency were realized and their feasibility was validated by long-term experiments with a proof-of-concept SOFC system.

(ii) The use of AOGR enabled increasing the fuel utilization of the system to 81% while maintaining the stack fuel utilization at a lower value, as required by the stack technology.

(iii) The voltage degradation of an SOFC stack in the system conditions corresponded to the laboratory results obtained by the stack manufacturer.

The suitability of basic BoP components and fundamental operational aspects for SOFC systems were resolved with the 5 kW system and experiments included operating a planar SOFC stack for 7000 hours [P1]. All components of this set-up, except for the afterburner and the power conversion unit, were found to be feasible for SOFC system use. The chosen BoP components upstream of the stack did not increase the inherent voltage degradation of the SOFC. The materials and the design of the plate-type heat-exchangers as well as the fuel processing system components were adopted in the proof-of-concept 10 kW system in [P2].

A reforming catalyst based on precious metal on a monolith support (manufactured by Süd-Chemie) was chosen for the fuel processing system. System experiments in [P1] confirmed that the precious metal catalyst used had the anticipated

advantages over Ni-based catalysts. The chosen catalyst had good stability under oxidizing and inert atmospheres, which enabled operating the reformer with steam as well as with air. Furthermore, the catalyst was ready for reforming even without first reducing the catalyst with a hydrogen-containing gas. The catalyst had a high activity, which resulted in a small reactor size (1x3" cylindrical monolith and gas hourly space velocities (GHSV) up to 40,000 h^{-1} were used [99]).

A complete design for a natural gas fuelled, grid-connected SOFC system was created and validated in [P2]. Figure 11 depicts the system constructed and its process layout design. The designed system has a modular structure in which the SOFC stack and the BoP -components are arranged into two interconnected modules: the BoP and the stack module.

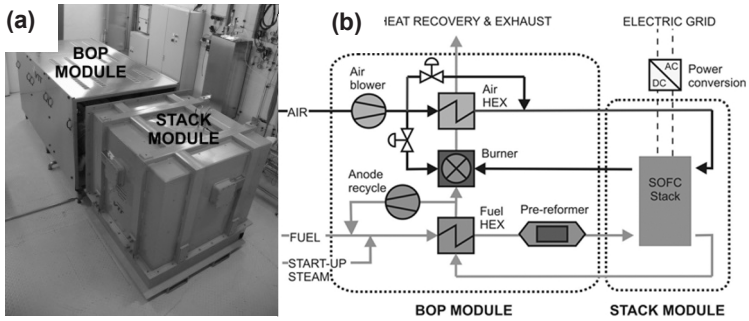

Figure 11 a) the 10 kW SOFC system and b) its process design. Adapted from [100]

The system used a 64-cell 10 kW power class planar SOFC stack provided by Versa Power Systems (VPS). Table 3 summarizes typical operational values for this specific stack design measured at the VPS laboratory test stand and at the 10 kW system's nominal operating conditions. Voltage and power output of the stack are lower in the system environment. Use of AOGR enabled a high system fuel utilization of 81.5%, whereas stack fuel utilization was kept at the desired value of ca. 62%. Consequently, the targeted 60% DC-efficiency was achieved.

Moreover, it should be noted that the stack was operated with higher air utilization (AU) compared to lab experiments, resulting in a 25% reduction in the cathode air flow rate. Lower air flow enabled decreasing the pre-heating duty of the air side heat exchanger, maintaining its size and pressure losses at a more reasonable level.

Table 3. Performance of the VPS SOFC stack in laboratory and system conditions

	Laboratory test [90]	10 kW system [P2]
Conditions		
Fuel	Synth. reformate	Natural gas
I / A	200	202
AU / %	15	20
FU_{sys} / %	-	81.5
FU_{sofc} / %	61.5	61–63
RR / %	-	68
Output		
U_{cell} / V	0.82	0.76
$P_{DC,SOFC}$ / kW	10.5	9.8
η_{DC} / %	48[1]	60[1]

[1]LHV of methane (803 kJ mol^{-1})

An external water supply and a separate steam generator were needed only during thermal cycling of the system. At stack currents higher than 115 A, the unit relies only on AOGR and no steam is fed to the system. Thermally self-sustained operation with the electric start-up heater switched off was achieved with a stack current of 160 A and higher.

At the nominal operating point the net AC output power and system efficiency were 7.1 kW and 43%, respectively (Table 4). The main reasons for not reaching the targeted 50% net efficiency during the first experiments reported in [P2] were higher-than-anticipated losses in the prototype power conversion equipment, which was optimized for reliability rather than efficiency, and in the DC current collection bus which had a high number of contacts with high contact resistances. It should be noted that the target of 50% net AC efficiency can be achieved by utilizing more efficient power conversion equipment, by using a recycle blower with lower power consumption and by optimizing the current collection as discussed in [30] and [101]. The improvement potential is presented for comparison in Table 4.

Table 4. Initial and improved performance of the 10 kW system.

	Initial [P2]	Improved
Input / kW		
$P_{fuel,\ in}$ (LHV) / kW	16.4	16.4
Losses / kW		
Current collection / kW	0.5	0.2 [101]
Power electronics / kW	1.2[1]	0.5[2]
Air blower / kW	0.8	0.8
Recycle blower / kW	0.3	0.1 [30]
Output		
$P_{DC,SOFC}$ / kW	9.8	9.8
P_{AC} / kW	7.1	8.2
η_{AC} / %	43	50

[1] η_{PCU} =87% [2] η_{PCU} =95%

During the experimental validation of the 10 kW system, the voltage degradation of the stack was measured to be less than 1% kh^{-1} at the system nominal operating point (Figure 12). The degradation rate corresponds to the results (0.95–2.6% kh^{-1}) reported by the stack manufacturer for their large area stacks [37] [64].

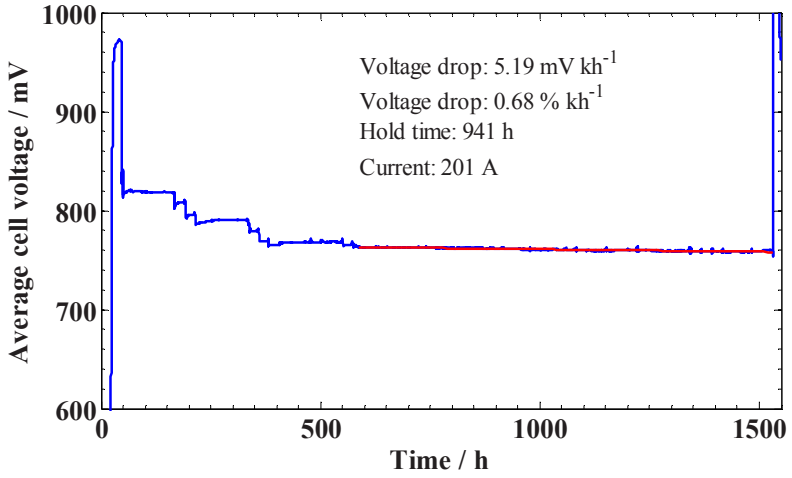

Figure 12. Voltage degradation of the stack under nominal operating conditions.

4.2 Operation of a pre-reformer with anode off-gas recycling [P3]

Publication [P3] addressed the research question 2: *What are the conditions for efficient and carbon-free operation of a fuel pre-reformer with anode off-gas recycling?* The conditions were investigated for a specific precious metal pre-reformer catalyst. The question is answered by summarizing the main results of [P3] as follows:

(i) Operation of the pre-reformer catalyst was efficient even at relatively high space velocities of 35,000 h^{-1} as the thermodynamic equilibrium was still reached at the reformer outlet. As a comparison, the conventional Ni-based catalysts have been used at much lower space velocities of 2,000–6,000 h^{-1} [70].

(ii) No carbon formation was observed to occur with the tested AOGR gas compositions down to a recirculation ratio of 0.2 and an O/C-ratio of 0.5. Thus the used type of pre-reformer does not impose operational or design constraints for SOFC systems with respect to carbon formation. This finding relaxes the operating constraints dictated by the thermodynamic equilibrium theory.

Figure 13 illustrates the improved operability of the pre-reformer catalyst compared to the carbon formation limits set by thermodynamic equilibrium. As the reformer does not dictate the minimum safe recirculation ratio with respect to carbon formation, lower values can be used if needed. Lower recirculation flow can alleviate the requirements for gas recirculation devices and decrease their power consumption.

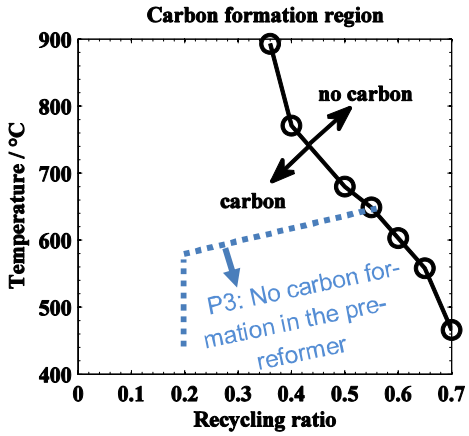

Figure 13. Temperature limit for carbon formation as a function of the recycling ratio of anode off-gas. Solid line: equilibrium value, Dashed line: experimentally defined value. Adapted from [69].

The experiments in [P1] were performed in steam reforming mode and more detailed evaluation of the catalyst's characteristics under AOGR conditions was of interest. A specific type of precious metal catalyst (Süd-Chemie FCR-HC35b) was therefore used for the study in [P3]. The same type of catalyst was later used for the 10 kW system in [P2]. The experimental work revealed that the pre-reformer reached thermodynamic equilibrium in AOGR operation mode in all tested conditions. Equilibrium was reached with AOGR gas even at the highest space velocities (Figure 14) of 35,000 h^{-1} achievable with the used test rig. Such a high space velocity enables the use of a relatively small-sized catalyst, thus promoting a compact reactor design. The 10 kW SOFC system presented in [P2], in which the reformer inlet flow rate is ca. 200 l_N min^{-1} under nominal operation conditions, would require a catalyst size of ca. 0.35 dm^3 if a GHSV of 35,000 h^{-1} was used as a dimensioning criterion.

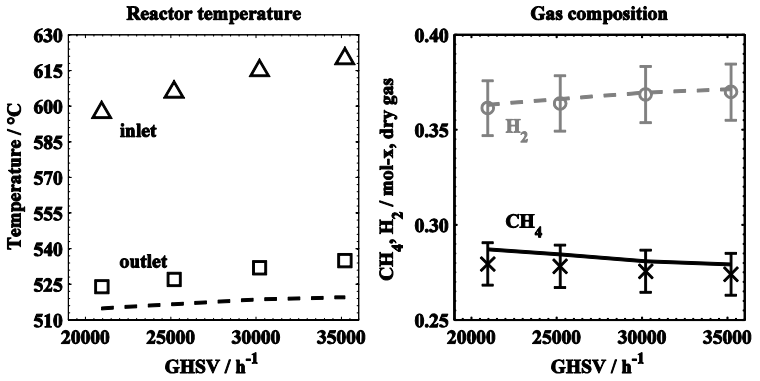

Figure 14. Performance of the pre-reformer catalyst in AOGR mode with a recycling ratio of 0.5. Inlet and outlet temperature (left) and molar fraction of methane and hydrogen at the reformer outlet (right) as a function of GHSV. Measured values are Δ : inlet temperature, □ : outlet temperature, x : methane and ○ : hydrogen. Calculated equilibrium values are presented with lines. [69]

Figure 15 illustrates the experiments performed to resolve the carbon-free operating domain. In Figure 15, the pre-reformer is operated periodically in conditions in which carbon formation is predicted to occur at thermodynamic equilibrium. Both the outlet gas composition and the temperature remained close to their equilibrium values for each condition. Furthermore, no traces of deposited carbon were detected when the reactor was purged with air after each hold period. Thus it was concluded that no carbon formation occurred that would affect operation of the reformer.

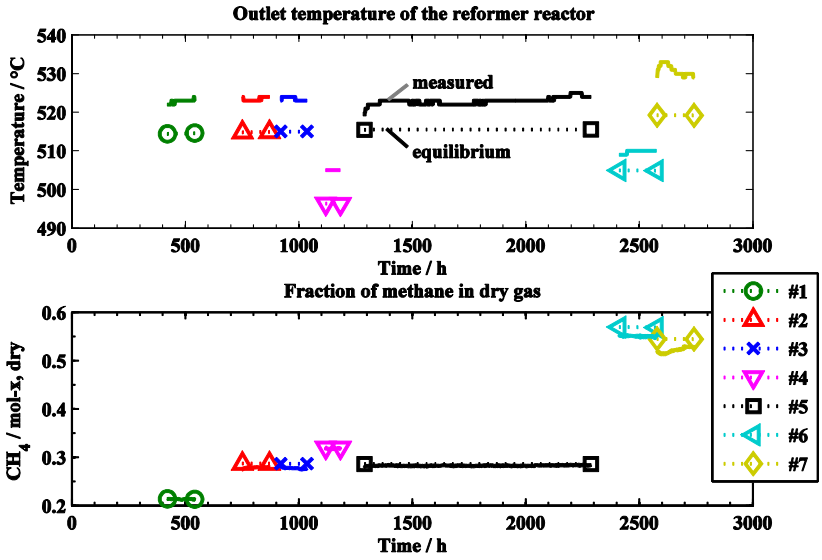

Figure 15. Temperature (above) and mole fraction of methane (below) at the reactor outlet during the experiment. The measured value is presented by a solid line and the calculated equilibrium value by a dashed line with markers at the ends. [69].

4.3 Leakages of an SOFC stack in the system environment [P4]

Publication [P4] addressed the research question 3: How is it possible to detect and quantify stack leakages and their effects in SOFC systems?

In short, the leakages can be quantified by using a diffusive mass transport model for the leakage flows and selected, simple gas component measurements in both the air and fuel side subsystems [P4]. The leakages in a stack are quantified in a real system environment, whereby the operational effects of the leakages are also assessed.

Figure 16 illustrates how the leakages alter the fuel utilization of the stack and produce additional heat in the stack due to combustion. It can be seen that the stack fuel utilization can be significantly affected by leakages, as the stack fuel utilization is increased by ca. 6 %-units. Likewise, combustion of the leakage generates over 500 W of additional heat within the stack and surroundings, which affects the thermal balance of the entire system.

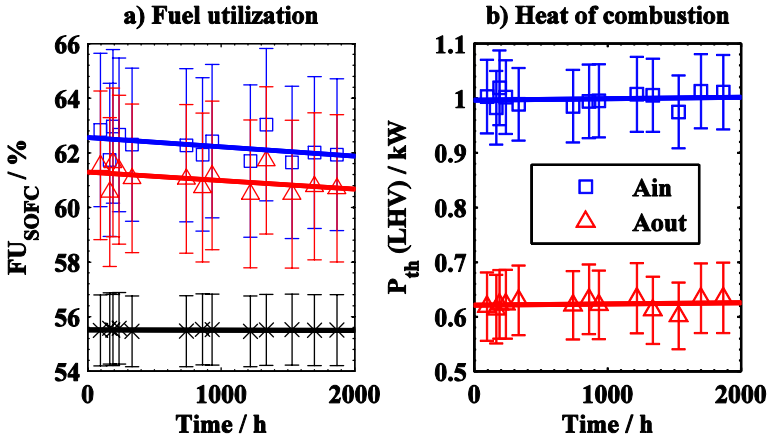

Figure 16. (a) SOFC stack fuel utilization and (b) heat of combustion using (□) anode inlet and (Δ) anode outlet gas composition for diffusive leakage at the stack inlet. (×) Ideal fuel utilization without leakages. [102]

Results of [P4] can be used to compensate for the effects of the leakages in the 10 kW SOFC system. To this end, the recirculation ratio and flow rate are increased to realize an actual stack fuel utilization of ca. 62%, which is more in line with the operating conditions used by the stack manufacturer [64]. The recirculation ratio and flow rate used to compensate the leakages are given in Table 5 and compared to non-compensated values. Additionally, ideal (no-leak) and actual (leakages taken into account) fuel utilization of the stack are given for comparison. It is necessary to increase the recirculation flow rate by 40% in order to maintain the stack fuel utilization at approximately 62%.

Table 5. Effect of stack leakages in the nominal operating conditions of the 10 kW system. System fuel utilization: 81%, Stack current: 200 A.

	Recycle ratio %	Recycle flow rate l_N min^{-1}	Ideal FU_{sofc} w/o leakage %	Actual FU_{sofc} as quantified in [P4] %
Non-compensated	60	125	61	67–69
Compensated with leakage taken into account	68	175	56	61–63

The main observation of the measurement method presented in [P4] is that the identification of the prevailing mass-transfer phenomena of the anodic leakage cannot be made only by analysing the fuel system gases. The fuel system gases consist of multiple compounds, and the leakages cannot be quantified reliably due to the uncertainty of the gas chromatographs used to measure the gas compositions in the experiments. However, the anodic leakages can be detected by measuring the fractions of CO_2 and H_2O of the leakages as well as O_2 in the air system. There, the oxidation of fuel leakage influences the CO_2 and H_2O fractions more than the uncertainty of the measurements.

In addition to the air system's measurements, simple leakage models for diffusive and viscous leakages are needed to distinguish the prevailing mass-transport mechanism of the fuel leakages. This distinction is possible by comparing the calculated H/C ratios obtained independently (i) by the leakage models and the fuel system gas analysis and (ii) by the air system gas analysis.

The analysis method was evaluated with a stack operated in the 10 kW SOFC system presented in [P2], and it was found that the used stack exhibited a characteristic, diffusive-type fuel leakage which remained constant over the 2000 hours of the experiment. Such an unchanging leakage can be considered as an inherent and characteristic property of the stack, and once quantified can be taken into account in the system design and operation.

4.4 Protection of the SOFC during system heat-up [P5]

Publication [P5] addresses the research question 4: How is it possible to protect the SOFC stack from re-oxidation without pre-mixed safety gases during system heat-up?

The anode can be protected by producing a hydrogen-containing reducing gas with the start-up steam generator and the fuel pre-reformer, instead of using a pre-mixed gas storage [P5]. Figure 17 illustrates the developed safety gas-free start-up strategy.

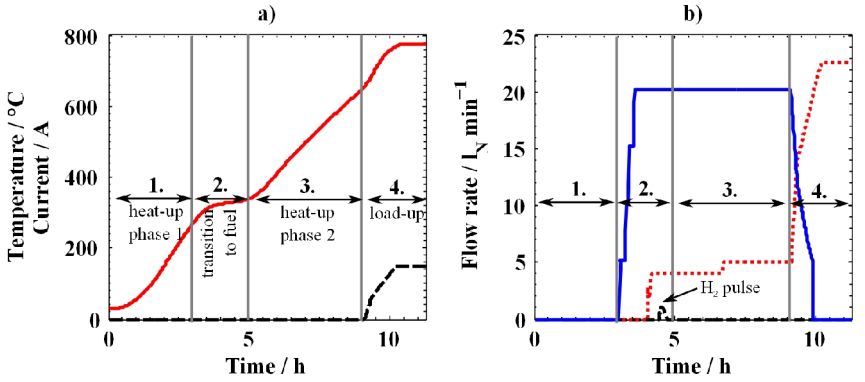

Figure 17. Safety gas-free start-up strategy validated with the SOFC system: a) the stack temperature (solid line) and current (dashed line) and b) the flow rates of hydrogen (dashed line), fuel (dotted line) and steam (solid line) [103]

In Figure 17, the system start-up commences by circulating air in the fuel system. The first heat-up phase is followed by a transition period, at a stack temperature of 200–300°C, during which steam and fuel supply are initiated to start the production of the reducing safety gases in the reformer and in the SOFC stack. After the production of reducing gas is started, the system is heated to the operating temperature, at which electric loading is commenced and the steam feed is shut off.

The start-up strategy was tested with the 10 kW system. The main findings of the start-up experiments were the following:

(i) An air leakage to the fuel system is problematic for the pre-reformer. Oxygen inhibits reforming reactions and production of the reducing safety gases at temperatures below 400°C. A short-duration hydrogen pulse decreases the light-off temperature of the pre-reformer. However, electric pre-heating of the reformer above 400°C to trigger the pre-reforming is preferred for system operation in order to eliminate the need for hydrogen gas altogether.

(ii) Due to the low-temperature oxidation of the stack, a pre-reformer is always necessary in a system having an AOGR loop and air leaking to the fuel system. The pre-reformer is required to remove oxygen from the anode inlet gas. Without the pre-reformer, the anode will remain in an oxidized state and prevent activation of steam-reforming reactions.

(iii) A loss of stack performance was observed when the stack was heated to 400°C prior to starting generation of the hydrogen-containing safety gas. Therefore, the generation of safety gas should be started already below 350°C, or at as low a temperature as possible, to prevent further oxidation and consequent damage to the Ni-cermet.

The start-up strategy proposed in [P5] utilizes existing BoP components, i.e a start-up steam generator, natural gas feed and fuel pre-reformer, instead of pre-mixed gas storage, and can decrease the size of the SOFC system. The 10 kW system requires a minimum of 250 dm^3 of space (5 pieces of 50 dm^3 steel gas containers) for the pre-mixed gas bottles, the amount needed for one 10 hour heat-up cycle. In contrast, the amount of water evaporated during the heat-up cycle of the same duration is ca. 10 dm^3. Arguably, filling up a water container with ion-exchanged water is cheaper and simpler than replacing the more cumbersome gas bottles.

4.5 Thermal management of an SOFC stack [P6, P7]

Publications [P6] and [P7] address the research question 5: How is it possible to estimate and regulate the internal temperature of an SOFC stack during system operation?

The temperature of an SOFC stack can be estimated by using a multivariate linear regression model (MLR) with current, air flow, air temperature and cathode outlet temperature as inputs [P6]. Furthermore, the stack temperature estimate provided by an MLR model is sufficiently accurate to enable feedback control of the stack temperature based on the estimate [P7].

Figure 18 illustrates the measured and estimated stack temperature and the resulting estimation error. At steady state, the error of the estimate is less than 2 °C. In transient states, in which the system inputs are changed successively in a stepwise or ramped manner, the error remains within 5 °C. In addition to the enhanced dynamic response, the use of the cathode outlet temperature as an MLR model input also enables capturing the stack degradation effects. The degradation of the stack's performance affects its heat production and is visible as a gradual increase of the stack temperature during the experiment.

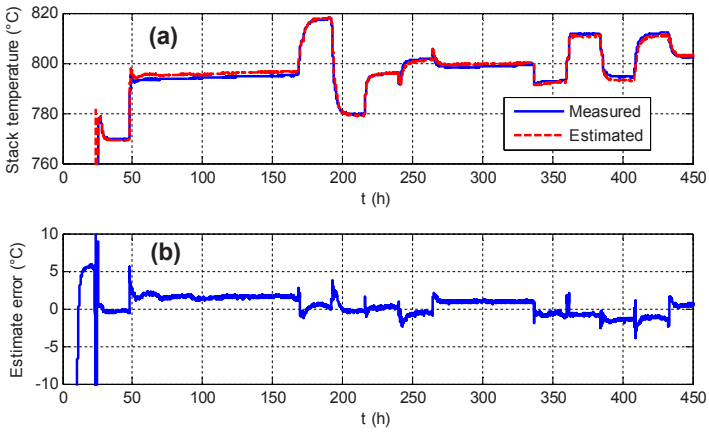

Figure 18. (a) The measured and estimated stack temperature and (b) the estimation error. [104]

Figure 19 depicts the results of experiments in which the estimate given by an MLR model was used as a feedback value for the stack temperature PID controller. In the experiments, the electric loading of the stack is changed (Figure 19a) while the setpoint of maximum temperature of the stack is set at 775°C (Figure 19b). The dynamic response of the estimate corresponds well to the measured maximum internal temperature. The stack temperature is controlled within 2°C of the desired value, the difference being due to the MLR estimate error.

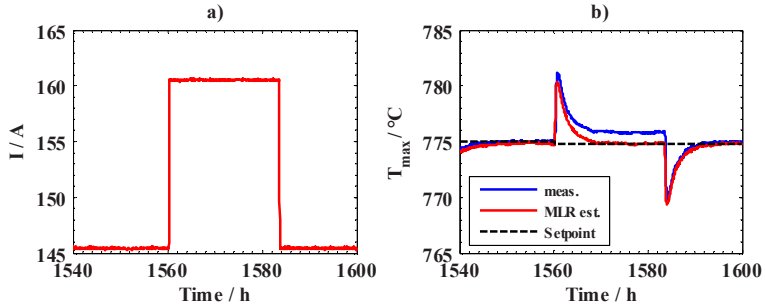

Figure 19. Load transient experiment with an MLR-based estimate. The subfigures show a) the stack current and b) the measured, estimated and setpoint values for stack maximum temperature. [105]

Development of the MLR models required obtaining the experimental data necessary to create the models. Selected system input variables, (stack current, air flow, air inlet temperature and fuel flow) were manipulated according to the design of

experiments (DoE) methodology. The manipulated input variables represent possible control levers available in an SOFC system.

It was found that measurement of the cathode outlet temperature conveys significant information concerning the behaviour of the stack internal temperature. This measurement is biased due to the stack temperature profile and as such does not provide an accurate estimate of the stack internal temperature. However, in addition to the controlled variables, the cathode outlet temperature was used as an MLR model input in order to increase the accuracy of the MLR estimate and to include the stack dynamics in the output of the otherwise static model. In other words, the effect of the system inputs on the stack internal temperature was revealed by the DoE, and the resulting data could be used to significantly increase the accuracy of the otherwise biased cathode outlet gas temperature measurement.

The accuracy and the applicability of the MLR-based estimates presented in [P6] and [P7] for stack temperature estimation and regulation illustrate the benefits of a systematic, designed, experimental procedure to obtain the required data to parameterize the models. Furthermore, the utilized full factorial experimental design enables quantifying the effects of the inputs with respect to the monitored output value. The simplicity and explicit nature of the MLR models makes their practical implementation in a control system quite straightforward.

5. Conclusions

The main contribution of this thesis to the field of the design and operation of SOFC systems is an underlying factor in the publications: the successful implementation of a grid-connected, natural gas fuelled, self-sustained proof-of-concept SOFC system having the potential to achieve 50% electrical efficiency.

The presented design and system components in [P1] and [P2] were demonstrated to be technically feasible and can be utilized in the future to develop commercial systems. The 10 kW SOFC system is one of the few reported actual implementations in which a blower-based AOGR has been used. The design of the system and the used components were validated by long-term experiments and thus demonstrated to be technically feasible. Moreover, the construction of actual proof-of-concept systems in [P1] and [P2] enabled applied research on specific topics related to system design and operation as discussed below.

In [P3] it was shown that efficient and safe operation of the pre-reformer based on a precious metal catalyst is possible in conditions in which carbon formation can occur according to the thermodynamic equilibrium. As a wider window of safe AOGR operation, the physical size and parasitic power consumption of the fuel processing equipment can be decreased. This helps to achieve a lower cost for the fuel pre-reformer, the gas recirculation equipment and other components of the fuel system.

The magnitude of stack leakages affects several important characteristics of a SOFC system. Therefore leakages have to be considered when designing and operating the systems. The analysis method presented in [P4] is applicable for in-situ quantification of SOFC stack leakages during their active and continuous operation in the system environment. The method can provide the necessary information for system designers and operators to assess and compensate for the effects of the leakages. Moreover, the method could be applied for durability and failure analysis of the SOFC stacks, e.g. to distinguish between the voltage decrease caused by leakages and by other degradation mechanisms.

The results presented in [P5] show that the SOFC system can be started without using premixed safety gases and without a significant loss of stack performance. Implementing such a heat-up strategy allows reducing the number and size of system components and increasing their servicing interval by significantly

reducing or completely eliminating the need for pre-mixed purge gas storage. Such simplifications help decrease the system capital and servicing costs.

The results of [P6] and [P7] are valuable when developing a control strategy for an SOFC system and designing the system's sensor arrangements. The results provide a means to eliminate the costly and complex internal temperature measurements of the stack. Instead, the temperature can be estimated and regulated on the basis of simpler and cheaper indirect measurements. A simple MLR estimator enables accurate control of the internal temperature of the stack, which helps to improve system performance and lifetime.

Altogether, the results contained in this thesis provide a diverse contribution to the field of research and development of SOFC systems. The use of actual system hardware kept the focus of the thesis on applied research and facilitated the solving of several specific, previously unpublished, practicalities related to the design and operation of SOFC systems. The presented solutions are readily implementable and can alleviate the challenges of commercialization of SOFC systems by simplifying system design and improving their operational capabilities.

Presently, a good level of know-how exists on the design, construction and operation of SOFC systems and currently available stacks meet the initial performance requirements for commercial deployment. However, high total cost of the systems and the inherent voltage degradation of the SOFC still remain as the main barriers to the widespread commercialization of this technology. The focus of any future technology development activities should be to realize low-cost and durable SOFC stacks and system components suitable for mass production.

References

[1] R. Payne, J. Love and M. Kah, “CFCL’s BlueGen Product,” *ECS Transactions,* vol. 35, no. 1, pp. 81-85, 2011.

[2] A. Mai, J. B. Iwanschitz, A. Schuler, R. Denzler, V. Nerlich and A. Schuler, “Hexis and the SOFC System Galileo 1000 N – past, present, future,” in *Proceedings 11th European SOFC and SOE Forum 2014*, Lucerne, 2014.

[3] M. Suzuki, Y. Takuwa, S. Inoue and K. Higaki, “Durability Verification of Residential SOFC CHP System,” *ECS Transactions,* vol. 57, no. 1, pp. 309-314, 2013.

[4] B. E. Corporation, 2012. [Online]. Available: www.bloomenergy.com. [Accessed 8 10 2014].

[5] Convion Ltd., 10 2014. [Online]. Available: http://convion.fi/index.html.

[6] FuelCellToday, 10 2014. [Online]. Available: http://www.fuelcelltoday.com/analysis/industry-review/2012/the-industry-review-2012.

[7] S. Mukerjee, K. Haltiner, R. Kerr, J. Kim and V. Sprenkle, “Latest Update on Delphi’s Solid Oxide Fuel Cell Stack for Transportation and Stationary Applications,” *ECS Transactions,* vol. 35, no. 1, pp. 139-146, 2011.

[8] J. Rechberger, A. Kaupert, C. Greisen, R. Johansson and L. Blum, “DESTA: SOFC APUs for Heavy Duty Truck Idling – a Progress Report,” in *Proceedings of 11th European SOFC & SOE Forum*, Lucerne, 2014.

[9] FuelCellToday, 10 2014. [Online]. Available: http://www.fuelcelltoday.com/analysis/industry-review/2013/the-industry-review-2013.

[10] “Bloom Energy Server,” Wikipedia, 22 11 2014. [Online]. Available: http://en.wikipedia.org/wiki/Bloom_Energy_Server. [Accessed 26 11 2014].

[11] FuelCellToday, 8 2012. [Online]. Available: http://www.fuelcelltoday.com/news-archive/2012/august/bluegen-domestic-fuel-cell-available-for-under-%C2%A320,000-in-the-uk. [Accessed 24 10 2014].

[12] E. Fontell, T. Phan, T. Kivisaari and K. Keränen, “Solid Oxide Fuel Cell System and the Economical Feasibility,” *Journal of Fuel Cell Science and Technology,* vol. 3, no. 3, pp. 242-253, February 2006.

[13] B. D. James, A. B. Spisak and W. G. Colella, “Manufacturing Cost Analysis of Stationary Fuel Cell Systems,” Arlington, 2012.

[14] E. Fontell, T. Kivisaari, N. Christiansen, J.-B. Hansen and J. Pålsson, “Conceptual study of a 250kW planar SOFC system for CHP application,” *Journal of Power Sources,* vol. 131, p. 49–56, 2004.

[15] E. Riensche, U. Stimming and G. Unverzagt, “Optimization of a 200 kW SOFC cogeneration power plant Part I: Variation of process parameters,” *Journal of Power Sources,* vol. 73, pp. 251-256, 1998.

[16] L. Blum, H.-P. Buchkremer, R. Steinbrech, B. De Haart, U. Reisgen and R. Steinberger-Wilckens, “Current Trends of SOFC Development at FZJ,” in *Proceedings of 8th European SOFC Forum*, 2008.

[17] L. Blum, U. Packbier, I. C. Vinke and L. J. deHaart, “Long-Term Testing of SOFC Stacks at Forschungszentrum Jülich,” *Fuel Cells,* vol. 13, no. 4, p. 646–653, 2013.

[18] L. Blum, P. Batfalsky, L. de Haart, J. Malzbender, N. H. Menzler, R. Petersen, W. J. Quadakkers, J. Remmel, F. Tietz and D. Stolten, “Overview on the Jülich SOFC Development Status,” *ECS Transactions,* vol. 57, no. 1, pp. 23-33, 2013.

[19] M. Noponen and T. Hottinen, “WFC20 Biogas Unit Operation,” in *Proceedings of 9th European SOFC Forum*, Lucerne, 2010.

[20] R. Peters, L. Blum, R. Deja, I. Hoven, W. Tiedemann, S. Küpper and D. Stolten, “Operation Experiencewith a 20 kW SOFC System,” *Fuel Cells,* vol. 14, no. 3, p. 489–499, 2014.

[21] R. George, “Status of tubular SOFC field unit demonstrations,” *Journal of Power Sources,* vol. 86, p. 134–139, 2000.

[22] J. Kiviaho, M. Halinen, M. Noponen, J. Saarinen, P. Simell and R. Rosenberg, “Solid Oxide Fuel Cell System in VTT,” *Journal of Fuel Cell Science and Technology,* vol. 4, no. 4, pp. 392-396, APril 2006.

[23] U. Riensche, J. Meusinger, U. Stimming and G. Unverzagt, “Optimization of a 200 kW SOFC cogeneration power plant. Part II: variation of the flowsheet,” *Journal of Power Sources,* vol. 71, pp. 306-314, 1998.

[24] R. Braun, S. Klein and D. Reindl, “Evaluation of system configurations for solid oxide fuel cell-based micro-combined heat and power generators in residential applications,” *Journal of Power Sources,* vol. 158, p. 1290–1305, 2006.

[25] P. Aguiar, C. Adjiman and N. Brandon, “Anode-supported intermediate-temperature direct internal reforming solid oxide fuel cell: II. Model-based dynamic performance and control,” *Journal of Power Sources,* vol. 147, p. 136–147, 2005.

[26] C. Stiller, B. Thorud, O. Bolland, R. Kandepub and L. Imsland, “Control strategy for a solid oxide fuel cell and gas turbine hybrid system,” *Journal of Power Sources,* vol. 158, p. 303–315, 2006.

[27] R. Peters, R. Deja, L. Blum, P. Pennanen, J. Kiviaho and T. Hakala, “Analysis of solid oxide fuel cell system concepts with anode recycling,” *Analysis of solid oxide fuel cell system concepts with anode recycling,* vol. 38, no. 16, pp.

6809-6820, 2013.

[28] F. Mueller, F. Jabbari and J. Brouwer, “On the intrinsic transient capability and limitations of solid oxide fuel cell systems,” *Journal of Power Sources,* vol. 187, p. 452–460, 2009.

[29] M. Halinen, J. Pennanen, O. Himanen, J. Kiviaho, P. Silventoinen, J. Backman and P. Salminen, “SofcPower 2007-2011 Loppuraportti,” Espoo, 2012.

[30] M. Halinen, J. Pennanen, O. Himanen, J. Kiviaho, P. Silventoinen, J. Backman, P. Salminen and A. Pohjoranta, “SofcPower 2007-2012 Project - The Finnish SOFC System Research Flagship,” *The Journal of Fuel Cell Technology,* vol. 13, no. 1, pp. 32-39, 2013.

[31] S. Tao, P. I. Cowin, C. T. G. Petit, R. Lan and J. T. S. Irvine, “Recent Progress in the Development of Anode Materials for Solid Oxide Fuel Cells,” *Advanced Energy Materials,* vol. 332, no. 3, p. 314, 2011.

[32] R. Knibbe, A. Hauch, J. Hjelm, S. D. Ebbesen and M. Mogensen, “Durability of Solid Oxide Cells - Review,” *Green,* vol. 1, pp. 141-169, 2011.

[33] W. Vielstich, A. Lamm and H. Gasteiger, Eds., Handbook of Fuel Cells: Fundamentals, Technology and Applications, 1st ed., vol. 4 Fuel Cell Technology and Applications: Part 2, Chichester: John Wiley & Sons, 2003.

[34] W. Vielstich, A. Lamm and H. Gasteiger, Eds., Handbook of Fuel Cells: Fundamentals, Technology and Applications, 1st ed., vol. 1: Fundamentals and Survey of Systems, Chichester: Jonh WIley & Sons, 2003.

[35] D. Shekhawat, J. Spivey and D. Berry, Eds., Fuel Cells: Technologies for Fuel Processing, 1st ed., Oxford: Elesevier, 2011.

[36] S. C. Singhal and K. Kendall, Eds., High Temperature Solid Oxide Fuel Cells: Fundamentals, Design and Applications, 1st ed., Oxford: Elsevier, 2003.

[37] B. Borglum, E. Tang and M. Pastula, “Development of Solid Oxide Fuel Cells at Versa Power Systems,” *ECS Transactions,* vol. 35, no. 1, pp. 63-69, 2011.

[38] I. Vinke, R. Erben, R.-H. Song and J. Kiviaho, “Installation and Operation of kW-Class Stacks from Jülich in External Laboratories,” in *Proceedings of 7th European SOFC Forum*, 2006.

[39] N. Shaigan, W. Qu, D. G. Ivey and W. Chen, “A review of recent progress in coatings, surface modifications and alloy developments for solid oxide fuel cell ferritic stainless steel interconnects,” *Journal of Power Sources,* vol. 195, p. 1529–1542, 2010.

[40] J. W. Fergus, “Metallic interconnects for solid oxide fuel cells,” *Materials Science and Engineering A,* vol. 397, p. 271–283, 2005.

[41] S. Deevi and W. Zhu, “Development of interconnect materials for solid oxide fuel cells,” *Materials Science and Engineering A,* vol. 348, pp. 227-243, 2003.

[42] J. Fergus, “Sealants for solid oxide fuel cells,” *Journal of Power Sources,* vol. 147, pp. 46-57, 2005.

[43] K. Lu and M. Mahapatra, “Glass-based seals for solid oxide fuel and electrolyzer cells – A review,” *Materials Science and Engineering R,* vol. 67, p. 65–85, 2010.

[44] M. Halinen, “Development and Control of 5 kW Solid Oxide Fuel Cell Demonstration Unit,” Espoo, 2005.

[45] M. Hauth, J. Rechberger, S. Megel and M. Kusnezoff, “Operating Results of the SOFC20 Stationary SOFC CHP System using a CFY-Stack Platform,” in *Proceedings of 11th European SOFC & SOE Forum*, Lucerne, 2014.

[46] O. Posdziech, M. Pruggmayer and M. Kunkis, “System Development Activities at sunfire,” in *Proceedings of 11th European SOFC & SOE Forum*, Lucerne, 2014.

[47] J. Hansen, “Direct Reforming Fuel Cells,” in *Fuel Cells: Technologies for Fuel Processing*, D. Shekhawat, J. Spivey and D. Berry, Eds., Oxford, Elsevier, 2011, pp. 409-450.

[48] N. Dekker, J. Ouweltjes and G. Rietveld, “Conversion of Simulated Biogas in a SOFC: The Effect of Organic Compounds,” *ECS Transactions,* vol. 7, no. 1, pp. 1465-1473, 2007.

[49] J. Rostrup-Nielsen and J. B. Hansen, “Steam Reforming for Fuel Cells,” in *Fuel Cells: Technologies for Fuel Processing*, D. Shekhawat, J. Spivey and D. Berry, Eds., Oxford, Elsevier, 2011, pp. 50-68.

[50] A. Faes, A. Hessler-Wyser, A. Zryd and J. Van Herle, “A Review of RedOx Cycling of Solid Oxide Fuel Cells Anode,” *Membranes,* vol. 2, no. 3, pp. 585-664, September 2012.

[51] V. Väisänen, R. T., H. J. and P. Silventoinen, “Design of 10 kW resonant push-pull DC-DC converter for solid oxide fuel cell applications »,” in *Power Electronics and Applications (EPE 2011), Proceedings of the 2011-14th European Conference*, Birmingham, 2011.

[52] R. Payne, J. Love and M. Kah, “Generating Electricity at 60% Electrical Efficiency from 1-2 kWe SOFC Products,” *ECS Transactions,* vol. 25, no. 2, pp. 231-239, 2009.

[53] H. Yoshida, T. Seyama, T. Sobue and S. Yamashita, “Development of Residential SOFC CHP System with Flatten Tubular Segmented-in-Series Cells Stack,” *ECS Transactions,* vol. 35, no. 1, pp. 97-103, 2011.

[54] M. Bertoldi, O. Bucheli and A. Ravagnia, “Development and Manufacturing of SOFC-Based Products at SOFCpower SpA,” in *Proceedings of 11th European SOFC & SOE Forum*, Lucerne, 2014.

[55] C. Adams, R. Barabasz, E. Dutton, G. Lin, A. Mohanram, Y. Narendar, J. Pietras, C. Qi, Z. Patterson, S. Ayhan, S. Poizeau and M. Zandi, “Saint-

Gobain's All Ceramic SOFC Stack: Architecture and Performance," in *Proceedings of 11th European SOFC & SOE Forum*, Lucerne, 2014.

[56] S. Megel, C. Dosch, S. Rothe, M. Kusnezoff, N. Trofimenko, V. Sauchuk, A. Michaelis, C. Bienert, M. Brandner, A. Venskutonis, W. Kraussler and L. S. Sigl, "CFY-stacks for use in stationary SOFC and SOEC applications," *ECS Transactions,* vol. 57, no. 1, pp. 89-98, 2013.

[57] R. Leah, A. Bone, A. Selcuk, M. Lankin, R. Pierce and L. Rees, "Robust, Low-Cost, Efficient Steel Cell Stack Development at Ceres Power," in *Proceedings of 11th European SOFC & SOE Forum*, Lucerne, 2014.

[58] B. Borglum, E. Tang and M. Pastula, "Solid Oxide Fuel Cell Development at Versa Power Systems," in *Proceedings of 11th European SOFC & SOE Forum*, Lucerne, 2014.

[59] Ceramic Fuel Cells, 10 2014. [Online]. Available: http://www.cfcl.com.au/Assets/Files/Gennex_Brochure_(EN)_Apr-2010.pdf.

[60] B. Borglum and H. Ghezel-Ayaghb, "Development of Solid Oxide Fuel Cells at Versa Power Systems and FuelCell Energy," *ECS Transactions,* vol. 57, no. 1, pp. 61-66, 2013.

[61] Wärtsilä, Topsoe Fuel Cells, "DEMO SOFC Project Summary," 10 2014. [Online]. Available: http://www.demo-sofc.eu/pdf/Laymans_report%20DEMO%20SOFC.pdf.

[62] M. Noponen and T. Korhonen, "Effects of Multiple Stacks with Varying Performances in SOFC System," in *Proceedings of 10th European SOFC Forum*, Lucerne, 2012.

[63] H. Weineisen and J. Poulsen, "Operation Results from the Topsoe PowerCore," in *Proceedings of 11th European SOFC & SOE Forum*, Lucerne, 2014.

[64] B. Borglum, E. Tang and M. Pastula, “The Status of SOFC Development at Versa Power Systems,” *ECS Transactions,* vol. 25, no. 2, pp. 65-70, 2009.

[65] M. Noponen, M. Halinen, J. Saarinen and J. Kiviaho, “Experimental Study of Anode Gas Recycling on Efficiency of SOFC,” *ECS Transactions,* vol. 5, no. 1, pp. 545-551, 2007.

[66] J. Jia, Q. Li, M. Luo, L. Wei and A. Abudula, “Effects of gas recycle on performance of solid oxide fuel cell power systems,” *Energy,* vol. 36, pp. 1068-1075, 2011.

[67] G. Samuelsen, Y. Yi, A. Rao and J. Brouwer, “Fuel flexibility study of an integrated 25kW SOFC reformer system,” *Journal of Power Sources,* vol. 144, pp. 67-76, 2005.

[68] M. Powell, K. Meinhardt, V. Sprenkle, L. Chick and G. McVay, “Demonstration of a highly efficient solid oxide fuel cell power system using adiabatic steam reforming and anode gas recirculation,” *Journal of Power Sources,* vol. 205, p. 377– 384, 2012.

[69] M. Halinen, O. Thomann and J. Kiviaho, “Effect of Anode off-gas Recycling on Reforming of Natural Gas for Solid Oxide Fuel Cell Systems,” *Fuel Cells,* vol. 12, no. 5, pp. 754-760, 2012.

[70] A. Nummela and M. Noponen, “Experimental Study on Effects of Anode Recirculation to Pre-Reforming of Natural Gas,” in *Proceedings of 9th European Fuel Cell Forum*, Lucerne, 2009.

[71] T. Hottinen, T. Lehtinen, J. Hansen and E. Fontell, “Operational Experiences from Wärtsilä 5 kW Test System with 4 Sofc Stacks,” in *Proceedings of the 2nd European Fuel Cell Technology and Applications Conference*, Rome, 2007.

[72] K. Föger, *Personal communication,* Wien, 2009.

[73] M. Peksen, R. Peters, L. Blum and D. Stolten, “Numerical modelling and experimental validation of a planar type pre-reformer in SOFC technology,” *International Journal of Hydrogen Energy,* vol. 34, pp. 6425-6436, 2009.

[74] R. Peters, E. Riensche and P. Cremer, “Pre-reforming of natural gas in solid oxide fuel-cell systems,” *Journal of Power Sources,* vol. 86, p. 432–441, 2000.

[75] G. Kolb, Fuel Processign for Fuel Cells, Weinheim: Wiley-VHC, 2008.

[76] R. Dietrich, J. Oelze, A. Lindermeir, C. Spitt, M. Steffen, T. Küster, S. Chen, C. Schlitzberger and R. Leithner, “Efficiency gain of solid oxide fuel cell systems by using anode off gas recycle,” *Journal of Power Sources,* vol. 196, p. 7152– 7160, 2011.

[77] J. F. B. Rasmussen, P. V. Hendriksen and A. Hagen, “Study of Internal and External Leaks in Tests of Anode-Supported SOFCs,” *Fuel Cells,* vol. 8, no. 6, pp. 385-393, 2008.

[78] R. Dietrich, C. Szepanski, A. Lindermeir, S. Stenger, R. Leithner, J. Hamje, R. Deichmann and L. Dörrer, “Multiple innovations on a portable propane driven 300 We SOFC system,” in *Proceedings of 11th European SOFC & SOE Forum*, Lucerne, 2014.

[79] Z. Wuillemin, N. Autissier, A. Nakajo, M. Luong, J. Van Herle and D. Favrat, “Modeling and Study of the Influence of Sealing on a Solid Oxide Fuel Cell,” *Journal of Fuel Cell Science and Technology,* vol. 5, no. 1, pp. 011016-(1-9), February 2008.

[80] M. Rautanen, O. Thomann, O. Himanen, J. Tallgren and J. Kiviaho, “Glass coated compressible solid oxide fuel cell seals,” *Journal of Power Sources,* vol. 247, pp. 243-248, 2014.

[81] A. Wood, M. Pastula, D. Waldbillig and D. Ivey, “Initial Testing of Solutions to Redox Problems with Anode-Supported Solid Oxide Fuel Cells,” in *Electrochemical Society Proceedings PV2005-07*, Pennignton, 2005.

[82] J. L. Young, V. Vedharathinam and V. I. Birss, “Reverse Cell Bias for the Prevention of Ni Oxidation During Air Exposure,” *ECS Transactions,* vol. 35, no. 1, pp. 1697-1706, 2011.

[83] T. Clausen, “Process for operating a high temperature fuel cell stack”. US Patent US 20130052548 A1, 28 2 2013.

[84] D. Yang, M. Steinbugler, R. D. Sawyer, L. Van Dine and C. Reiser, “Procedure for starting up a fuel cell system having an anode exhaust recycle loop”. USA Patent US 7250229 B2, 31 7 2007.

[85] J. Ruokomäki, “Method and arrangement for utilizing recirculation for high temperature fuel cell system”. World Patent WO 2013117810 A1, 15 8 2013.

[86] A. Nakajo, F. Mueller, J. Brouwer, J. Van herle and D. Favrat, “Progressive activation of degradation processes in solid oxide fuel cell stacks: Part II: Spatial distribution of the degradation,” *Journal of Power Sources,* vol. 216, pp. 434-448, 2012.

[87] A. Nakajo, Z. Wuillemin, J. Van herle and D. Favrat, “Simulation of thermal stresses in anode-supported solid oxide fuel cell stacks. Part I: Probability of failure of the cells,” *Journal of Power Sources,* vol. 193, pp. 203-215, 2009.

[88] S. Reuber, A. Pönicke, C. Wunderlich and A. MIchaelis, “Eneramic Power Generator- A Reliable and Cycleable 100W SOFC System,” *ECS Transactions,* vol. 57, no. 1, pp. 161-169, 2013.

[89] S. Megel, M. Kusnezoff, N. Trofimenko, V. Sauchuk, J. S. ,. J. B. ,. W. Schilm, A. Michaelis, C. Bienert, M. Brandner, A. Venskutonis, S. Skrabs and L. Sigl, “CFY-Stack: from electrolyte supported cells to high efficiency SOFC stacks,” in *Proceedings of 10th European SOFC Forum*, Lucerne, 2012.

[90] B. Borglum, “Development of Solid Oxide Fuel Cells at Versa Power Systems,” 17 11 2009. [Online]. Available: http://www.fuelcellseminar.com/assets/2009/HRD24-3_0430PM_Borglum.pdf.

[Accessed 18 4 2013].

[91] W. B. Guan, H. J. Zhai, L. Jin, C. Xu and W. G. Wang, “Temperature Measurement and Distribution Inside Planar SOFC Stacks,” *Fuel Cells,* vol. 12, no. 1, pp. 24-31, 2012.

[92] J. Herring, J. E. O’Brien, C. Stoots, G. Hawkes, J. Hartvigsen and M. Shahnam, “Progress in high-temperature electrolysis for hydrogen production using planar SOFC technology,” *International Journal of Hydrogen Energy,* vol. 32, p. 440 – 450, 2007.

[93] M. Fardadi, D. McLarty and F. Jabbari, “Actuator Limitations in Spatial Temperature Control of SOFC,” *Journal of Fuel Cell Science and Technology,* vol. 10, no. 031005, pp. 1-10, June 2013.

[94] F. Mueller, M. Fardadi and F. Jabbari, “Feedback control of solid oxide fuel cell spatial temperature variation,” *Journal of Power Sources,* vol. 195, p. 4222–4233, 2010.

[95] M. Sorrentino and C. Pianese, “Model-based development of low-level control strategies for transient operation of solid oxide fuel cell systems,” *Journal of Power Sources,* vol. 196, p. 9036– 9045, 2011.

[96] D. Montgomery, Design and Analysis of Experiments, 8th ed., Singapore: John Wiley & Sons, 2009.

[97] M. Santarelli, M. Calì and P. Leone, “Design of experiments for fitting regression models on the tubular SOFC CHP100kWe: Screening test, response surface analysis and optimization,” *International Journal of Hydrogen Energy,* vol. 32, p. 343 – 358, 2007.

[98] M. Santarelli, P. Leone, M. Cali and G. Orsello, “Experimental evaluation of the sensitivity to fuel utilization and air management on a 100kW SOFC system,” *Journal of Power Sources,* vol. 171, pp. 155-168, 2007.

[99] M. Halinen, M. Noponen, J. Saarinen, P. Simell and J. Kiviaho, “Characterization and Control of Autothermal Reformer for SOFC Applications,” in *Fuel Cell Seminar Conference CD*, Honolulu, 2006.

[100] M. Halinen, M. Rautanen, J. Saarinen, J. Pennanen, A. Pohjoranta, J. Kiviaho, M. Pastula, B. Nuttall, C. Rankin and B. Borglum, “Performance of a 10 kW SOFC Demonstration Unit,” *ECS Transactions,* vol. 35, no. 1, pp. 113-120, 2011.

[101] M. Halinen, A. Pohjoranta, L. Kujanpää, V. Väisänen and P. Salminen, “Summary of the RealDemo - project 2012-2014,” Espoo, 2014.

[102] M. Halinen and J. Pennanen, “Analysis of leakages in a solid oxide fuel cell stack in system environment,” *Fuel cells,* vol. 2, p. 15, 2015.

[103] M. Halinen, O. Thomann and J. Kiviaho, “Experimental study of SOFC system heat-up without safety gases,” *International Journal of Hydrogen Energy,* vol. 39, pp. 552-561, 2014.

[104] M. Halinen, A. Pohjoranta, J. Pennanen and J. Kiviaho, “Stack temperature estimation in system environment by utilizing the design of experiments methodology,” *ECS Transactions,* vol. 57, no. 1, pp. 205 - 214, 2013.

[105] M. Halinen, A. Pohjoranta, J. Pennanen and J. Kiviaho, “Application of Multivariable Regression Model for SOFC Stack Temperature Estimation in System Environment,” *Proceedings of 11th European SOFC & SOE Forum 2014,* 2014.

[106] L. G. J. de Haart, J. Mougin, O. Posdziech, J. Kiviaho ja N. Menzler, ”Stack Degradation in Dependence of Operation Parameters the Real-SOFC Sensitivity Analysis,” *Fuel Cells,* osa/vuosik. 9, p. 794, 2009.

[107] M. Halinen, J. Saarinen, M. Noponen, I. Vinke and J. Kiviaho, “Experimental Analysis of Performance and Durability of SOFCdemonstration Unit,” *Fuel Cells,* vol. 10, no. 3, pp. 440-452, 2010.

[108] V. Väisänen, T. Riipinen and P. Silventoinen, “Effects of Switching Asymmetry on an Isolated Full-Bridge Boost Converter,” *IEEE Transactions on Power Eletronics,* vol. 25, no. 8, p. 2033, 2010.

PUBLICATION [P1]

Experimental Analysis on Performance and Durability of SOFC Demonstration Unit

In: Fuel Cells 10 (3), pp. 440-452

ORIGINAL RESEARCH PAPER

Fuel Cells DOI: 10.1002/fuce.200900152

Experimental Analysis on Performance and Durability of SOFC Demonstration Unit

M. Halinen[1]*, J. Saarinen[1], M. Noponen[1a], I. C. Vinke[2], J. Kiviaho[1]

[1] VTT Technical Research Centre of Finland, Fuel Cells, P.O. Box 1000, Biologinkuja 5, Espoo, FI-02044 VTT, Finland
[2] Forschungszentrum Jülich GmbH, Institute of Energy Research -Fuel Cells (IEF-3), D-52425 Jülich, Germany

Received August 06, 2009; accepted December 02, 2009

Abstract

A technical description and experimental analysis of a SOFC demonstration unit is presented. The unit contains most of the primary BoP-components of a complete SOFC system, except of air and fuel recirculation equipment or fuel system compressor. Natural gas is used as the fuel and electricity is supplied to the electric grid. A 5 kW power class planar SOFC stack from Research Centre Jülich is assembled to the demo unit and a long-term experiment is conducted to assess the characteristic performance and durability of different components of the unit (e.g. the SOFC stack, the fuel pre-reformer and air heat exchangers). The evolution of absolute voltage drop of the stack over time is found to be of the same magnitude when compared to short stack experiments. Thus, other system components are not observed to cause an increase in the characteristic voltage drop of the stack. Two BoP-components, the afterburner and the power conversion unit failed to operate as designed. The performance of other BoP-components i.e. fuel pre-reformer and heat exchangers were satisfactory during the test run, and no significant performance loss could be measured.

Keywords: Balance of Plant, Durability, Experimental Results, Solid Oxide Fuel Cell, Stack, Voltage Degradation

1 Introduction

Solid oxide fuel cells (SOFCs) are considered an advantageous technology in energy production due to the high fuel conversion efficiency, modular design possibilities and fuel flexibility. High operating temperature makes SOFCs well suited for combined heat and power production (CHP) or for hybrid systems where the SOFC stack is coupled with a gas turbine. Fuel processor design is simplified compared to low temperature fuel cell types due to high operating temperature that enables direct oxidation of carbon monoxide and the use of hydrocarbon fuels *via* internal reforming reactions. The theoretical efficiency of the SOFC is not governed by size when compared to e.g. Carnot- or Rankine-cycle based energy production. Thus, SOFCs can be utilised for various applications with different power scale e.g. auxiliary power units for cars and trucks, residential and distributed CHP or stationary power production.

The widespread commercialisation of the SOFC technology is hindered by relatively higher cost of the SOFC systems when compared to the established technology for energy production e.g. engines or gas turbines. The price for both SOFC stacks along with other system components is high and the availability of products is poor due to the absence of developed markets and production. Along with the reduction of cost, long lifetime and high availability are prerequisites for a SOFC system for both stationary and micro CHP applications. The inherent voltage degradation phenomenon of the SOFC stacks is the most important factor that affects the durability and lifetime of a SOFC system. For stationary applications, voltage degradation rates below 0.25% kh^{-1} have to be achieved to ensure a long enough lifetime for the products [1, 2]. Currently, operating times for planar SOFC stacks that

[*] *Corresponding author, matias.halinen@vtt.fi*
[a] *Present affiliation: Wärtsilä, Product Centre Ecotech, Fuel Cells*

span up to and over 10,000 h with degradation rates below 1% kh^{-1} have been reported [3–5].

In addition to the SOFC stack, also the other components of the system, and the system as a whole, must endure years of continuous operation without unreasonable performance degradation or component failures. In the absence of large-scale production of dedicated components and peripherals for SOFC systems, the lifetime and performance of system components are not well established. Operation times of over thousands of hours for complete SOFC systems with a varying degree of availability have been achieved and reported [3, 6–9]. However, the level of reporting is typically very general and no information is given on the fundamental process parameters such as fuel and air utilisation, or current density during the operation of the system. Additionally, the effect of different system components on the performance and durability of the system as a whole is not assessed.

It can be argued that a more comprehensive understanding of issues related to the reliability and durability of SOFC systems is needed in order to attain similar operation times and degradation rates for complete SOFC systems when compared to the lifetime of individual stacks. Therefore, long-term experiments with complete SOFC systems are needed to measure and determine the effect of system components on the degradation and lifetime of SOFC stack. In this paper, the technical design and experimental analysis of a SOFC demonstration unit are presented. The unit was designed and constructed in a Finnish publicly funded SOFC research and development programme, which consisted of system and BoP-component development, system modelling and characterisation of SOFC cells and short stacks in system relevant operating conditions [10, 13, 20, 24]. The unit was constructed in order to demonstrate SOFC technology and assess the performance, durability and reliability of a complete grid connected SOFC system with natural gas as the fuel [10]. Moreover, the experimental results obtained with the unit could be used to develop and validate modelling tools for SOFC systems [11–13]. Results from a 7,000 h test run with a 5 kW power class stack are presented. Characteristic performance and durability of different system components e.g. fuel processing unit, heat exchangers, and the SOFC stack are reported.

2 Experimental

2.1 System Layout and the SOFC Stack

The demonstration unit included all the most important balance of plant components (BoP) of a SOFC system i.e. a planar stack, fuel pre-reformer unit, power conversion and grid interconnection equipment, heat exchangers for air and fuel, a catalytic burner, a blower for cathode air and mass flow controllers for other reactants, automation and control system, and purge gas containers for system shutdown and start-up situations (Figure 1).

The unit was constructed in order to demonstrate SOFC technology, assess the durability and reliability of SOFC stacks and BoP-components with long-term testing for several thousands of hours and to study the characteristic performance of different components and the interactions between the components. In order to obtain characteristic measurement data from individual components, a non-integrated design was applied. The intention with the non-integrated design was to reduce the effect of surface-to-surface heat transfer between components and to make modifications and

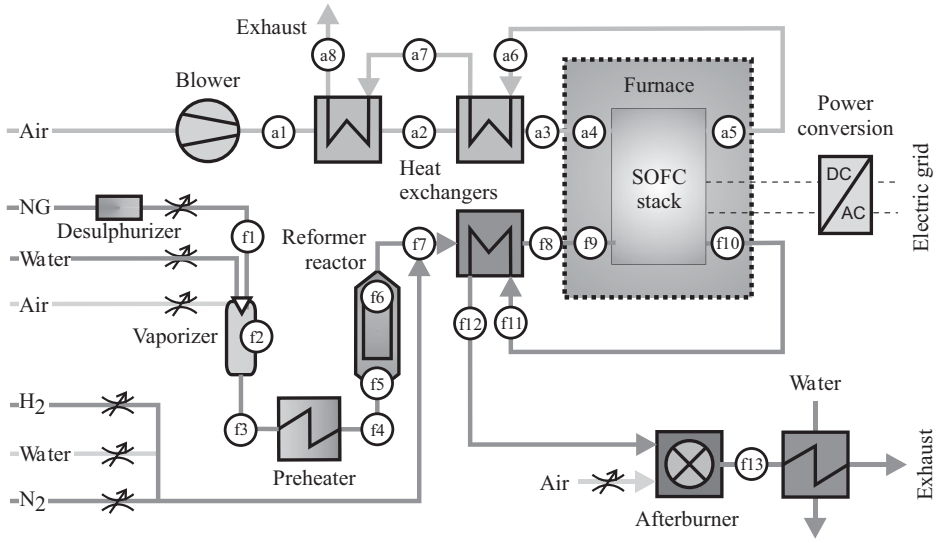

Fig. 1 Principle layout of the SOFC demonstration unit. Numbered circles represent measurement positions at the air and fuel systems of the unit.

replacements of different components easy. Thus, the unit was not designed to be thermally self-sufficient. Components and piping that operated above the room temperature were insulated with ceramic fibre insulation felts (isoTHERM S) and mineral wool sleeves. Additionally, the heat loss in the pipelines between the heat exchangers, the reformer unit and the stack was compensated with electric trace heating elements. Furthermore, it was necessary to position the SOFC stack in a furnace to make the assembly and curing of the stack possible on-site. The furnace was also used for start-up and to influence the temperature of the stack during system operation. Heating elements were used in the fuel system to vaporise the water and preheat the gas before the reformer reactor.

In order to collect relevant measurement information of the different components of the system, temperature and pressure were measured at several positions at the fuel and air systems. At the fuel system, temperature was measured at positions f2–f7 and f9–f13, and pressure at positions f1, f2, f7, f8, f11 and f12, depicted in Figure 1. At the air system, the temperature was measured at positions a1-a8 and the pressure at positions a1, a3, a6 and a8. Thermocouples (K-type, Class 1, ± 4 °C) were used for all temperature measurements. Pressure was measured with digital differential pressure meters (0–1,000 ± 3 mbarg, Keller PR-33).

The SOFC stack used in the unit was designed, manufactured and assembled by Forschungzentrum Jülich (FZJ) [14]. It utilised planar anode-supported cells with metallic interconnect plates made from CroFer22APU steel, which were coated with a MnOx/LCC10 contact layer at the air side. Glass-ceramic seals (Glass #76) were used to seal the stack. Fuel and air were distributed to cells in counter-flow pattern with internal manifold [15]. The 5 kW class stack used in the experiments consisted of 50 rectangular unit cells with an active area of 361 cm^2. The stack was resting on top of ceramic bricks inside the furnace. The inner dimensions of the furnace were 1,100 mm × 1,100 mm, the inner height was 640 mm and the thickness of the insulation layer was 150 mm. The heating elements of the furnace were situated on two opposite sides of the furnace. Current was collected from the end plates of the stack with steel bars that were led through the bottom of the furnace. Gas pipelines were, likewise, led through the bottom of the furnace.

The voltage was measured individually from all 50 unit cells in the stack with platinum wires that were spot-welded to the interconnect plates and end plates of the stack. The maximum error for the voltage measurements was ±9 mV. The flow-wise temperature profile was measured from interconnect plates situated above cells 3, 25 and 48, counting from the bottom of the stack. Thermocouples (K-type, Class 1) were used for the temperature measurements. The thermocouples were inserted inside 35 mm deep holes in the interconnect plates. In addition, the inlet and outlet temperatures of the fuel and air were measured from the pipeline ~10 cm from bottom plate of the stack (positions a4, a5, f9 and f10 in Figure 1).

2.2 Fuel System

The conventional nickel-cermet anode used in SOFCs is an effective steam-reforming catalyst, and therefore, able to convert hydrocarbons to hydrogen and carbon monoxide that can be utilised in electrochemical reactions. However, complete internal reforming can lead to local cooling at the fuel inlet area caused by a fast endothermic steam reforming reactions, and large temperature gradients can develop which may lead to cell cracking. Additionally, heating the fuel directly to operating temperature of the stack without pre-reforming of the fuel at lower temperatures increases the probability of hydrocarbon cracking and carbon formation in the heat exchangers or pipelines [16]. Without pre-reforming, some higher hydrocarbons can coke the nickel substrate at the anode electrode resulting in performance degradation and ultimately destruction of the cell [17, 18]. Due to the above-mentioned issues, prereforming of hydrocarbon fuels is usually necessary.

With natural gas, where the methane is the main constituent of the fuel, the degree of pre-reforming (*DoR*) of methane should be selected to optimise system-operating conditions. At nominal operating conditions, it is beneficial to maximise the amount of internal reforming reactions as the endothermic steam reforming of methane cools down the stack and decreases the need for surplus cathode air, which improves electrical efficiency [19]. At part-load and system stand-by situations, the amount of heat losses from the system is increased with respect to the heat produced by the stack. Therefore, in these situations, it may be beneficial to increase the *DoR* and limit the amount of methane fed into the stack [13]. As a result, the temperature and the voltage of the stack are increased, which can improve the system efficiency.

The reformer unit for natural gas used in the system could be operated at steam reforming conditions and, additionally, air could be supplied into the reactor to utilise exothermic partial oxidation reactions [20–22]. It consisted of mass flow controllers for natural gas (0–35.0 ± 0.5 l_N min^{-1}), water (0–80 ± 1 g min^{-1}) and air (0–60.0 ± 0.7 l_N min^{-1}), sulphur removal reactor, vaporiser, preheater, reactor chamber equipped with a proprietary monolithic catalyst (Süd-Chemie) and a heat exchanger before the stack. The natural gas used in Finland contains 4–10 ppm of sulphur containing THT odorant, and if not removed from the natural gas, it can deactivate the anode, lower the cell voltage and cause increased degradation [20]. The THT odourant was removed with an absorbent (Süd-Chemie) operating at room temperature. The adsorbent was changed on regular basis to keep the fuel supply free of sulphur. Concurrently, the impurities in the water supply were removed with ion-exchange resin. Natural gas and water were fed through a gas atomising nozzle into the vaporisation chamber. The supply pressure for natural gas and water was ~3 barg. Air was fed into the vaporisation chamber through a separate inlet. The reactor and the catalyst were not heated during operation. The heat used in the steam reforming reaction was provided by pre-

heating the inlet gases with electric heaters. Additionally, heat was supplied to the reactor by exothermic partial oxidation reactions when air was fed to the reformer unit. Temperature was measured at the reactor inlet, from the leading surface of the catalyst and at the reactor outlet (positions f4, f5 and f6 in Figure 1). Pressure was measured from the natural gas inlet before the gas atomising nozzle and from the vaporisation chamber (positions f1 and f2). A heat exchanger was situated between the reactor and the stack in order to increase the temperature of the fuel before the stack inlet. The heat exchanger was of a welded plate type and it was manufactured in-house. Temperature (positions f7, f8 and f11) and pressure (positions f7, f8, f10 and f11) were measured before and after the heat exchanger. Steel grade 1.4404 was used for the vaporiser and steel grade 1.4835 was used for all other components and piping at the fuel system of the demonstration unit.

Reformer exhaust gas was analysed with an online gas analyser (Sick S710 series) and with gas chromatographs (HP 6850A and HP 5890 Series II). The accuracy of the online analyser was further improved by calibrating it with varying gas mixture that correspond the different compositions of the exhaust gas. After calibration, the accuracy of the online analyser was ±0.5% for CO, CO_2 and CH_4 and ±1% for H_2. The composition of the exhaust gas on wet basis was calculated on the basis of carbon and nitrogen mass balances solved with the inlet mass flow measurements for air, water and natural gas and with exhaust gas analysis.

The unit could also be operated with gas mixture containing hydrogen (0–70.0 ± 0.8 l_N min^{-1}), nitrogen (0–70.0 ± 0.8 l_N min^{-1}) and steam (0–200 ± 2 gh^{-1}). Water was evaporated and mixed with gases by using a temperature-controlled evaporative mixer (Bronkhorst CEM-202). The gas mixture could be used to reduce the anode substrate after the stack assembly, as fuel during system operation and as purge gas during the heating and cooling of the unit to keep the anode substrate at reducing atmosphere.

Unused fuel in the anode exhaust gas was oxidised with air in a catalytic burner. The burner consisted of four successive segments equipped with cylindrical monolith catalysts. The burner and catalysts were manufactured in-house. Each catalyst segment had an individual air inlet. Air was supplied to the burner with a thermal mass flow controller (0–500 ± 6 l_N min^{-1}) and divided between the segments with rotameters. Downstream from the burner, the exhaust gas was fed through a water-cooled heat exchanger in order to retrieve the heat and condensate the water vapour before the exhaust.

2.3 Air System

Ambient air provides the source of oxygen, which is needed for electrochemical reactions at the cathode, and the air can be fed into the stack e.g. with air blowers. The use of over-stoichiometric amounts of air is necessary to dissipate the heat produced by the SOFC stack under electrical loading and prevent overheating of the stack to excessive operating temperatures. The inlet ambient air has to be preheated closer to the operating temperature of the stack to avoid local cooling of the stack at the air inlet, which could cause damaging temperature gradients or decrease the stack voltage under electric current by lowering the operating temperature [16]. The needed over-stoichiometric amount of air can vary between 3 and 10 (U_{AIR} between 0.10 and 0.33) depending on the *DoR* and the permissible temperature increase of air in the stack [19]. Such amounts of air lead to large air preheat duty and the energy needed for preheating must be recuperated from the stack's exhaust gases in order to achieve practical system efficiencies.

Ambient air was supplied to the unit with two-side channel blowers connected mechanically into series (Ventur SC-20C). Two blowers were used to reach pressures above 300 mbar. A filter was present at the blower inlet to remove particles from the air. Rotation speed of the blower was controlled with an inverter and the air flow was measured with a thermal mass flow metre (0–1,000 ± 20 l_N min^{-1}). Two heat exchangers for low and high temperature were connected in series in order to pre-heat inlet air to the stack. The design with two heat exchangers was chosen for the air system in order to reduce the temperature difference between the inlet and outlet and thus the thermal stresses induced to the heat exchangers. Concurrently, poor commercial availability of single heat exchanger that would meet the specified operating temperature necessitated this approach.

The low temperature heat exchanger was of a fully welded plate type (Raucell 120-23). Maximum operating temperature for this heat exchanger was designed to be below 450 °C. The high temperature heat exchanger was of a tube and shell type designed and manufactured in-house, and the maximum operating temperature was designed to be below 800 °C. Steel grades used in the construction of the heat exchangers were 1.4404 and 1.4835 for lower and higher operating temperature, respectively. Temperature was measured before, after and between the heat exchangers at cold and hot sides (positions a1, a2, a3, a6, a7 and a8 in Figure 1). Pressure was measured before and after the two heat exchangers at hot and cold sides (positions a1, a3, a6, and a8).

2.4 Power Conditioning Equipment and Automation System

Power conditioning equipment is needed in SOFC systems in order to increase the stack's DC voltage high enough to enable high efficiency DC power conversion to AC power and synchronisation with the electricity grid. Power conditioning and grid interconnection equipment consisted of DC–DC converters, regenerative inverter, LC-filter and transformer. DC–DC converters were used to increase the voltage of the SOFC stack to ~400 VDC required by the inverter. The inverter transmuted DC to 200 VAC. A LC-filter was used to compensate the possible current and voltage disturbance from the system to electric grid. Finally, a transformer was used to increase the voltage from 200 to 400 VAC. The power

conversion unit was manufactured from off-the-shelf components by Verteco Inc. Electric current from the stack to the power conversion unit was measured using a shunt resistor (Metrix Electronics) with a maximum error of ±0.7 A. Alternatively, the stack could be operated without the power conversion unit by dissipating the produced electricity with a DC load (Chroma 63203) e.g. during initial characterisation of the stacks with hydrogen as a fuel. The DC load was connected parallel to the stack with grid interconnection equipment. The maximum error for the current measurement of the DC load was ±1.2 A.

In order to provide the capability for long term testing in a safe and reliable way, the demonstration unit was designed to be capable of unmanned operation. This was made viable by constructing an automation and control system, which consisted of a standard industrial PLC (Schneider Premium Series) and a PC-based monitoring station. The PC-based monitoring station was used as a human-machine-interface and as a measurement database. During unmanned operation, several critical process measurements i.e. individual cell voltages, temperature of the inlet and outlet gases of the stack, supply pressure of the reactants, air blower or power conditioning faults, temperature of the reformer reactor and system-wide pressure measurements were used to monitor the safe operating conditions of the unit. If the critical process measurements deviated beyond predefined limits, the unit was brought to a stand-by state by disconnecting the stack from the electric grid and aborting the fuel feed to the unit. Air and safety gas containing 97% Ar and 3% H_2 were supplied from gas bottles to the respective sides of the unit to keep the anode at reducing and cathode at oxidising atmosphere. The gas flow through the system during emergency shutdown situations was set to be ~1 l_N min^{-1}.

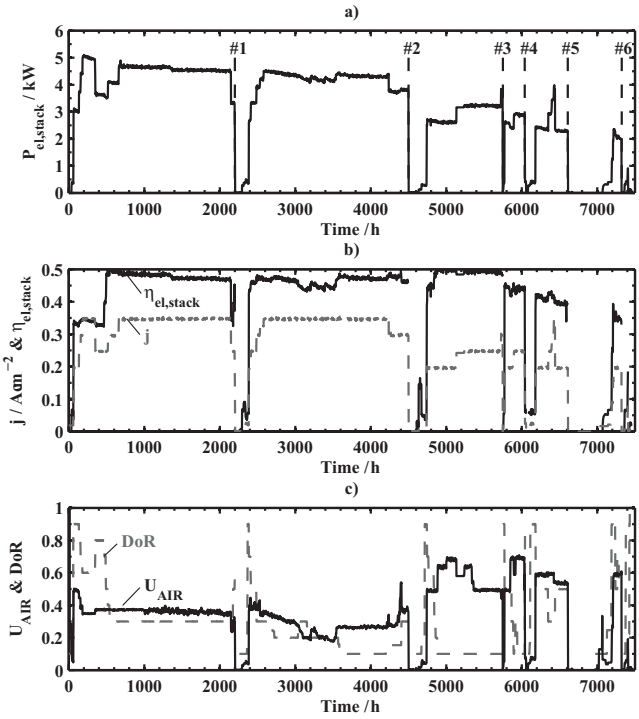

Fig. 2 Operating conditions of the demonstration unit and the electric power of the stack during the experiment. a) Gross electric power of the stack ($P_{el,stack}$). b) current density (j, dashed line) and gross electric efficiency ($\eta_{el,stack}$, solid line). c) Air utilisation (U_{AIR}, solid line) and degree of pre-reforming (*DoR*, dashed line). Shutdown situations are marked with numbers in the top figure.

3 Results and Discussion

3.1 Performance and Durability of the Stack

A long-term test run for a total period of 7,000 h was conducted with the demonstration unit, during which the stack was electrically loaded for over 6,000 h. During the experiment, the system was operated both at steady-state operating conditions, to assess the durability of the stack and BoP-components, and at varying operating conditions, to measure the characteristic operation of the unit components. The gross DC power ($P_{el,stack}$) of the stack along with the gross DC efficiency ($\eta_{el,stack}$), the current density, the air utilisation (U_{AIR}) and the degree of pre-reforming (*DoR*) of the fed methane (98% in natural gas) during the experiment are depicted in Figure 2. During the first 500 h of the experiment, fuel utilisation (U_{FUEL}) of the stack was 51%. During 500 to 4,500 h, U_{FUEL} was kept at 71% and the current density at 0.35 A cm^{-2} in order to measure the durability of the unit at nominal operating conditions. During this period, the $P_{el,stack}$ was between 4.5 and 5 kW and the $\eta_{el,stack}$ between 45 and 50%, depending on the operating parameters and duration of the experiment. After 4,500 h, the unit was used at lower current densities to measure the performance at part-load conditions at 0.2–0.25 A cm^{-2}, and also at lower operating temperature. Until 5,900 h, temperature of the furnace was kept at 780 °C during which $\eta_{el,stack}$ of 50% was achieved at part-load operating conditions. After 5,900 h, furnace temperature was decreased to 730 °C and a lower $\eta_{el,stack}$ of 40–45% was measured due to decreased stack voltage. At the end of the long term testing, at 7,000 h, the stack was insulated and the unit was operated without heating of the furnace in order to measure the effect of varying *DoR* to the temperature, voltage and effciency of the stack.

The demonstration unit and the stack could be operated over a wide range of operating conditions. During the experiment, the *DoR* varied between 0.1 and 0.9, U_{FUEL} between 0.51 and 0.71 and U_{AIR} between 0.17 and 0.68 when the cur-

rent density was at or above 0.2 A cm^{-2}. For the major part of the test, when the furnace was in use, varying the *DoR* did not result in significant changes in the temperature or voltage of stack, and the stack could be operated with *DoR* of 0.1 between 0.25 and 0.35 A cm^{-2}. At the end of the long term testing, when the furnace was not in use, a more pronounced effect of the *DoR* was observed, and *DoR* below 0.5 could not be achieved with 0.2 A cm^{-2}. This was due to the temperature smoothing effect of the furnace because of its high heat transfer area: the higher the temperature of the stack was with respect to the furnace temperature, the higher were the heat losses from the stack and vice versa. Therefore, the use of furnace affected the thermal balance of the stack to a great extent and provided an increased operability for the system, which would not have been possible without the furnace. It was observed that at low U_{AIR} values, the stack voltage decreased as the temperature of the stack was decreased due to increased air flow rate (Figure 2, 3,000–3,500 h). Interestingly, the operability of the stack was maintained at high U_{AIR} (above 0.33 [19]) values and no overheating of the stack occurred. This can be explained again by the use of furnace during the experiment.

As can be seen in Figure 2, the experiment was interrupted and the electric loading of the stack discontinued several times during the test run. Shutdown #1 at 2,200 h was initiated due to system servicing. The system was brought to a standby state and switched to hydrogen-nitrogen purge gas in order to clean the atomising nozzle of the fuel processor. The nozzle was clogged due to saturation of the ion-exchange resin, and the impurities present in the water deposited at the orifice of the nozzle. This induced a pressure drop increase over the nozzle (between f1 and f2), which would have eventually hindered the fuel and water flow to the fuel processing unit. As the ion-exchange mass was changed on a more regular basis based on the conductivity measurement of the water, clogging was not observed later during the experiment. Shutdown #2 at 4,500 h, occurred automatically due to supply failure of the natural gas and the system was brought to emergency shutdown. The fuel and air feeds were immediately discontinued and the unit was purged with a safety gas from gas bottles. Shutdowns #3 and #4 at 5,800 and 6,100 h, respectively, occurred automatically due to high pressure and low voltage alarms caused by partially frozen exhaust pipeline. The dew point of the anode exhaust gas after heat recovery and condensation was ~10 °C and the coincident outside temperature was –20 °C. As a result, the water vapour left in the exhaust gas froze in the exhaust pipeline obstructing the gas flow. The problem was solved by installing an electric trace heater to the exhaust pipeline.

After each of the above-mentioned shutdown situations, the individual cell voltages were compared at identical operating conditions with respect to current density, U_{FUEL}, U_{AIR}, *DoR* and furnace and stack temperature. The difference between individual cell voltages was at maximum ±20 mV before and after each shutdown, as some of the cells exhibited an increase in voltage. An exception to this was after the shutdown #3 at 5,800 h, where the flow of air purge gas was cut off for 3 h, due to exhaustion of purge air container, resulting in a significant loss of performance in cells number 1 and 7. With respect to these results, it can be concluded that the shutdown routines developed for the unit, if executed in a designed manner, along with a robust enough stack design, were sufficient to bring the system down safely without relevant decrease in the performance.

The shutdown #5 at 6,400 h was initiated to cool down the stack to room temperature to assemble insulation layer as the adjacent cells to cell #8 had already started to show progressive decrease in voltage after the shutdown at 5,800 h. The stack was then insulated with microporous insulation layer, heated back up to operating temperature mainly by pre-heating the inlet gases of the stack, and operated for another ~200 h. During this time, the effect of *DoR* on the temperature, voltage and efficiency of the stack was measured without external heating of the furnace. The final shutdown #6 at 7,400 h was initiated automatically due to progressive failures of the cells adjacent to short-circuited cell #8, which led to increasing leakages between the fuel and air sides of the stack and excessive temperatures, both in the stack and at the exhaust pipeline due to the burning of the fuel. This was seen as a catastrophic failure of the stack.

Additionally, between 2,500 and 3,500 h recurring difficulties related to the control of the inlet cathode air flow caused a steady increase in the inlet air flow, which manifests as a decrease of U_{AIR} in Figure 2. As a result of increased inlet air, the stack was cooled down progressively and the temperature and voltage of the stack were decreased. This decrease in voltage is seen as a decrease in $P_{el,stack}$ in Figure 2, as the stack was used with constant current density. The problem was solved by reconfiguring the control loop for cathode air, and thus a steady supply of air was restored.

Polarisation of the 5 kW stack was measured with hydrogen immediately after assembly and curing. After the curing and evaluation of stack performance with hydrogen, the unit and the stack were cooled down to ambient temperature for inspection and heated back to operating temperature to commence the experiments. Individual cell voltages of the stack with hydrogen at current density of 0.25 A cm^{-2} are depicted in Figure 3. Additionally, individual cell voltages measured during the experiment with reformed natural gas at 0.35 A cm^{-2} are shown for comparison. The distribution of individual cell voltages is identical with hydrogen and reformate gas i.e. the initial thermal cycle did not cause changes in the voltage distribution. Voltage of the cell #1 (bottom cell) was 50–100 mV lower compared to the other cells, and short-circuit was measured in the cell #8. The other cell voltages were within ±25 mV and similar values have been reported previously for FZJ stacks [23]. A slight increase in the voltage is observed towards the top of the stack, which is probably caused by the heating effect of the furnace, and due to the heat loss through the ceramic bricks at the bottom of the furnace. The differences between individual cell voltages, which are more pronounced in the middle of the stack (cells 20–30),

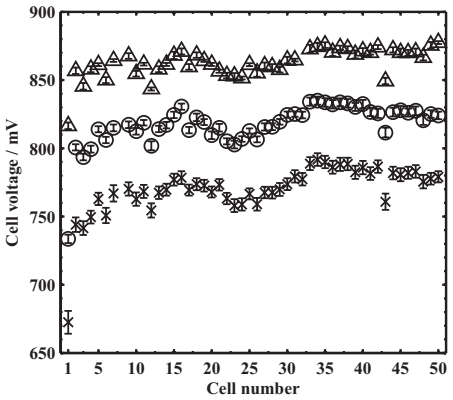

Fig. 3 Unit cell voltages of the stack at △ : hydrogen, U_{FUEL} = 0.6, j = 0.25 A cm^{-2}; ○ : natural gas, U_{FUEL} = 0.51, j = 0.35 A cm^{-2}; × : natural gas, U_{FUEL} = 0.71, j = 0.35 A cm^{-2}. Cell number 1 is located at the bottom of the stack. Error bars represent 2σ error.

can be due to differing contact resistances caused by inhomogeneous settling of the stack during the stack assembly and curing.

I–V curves of the stack with reformed natural gas at U_{FUEL} of 51% and 71% are depicted in Figure 4. After each current step, the system was left to stabilise for at least 24 h to reach new system-wide steady-state conditions i.e. so that no changes in the temperature measurements were observed. The time between the two different *I–V* curves depicted in Figure 4 is ~250 hundred hours. Electric power of 5.1 kW with U_{FUEL} of 51% was achieved at 0.35 A cm^{-2}. However, the $\eta_{el,stack}$ was only 33–35% due to low fuel utilisation level of the stack and also due to high inlet air O_2/C -ratio to the reformer, as part of the natural gas was oxidised already in

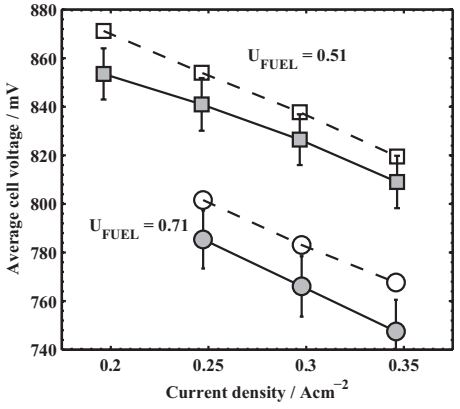

Fig. 4 Average unit cell voltage of the stack *versus* current density where U_{FUEL} is ○ = 0.71 and □ = 0.51. Fuel is pre-reformed natural gas. Solid line and filled marker: actual values measured from the stack. Dashed line and open marker: averaged values without cell #8. Error bars represent 2σ error.

the reformer reactor (see Section 3.2). The efficiency was improved by higher fuel utilisation and lower inlet air O_2/C ratios, as relatively larger fraction of the inlet fuel was used to produce electricity. With U_{FUEL} of 71%, electric power of 4.7 kW was achieved and the $\eta_{el,stack}$ was increased to ~48%. The short-circuited cell caused a decrease in the performance of the stack by lowering the stack voltage up to 2.5% during the *I–V* measurements. However, despite the performance loss, the robustness of the stack design towards short-circuits was demonstrated as stable operation was maintained up to 6,000 h during the experiment.

Performance degradation of varying magnitude was observed in the stack throughout the experiment. The measurements from the 5 kW stack were compared to the inherent voltage degradation of stacks with similar design and materials. The performance degradation of SOFC stacks is typically measured by operating the stack galvanostatically at constant operating conditions for several thousands of hours. The degradation can then be calculated from the absolute [$\Delta U \Delta t^{-1}$ (mV kh^{-1})] or relative [$\Delta U U_1^{-1} \Delta t^{-1}$ (%kh^{-1})] voltage drop over time and the resulting value can be used to express the durability of the stack. As the demonstration unit and the stack were used in varying operating conditions throughout the experiment, it is impossible to calculate any single value for stack voltage drop for the entire duration of the test based on the above described practice. Instead, the degradation of the stack is evaluated here by observing the evolution of absolute voltage drop of the stack voltage over time.

The average cell voltage of the stack during the experiment is depicted in Figure 5a. The absolute voltage drop is calculated with linear regression for all periods at steady-state operating conditions over 100 h. Measurements from the short-circuited cell (#8) are not used in the linear regression, as this generates step transitions in the voltage, which would produce misleading values for linear regression. Additionally to the steady-state conditions, the voltage drop is calculated with linear regression between periods where operation at identical conditions was resumed. The time periods and operating conditions used to calculate the absolute voltage drop, along with the results of linear regression are summarised in Table 1.

The resulting values for absolute voltage drop over time are depicted in Figure 5b. The absolute voltage drop was 20–135 mV kh^{-1} during the first 400 h of operating conditions and the voltage drop gets smaller over time. After the initial 400 h, the voltage drop settles at 6–12 mV kh^{-1}. After 4,000 h, the result suggests that the voltage drop is again increasing. Comparable values of absolute voltage drop over time for similar first generation (1-G) F-design short stacks have been reported by de Haart et al [5]. With 1-G short stacks, the initial voltage drop was 100–135 mV kh^{-1} during the first 300 h, which corresponds to the values obtained in the demonstration unit. Concurrently, after the initial drop in voltage, a linear decrease in voltage was measured over time. The linear decrease of voltage for 1-G short stacks was 6 mV kh^{-1} at 0.3 A cm^{-2}, and 16 mV kh^{-1} at 0.4 A cm^{-2}, which again corre-

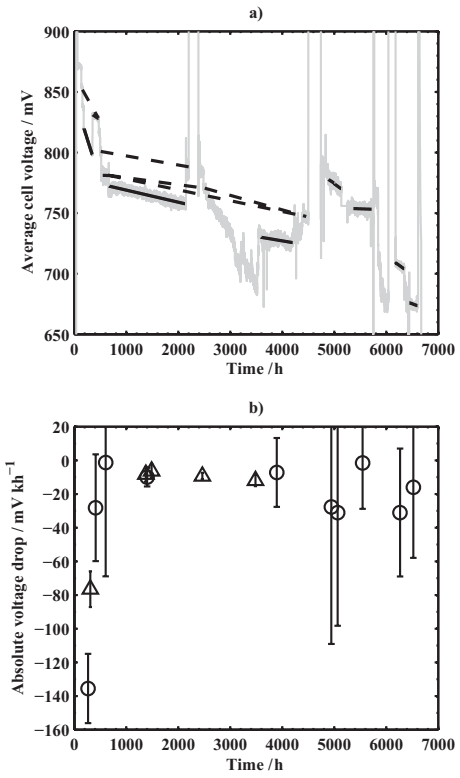

Fig. 5 Evolution of the stack voltage during experiment. a) Average cell voltage of the stack over time without cell #8 (grey line), linear fit for voltage at steady-state operating conditions (black solid line) and linear fit between identical operating conditions (black dashed line). b) Voltage decrease obtained with linear fitting at steady-state operating conditions (○) and between identical operating conditions (△). Error bars represent 2σ error in linear fit.

Table 1 Time period and operating conditions where the absolute voltage drop over time is calculated with linear regression. Error estimate for linear regression that meets 2σ variance in voltage measurements.

t_1	t_2	j	U_{FUEL}	U_{AIR}	Inlet O_2/C	Operating	ΔU	ΔU 2σ error
Hours		A cm^{-2}				Conditions	mV kh^{-1}	mV kh^{-1}
185	345	0.35	0.51	0.35	0.25	Steady-state	–136	21
156	462	0.25	0.51	0.38	0.30	Identical	–77	11
355	465	0.25	0.51	0.37	0.35	Steady-state	–28	32
545	660	0.30	0.71	0.37	0.10	Steady-state	–1	68
670	2 130	0.35	0.71	0.36	0.10	Steady-state	–10	6
510	2 428	0.25	0.71	0.38	0.19	Identical	–8	4
650	2 509	0.30	0.71	0.38	0.10	Identical	–6	4
650	4 460	0.30	0.71	0.37	0.10	Identical	–9	2
2 509	4 460	0.30	0.71	0.38	0.10	Identical	–12	3
3 590	4 200	0.35	0.71	0.26	0.00	Steady-state	–7	20
4 890	5 000	0.20	0.71	0.64	0.00	Steady-state	–28	81
5 000	5 130	0.20	0.71	0.68	0.00	Steady-state	–31	67
5 370	5 720	0.25	0.71	0.49	0.00	Steady-state	–2	27
6 190	6 345	0.20	0.71	0.59	0.20	Steady-state	–31	38
6 445	6 600	0.20	0.70	0.54	0.20	Steady-state	–16	42

spond to the values between 1,000 and 4,000 h of operation presented in Figure 5b. When the 1-G short stacks were used at current a density of 0.4 A cm^{-2} or higher, the voltage drop started to increase progressively before 3,000 h of operation. This progressive degradation was observed to increase towards higher current densities. After 4,000 h, the stack in the demonstration unit exhibits signs of progressive voltage decrease as well. However, relatively large error margin for the absolute voltage drop, due to measurement noise and short period of constant operation conditions, prevents obtaining a reliable value for the magnitude of progression. Nevertheless, both the magnitude and the different periods in the evolution of the absolute voltage drop over time correspond well between the 5 kW stack and similar 1-G stacks. Therefore, it can be concluded that the voltage degradation of the stack is inherent to the stack design itself i.e. no distinct increase in the degradation is observed due to choice of BoP-components, materials and design or system operating conditions.

3.2 Performance and Durability of BoP-components

The performance of the BoP-components used in the demonstration unit was suffcient to obtain the designed electrical output for the stack with gross electric efficiency of 45–50%. Fuel processing unit, air and fuel heat exchangers and the automation system worked as designed and performed reliably during the test run. The performances of the afterburner and power conversion unit were sub-optimal, but did not impede the performance of the stack.

The fuel reformer used in the demonstration unit provided means to control the degree of pre-reforming of the natural gas by varying the inlet air O_2/C-ratio and the H_2O/C-ratio [22]. By increasing the inlet air O_2/C-ratio, the faradic equivalent current efficiency of the reformer is lowered [24], as the part of the inlet fuel reacts with oxygen *via* partial oxidation reactions (Eq. 1).

$$\eta_{far} = \left(1 - 0.5 \times \frac{O_2}{C}\right) \quad (1)$$

In order to minimise the risk of carbon formation in the reactor, fuel pipelines and stack, the H_2O/C-ratio was increased as the O_2/C-ratio was decreased. The minimum H_2O/C-ratio in relation to O_2/C-ratio was selected to exhibit no graphite formation at thermodynamic equilibrium above 350 °C, and was defined according to Equation 2.

$$\frac{H_2O}{C} = 1.44 \times \left(\frac{O_2}{C}\right)^2 - 2.88 \times \frac{O_2}{C} + 2 \quad (2)$$

The effect of varying inlet air O_2/C-ratio to the outlet temperature (position

f6, Figure 1) of the reactor and on the gas composition of the reactor exhaust gas is depicted in Figure 6. The temperature at the reactor inlet (position f5) varied between 530 and 550 °C. At steam reforming mode (O_2/C ratio = 0), the *DoR* of methane in the natural gas was ~10%, and the *DoR* of ethane and propane was above 97% while the rest of the higher hydrocarbons in the natural gas were below detection limit. It should be noted that the *DoR* was nearly proportional to the inlet O_2/C-ratio and at O_2/C-ratio of 0.4 the degree of pre-reforming was increased to 90%. Concurrently, η_{far} decreased from 100% at steam reforming mode to 80% at O_2/C-ratio of 0.4.

The experimental results of the reformer characterisation were compared to the thermodynamic equilibrium at corresponding conditions. The equilibrium temperature and the composition of the reformate gas was calculated with Cantera toolbox [25] using GRI-Mech 3.0 reactions developed for natural gas combustion [26]. Equilibrium was solved for an adiabatic system, where the total enthalpy and pressure between reactants and products were kept constant. Temperature measurement at the reactor inlet (Figure 6) and measurements from mass flow controllers were used to define inlet gas mixture temperature and composition.

The experimental values are within the error limits when compared to the corresponding equilibrium values, except at O_2/C -ratios below 0.1 (Figure 6). At O_2/C -ratios below 0.1 the measured outlet temperature methane concentration are higher with respect to the equilibrium values. This deviation can be due to the catalyst kinetics, which limit the extent of the endothermic steam reforming reactions, as both the methane concentration and temperature at the outlet are higher than the corresponding equilibrium values.

Ageing of a natural gas pre-reformer catalyst can be assessed by observing the change in the methane conversion over time [27]. Decrease in the catalyst activity towards conversion of methane with an adiabatic reactor would show as decrease in the *DoR* and increase in the reactor outlet temperature, as less methane is consumed by endothermic steam reforming reactions. The long-term performance of the catalyst with respect to *DoR* and reactor outlet temperature is depicted in Figure 7. Again, both experimental and equilib-

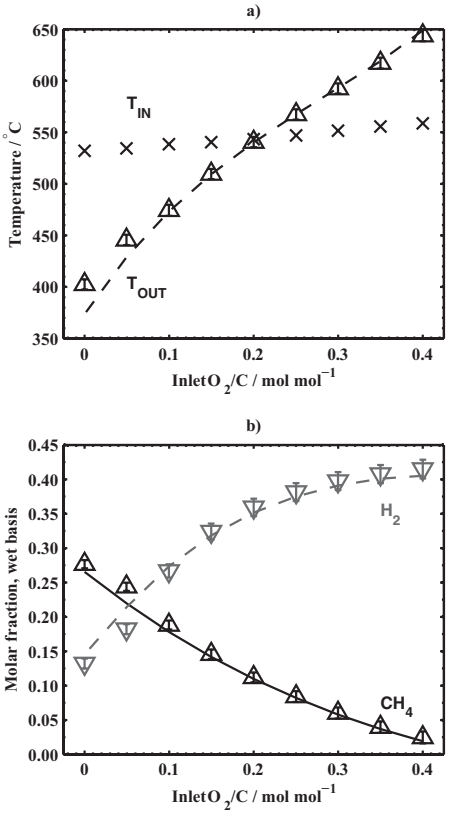

Fig. 6 Inlet O_2/C-ratio *versus* a) x = temperature at the reactor inlet and △ = temperature at the reactor outlet and b) ▽ = molar fraction of hydrogen and △ = molar fraction of methane. Markers represent the measured values and lines the equilibrium values.

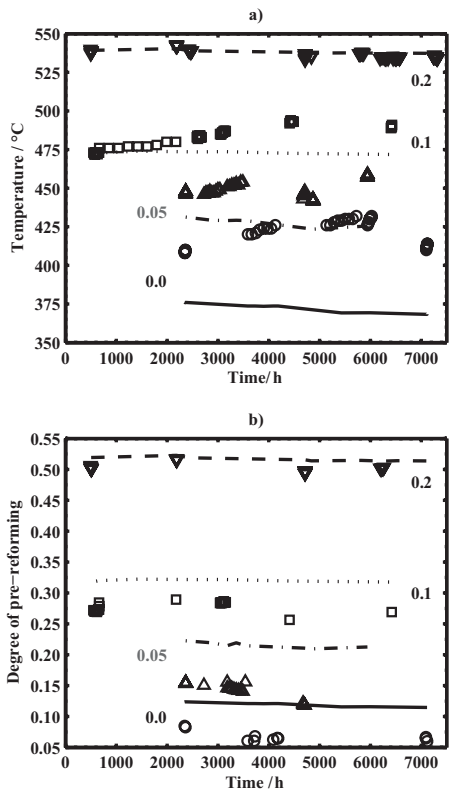

Fig. 7 a) Temperature at the reactor outlet and b) degree of pre-reforming gas during the test run with varying inlet air O_2/C -ratio. Markers represent the measured values and lines equilibrium values. Inlet air O_2/C -ratio was 0.0 (○, solid line), 0.05 (△, dash-dot), 0.1 (□, dotted) and 0.2 (▽, dashed).

rium results are presented. The performance can be evaluated with several inlet O_2/C -ratios as the demo unit was used at varying conditions. With inlet O_2/C -ratio of 0.2, no changes in either the temperature or the *DoR* can be seen over time. With lower O_2/C -ratios, the difference in the reactor outlet temperature increases by a maximum of 25 °C as the experiment proceeds further when compared to equilibrium values. A similar effect can be perceived with *DoR*, but the effect is not so pronounced as with temperature. These results indicate that some deactivation of the catalyst occurred, as the extent of steam reforming reactions decreased during the test run. Moreover, the deactivation can be more pronounced towards lower O_2/C -ratios, where larger portion of the methane is converted *via* steam reforming instead of partial oxidation reactions. However, the changes in the temperature are within 25 °C and the corresponding change in the *DoR* is only a few percent units. It can be argued that a deactivation of this magnitude is not an issue in the system operation, as the heat balance of the system is not significantly changed.

The characteristic performance of the air heat exchanger bundle is depicted in Figure 8a. It can be seen that the inlet air (position a3) was preheated to 530–580 °C and the temperature was increasing with the inlet air flow. The conductance of the heat exchanger bundle was 28.5 W K^{-1} and 79 W K^{-1} with 200 l_N min^{-1} and 600 l_N min^{-1}, respectively. The conductance increased linearly as a function of air flow rate. The relative decrease in temperature at lower air flow rates is due to considerable heat losses from the air exhaust pipeline between the stack and the heat exchangers, and from the heat exchanger bundle itself. Heat loss was calculated to be 13–15% from the hot air flow in the heat exchangers and 6–12% in the stack exhaust pipeline, depending on the air flow rate (data not shown). The temperature difference between the air flows at the stack end of the heat exchanger bundle remained at 150 ± 10 °C, regardless of the variation in the inlet air flow rate and the temperature of the hot air from the stack.

The characteristic performance of the air heat exchanger bundle remained constant during the test run. Figure 8b depicts the difference between temperature measurements at the stack end and blower end of the heat exchanger bundle. It is clear that the temperature difference remains at the above mentioned 150 ± 10 °C over time with some fluctuations caused by system stand-by situations. This indicates that the heat-transfer properties of the heat exchangers remain unchanged during the experiment. Likewise, no changes in the characteristic pressure drop at the hot side and the cold side of the HEX bundle were measured (data not shown).

No changes in the pressure losses at the fuel heat exchanger were observed over time. The pressure loss at each side of the fuel exchanger and in the fuel side of the stack was 5–20 mbar depending on inlet fuel flow rate, degree of pre-reforming and fuel utilisation of the stack. The pressure loss of the reformer reactor was below 5 mbar, while the vaporiser and fuel heater contributed 40–100 mbar to the total backpressure of the fuel system. The total backpressure of the components at the fuel system remained below 200 mbar

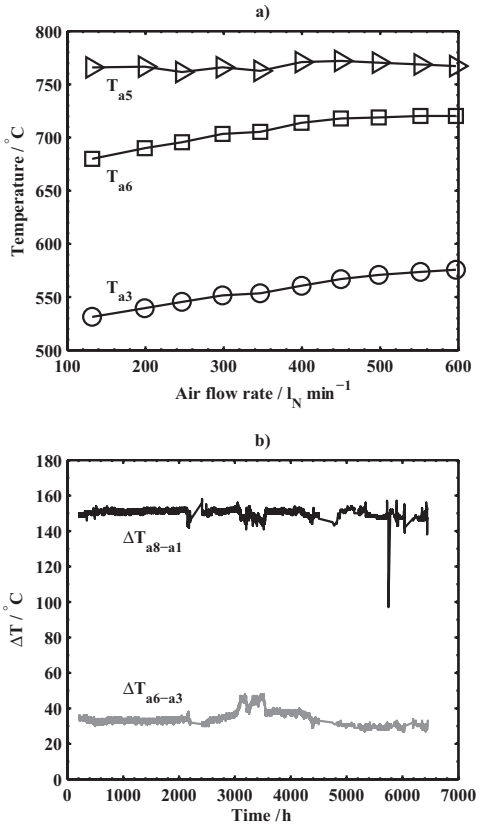

Fig. 8 Operation of the heat exchangers at the air system. a) Temperature of the air at the fresh side outlet of the HEX (▷), hot side inlet of the HEX (○) and at the stack exhaust (□). b) Temperature difference the inlet and out-let gases at the hot end and cold end of the HEX bundle, respectively. Current density was 0.2–0.35 A cm^{-2} during the measurements.

during the experiment. The heat transfer properties of the fuel heat exchanger cannot be evaluated reliably as the trace heating elements inflicted bias to the temperature measurements of the fuel and exhaust gases. Additionally, the vicinity of the air heat exchanger of considerably larger mass may have caused bias in the measurements as the heat exchangers were insulated under the same insulation layer. However, the heat exchanger operated through the entire test run and provided sufficient pre-heating of inlet fuel to operate the unit.

In atmospheric SOFC systems, the air blower is typically largest consumer of electric power among all auxiliary components [19]. Therefore, the characteristic backpressure of a SOFC system largely defines the parasitic power losses and the resulting decrease in the electric efficiency. The backpressure at different measurement positions at the air system *versus* the inlet air flow, along with the calculated power consumption of the air blower, are depicted in Figure 9. The power consumption of the air blower as a function of the air flow rate is calculated with fan efficiency of 25% and the total

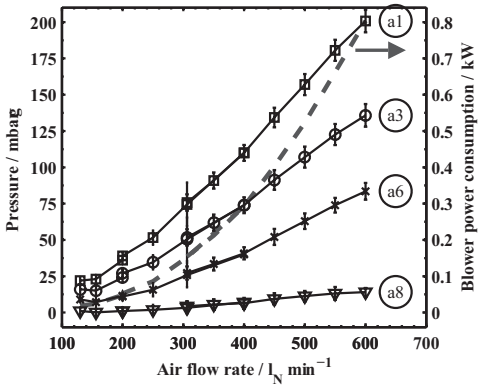

Fig. 9 Pressure at different measurement positions at air system (solid line and markers) and the power consumption of the blower (dashed line). Current density was 0.25–0.35 A cm^{-2} during the measurements. Error bars represent 2σ error.

backpressure of the system (a1, Figure 1). Constant total efficiency (electricity to pV-work) was assumed for the entire operating range of the blower. The power consumption of the blower is calculated to be 300 W at 400 l_N min^{-1}, which corresponds 26% of U_{AIR} at a current density of 0.35 A cm^{-2}. With $P_{el,stack}$ of 4.5–5 kW, the power consumption of the blower is below 10% of the gross stack electric power, and the decrease in the $\eta_{el,stack}$ is below 3%-units. The pressure loss of each component at the air system contributes to the total backpressure. With 400 l_N min^{-1}, the individual pressure losses of the hot and cold side of the heat exchanger bundle, and the stack are ~30 mbar. With this backpressure, the use of regular side-channel blowers is feasible as the parasitic power losses caused by the air blower remain below 300 W and the resulting decrease in the electrical efficiency is kept at an adequate level.

Two BoP -components, the power conversion unit and the afterburner, failed to operate as expected. The SOFC stack was connected to the electric grid with a power conversion unit whenever electric load was applied during the test run. A current setpoint was imposed on the power conversion unit, which limited the current density of the stack to the desired value. However, at maximum, half of the electricity produced by the stack could be supplied to the grid as the power conversion equipment caused an increasing voltage ripple on the stack at higher current levels. Therefore, the stack was loaded in parallel with the DC load to limit the current to the power conversion unit and to obtain high enough current densities for the test.

Cabling losses were 5–10%, calculated as loss of voltage between the stack end plates and the power conversion unit, and redesign of the current collection and cabling is required to decrease the losses. The conversion efficiency from DC input to AC output of the power conversion unit was ~70% with 2.5 kW input power. DC–DC converters that increased the DC voltage of the stack to 400 VDC for the inverter were the primary cause for the poor efficiency, having efficiency of ~80%. The low efficiency of the power conversion unit is partly explained by the use of regular off-the-shelf components that were not optimised for the low voltage and high current output of the stack. Significant improvements in the power conversion unit can be expected by utilising customised components.

Shortly after the stack assembly and system start-up, the burner failed to ignite and burn the anode off-gas from the stack. The failure was probably caused by condensation of liquid water to the surface of the catalysts during commissioning of the stack and the first thermal cycle. The condensed water rinsed away the catalytically active material, and no oxidation of fuel could occur in the afterburner. Prior to the long term testing, the afterburner was characterised in a separate test bench [24] and an endurance test of 1,000 h was conducted before assembling the burner to the demo unit. During the endurance test the burner showed no measurable decrease in performance. In the future experiments, a more robust afterburning catalyst tolerant to water condensation is needed or the condensation has to be prevented by redesigning the burner.

4 Conclusion

A SOFC demonstration unit was designed and constructed. The unit was operated with a planar SOFC stack for a total of over 7,000 h. During the test run the performance and durability of the stack and other BoP-components were assessed. Two components, the afterburner and the power conversion unit failed to operate as intended, but the performance of other components was satisfactory during the test run. The SOFC stack used in the system showed stable operation for long term testing and towards several shutdown situations, even with one cell in short-circuit.

The heat exchanger bundle at the air system operated with sufficient effectiveness to pre-heat the inlet air for stack operation. The total pressure losses at the air system were low enough to make use of regular side channel blowers feasible. At the fuel system, the combined effect of high heat loss and the use of trace heating prevented the assessing of the effectiveness of the heat exchanger. Nevertheless, the fuel heat exchanger was used successfully throughout the experiment and no distinct changes in the pressure loss or stack inlet temperature at the fuel side were observed. The operational characteristics of the reformer unit are assessed by comparison with thermodynamic equilibrium. A minor decrease in the DoR of the reformer was measured during the test run, but the change is not significant for system operation and was not observed to impede the performance of the stack.

The evolution of the voltage drop of the 5 kW power class stack used during the test run corresponds with the measurements conducted with similar short stacks. A period of large initial drop in voltage, followed by a period of nearly con-

stant voltage drop, is evident in the experimental results. Moreover, both the magnitude and time scale of these two phenomena match with the short stack experiments. It can, therefore, be concluded that the different system components, e.g. reformer or heat exchangers upstream of the stack, and varying operating conditions during the test run, did not cause a measurable increase in the inherent voltage degradation of the stack.

Acknowledgements

The authors would like to thank Wärtsilä Oyj, Automation Technology Laboratory of Helsinki University of Technology and Verteco Inc. for participating in the designing of the 5 kW SOFC unit. Forschunzentrum Jülich is gratefully acknowledged for providing and assembling the stacks for the unit. Dr L.G.J. (Bert) de Haart is acknowledged for his valuable input on operational issues with the stack. Mr. Reinhard Erben is thanked for his involvement in the stack assembly and instrumentation. Mr. Kari Koskela and Mr. Jorma Stick are specially acknowledged for their valuable effort in the construction of the unit. Funding for this study was obtained from FINSOFC and SofcPower projects. Finnish Funding Agency for Technology and Innovation in Finland (TEKES) as well as the companies that participated in the projects are gratefully acknowledged for their financial support.

List of Symbols

j	current density, A cm^{-2}
I_{stack}	total current of the stack, A
$P_{el,stack}$	gross DC electric power of the stack, $U_{stack}I_{stack}$, W
$\eta_{el,stack}$	gross DC electric efficiency of the stack, $\frac{P_{el,stack}}{\dot{n}_{NG}\Delta H_{NG,LHV}}$
$\Delta H_{NG,LHV}$	lower heating value for natural gas in Finland, 805.68 kJ mol^{-1}
T	temperature, °C
U	voltage, V
$\dot{n}$	molar flow rate, mol s^{-1}
NTP	normal temperature (0 °C) and pressure (101,325 Pa)
F	Faradys's constant (96,485 C mol^{-1})
G	conductance of a heat exchanger $\frac{\dot{n}(h_{cold,out}-h_{cold,in})}{\Delta T_{ln}}$, W K^{-1}
ΔT_{ln}	logarithmic mean temperature difference for a counter-flow heat exchanger $\frac{(T_{hot,out}-T_{cold,in})-(T_{hot,in}-T_{cold,out})}{\ln((T_{hot,out}-T_{cold,in})/(T_{hot,in}T_{cold,out}))}$, K
h	specific enthalpy or enthalpy increment, W mol^{-1} K^{-1}
U_{AIR}	air utilisation of the stack, $\frac{I_{stack}}{0.21\dot{n}_{AIR}4F}$
U_{FUEL}	fuel utilisation of the stack
Inlet O_2/C	air oxygen to fuel carbon ratio at the reformer inlet
Inlet H_2O/C	water to fuel carbon ratio at the reformer inlet
DoR	degree of pre-reforming of methane of the reformer $\frac{\dot{n}^{in}_{CH_4}-\dot{n}^{out}_{CH_4}}{\dot{n}^{in}_{CH_4}}$
σ	standard deviation

References

[1] L. Blum, H-P Buchkremer, R. W. Steinbrech, B. De Haart, Uwe Reisgen, R. Steinberger-Wilckens, Current Trends of SOFC Development at Forschungzentrum Juelich, Proc. 8th European SOFC Forum, Conference CD, **2008**, File No. B0306.

[2] E. Fontell, T. Kivisaari, N. Christiansen, J.-B. Hansen, J. Pålsson, *J. Power Sources* **2004**, *131*, 49.

[3] Y. Kayahara, M. Yoshida, Residential CHP Program by Osaka Gas Company and KYOCERA Corporation, *Proc. 8th European SOFC Forum*, Conference CD, **2008**, File No. B0304.

[4] N. Christiansen, J. B. Hansen, H. Holm-Larsen, M. Joergensen, L. T. Kuhn, P. V. Hendriksen, A. H. S. Linderoth, Solid Oxide Fuel Cell Research and Development at Topsoe Fuel cell A/S and Risoe/DTU, *Proc. 8th European SOFC Forum*, Conference CD, **2008**, File No. B0304.

[5] L. G. J. de Haart, J. Mougin, O. Posdziech, J. Kiviaho, N. H. Menzler, Stack Degradation in Dependence of Operation Parameters the Real-SOFC Sensitivity Analysis, Fuel Cells, **2009**, *9*, 794.

[6] E. Fontell, T. Hottinen, T. Lehtinen, Progress of the Wärtsilä Fuel Cell Program, *Proc. 8th European SOFC Forum*, Conference CD, **2008**, File No. B0406.

[7] T. Hottinen, T. Lehtinen, J. Hansen, E. Fontell, Operational Experiences from Wärtsilä 5 kW Test System with 4 SOFC Stacks, *Proc. 2nd European Fuel Cell Technology and Applications Conference*, **2007**, pp. 45–46 (EFC2007–39026).

[8] R. A. George, *J. Power Sources* **2000**, *86*, 131.

[9] S. Mukerjee, K. Haltiner, R. Kerr, L. Chick, V. Sprenkle, K. Meinhardt, C. Lu, Y. Kim, S. Weil, *ECS Trans.* **2007**, *7*, 59.

[10] J. Kiviaho, M. Halinen, M. Noponen, J. Saarinen, Finnish Platform for SOFC Research and Development, Fuel Cell Seminar 30, Conference CD, **2006**.

[11] A. Gubner, J. Saarinen, J. Ylijoki, D. Froning, A. Kind, M. Halinen, M. Noponen, J. Kiviaho, Dynamic Co-Simulation of Solid Oxide Fuel Cell (SOFC) and Balance of Plant (BoP) by Combining an SOFC Model with the

BoP-Modelling tool APROS, Proc. 7th European SOFC Forum, Conference CD, **2006**, File No. B092.
[12] T. Ollikainen, J. Saarinen, M. Halinen, T. Hottinen, M. Noponen, E. Fontell, J. Kiviaho, *ECS Trans.* **2007**, *7*, 1821.
[13] J. Saarinen, M. Halinen, A. Gubner, M. Noponen, J. Ylijoki, A. Kind, J. Kiviaho, Steady-State Simulation Study of Thermal Management of Planar SOFC Stack, Fuel Cell Seminar 30, Conference CD, **2006**.
[14] I. Vinke, R. Erben, R.-H. Song, J. Kiviaho, Installation and Operation of kW-Class Stacks from Jülich in External Laboratories, *Proc. 7th European SOFC Forum, Conference CD*, **2006**, File No. B036.
[15] R. Steinberger-Wilckens, I. C. Vinke, L. Blum, L. B. de Haart, J. Remmel, F. Tietz, W. Quadakkers, Progress in Stack Development at Forschungzentum Jülich, *Proc. 6th European SOFC Forum* **2004**, *1*, 11.
[16] J. J. Hartvigsen, S. Elangovan, A. Khandkar, System design, in: *Handbook of Fuel Cells Fundamentals, Technology and Applications, Vol. 4*, **2003**, pp. 1071–1085, ISBN: 0-471-49926-9.
[17] N. Dekker, J. Outweltjes, G. Rietveld, *ECS Trans.* **2007**, 7, pp. 1465.
[18] H. Timmermann, W. Sawady, D. Campbell, A. Weber, R. Reimert, E. Ivers-Tiffé, *J. Electrochem. Soc.* **2008**, *155*, B354.
[19] E. Riensche, U. Stimming, G. Unverzagt, *J. Power Sources* **1998**, *73*, 251.
[20] M. Noponen, M. Halinen, J. Kiviaho, J. Saarinen, *J. Fuel Cell Sci. Tech.* **2006**, *3*, 444.
[21] M. Noponen, M. Halinen, J. Saarinen, J. Kiviaho, *ECS Trans.* **2007**, *5*, 545.
[22] M. Halinen, M. Noponen, J. Saarinen, J. Kiviaho, Characterization and Control of a Autothermal Reformer for SOFC Applications, Fuel Cell Seminar 30, Conference CD, **2006**.
[23] L. Blum, H.-P. Buchkremer, S. Gross, A. Gubner, L. B. deHaart, H. Nabielek, W. Quadakkers, U. Reisgen, M. J. Smith, R. Steinberger-Wilckens, R. Steinbrech, F. Tietz, I. Vinke, **2007**, Fuel Cells 3, pp. 204–210.
[24] J. Saarinen, M. Halinen, J. Ylijoki, M. Noponen, P. Simell, J. Kiviaho, *J. Fuel Cell Sci. Tech.* **2007**, *4*, 397.
[25] D. Goodwin, An open-source, extensible software suite for cvd process simulation, Proceedings of CVD XVI and EuroCVD 14, The Electrochemical Society PV 2003-2008, **2003**, pp. 155–162, see also http://www.cantera.org/.
[26] G. Smith, GRI-MECH 3.0, http://www.me.berkeley.edu/gri_mech/.
[27] R. Peters, E. Riensche, P. Cremer, *J. Power Sources* **2000**, *86*, 432.

PUBLICATION [P2]

Performance of a 10 kW SOFC Demonstration Unit

In: ECS Transactions 35 (1), pp. 113-120

ECS Transactions, 35 (1) 113-120 (2011)
10.1149/1.3569985 ©The Electrochemical Society

Performance of a 10 kW SOFC Demonstration Unit

M. Halinen[a], M. Rautanen[a], J. Saarinen[a], J. Pennanen[a], A. Pohjoranta[a], J. Kiviaho[a]
M. Pastula[b], B. Nuttall[b], C. Rankin[b], B. Borglum[b]

[a] VTT Technical Research Centre of Finland, Espoo, Finland
[b] Versa Power Systems Ltd., Calgary, AB, Canada

Experimental results of the performance of a solid oxide fuel cell (SOFC) unit are presented. The unit was designed, manufactured and tested at the VTT Technical Research Centre of Finland. The 10 kW power class SOFC stack and stack module were designed and manufactured by Versa Power Systems (VPS). A successful commissioning test of the unit was conducted in 2010. Long term testing of the unit was started in November 2010. The unit has been operated with natural gas for over 1500 hours supplying electricity to the local grid. The unit has shown robust and uninterrupted performance. Stack DC efficiency of 60% and system net AC efficiency of 43% has been measured during the operation.

Introduction

The high electrical efficiency obtained with SOFC-based power plants is the key benefit of the SOFC technology when competing in the power production market against conventional production technologies. However, a sufficiently long lifetime of both the SOFC stacks, as well as the necessary Balance of Plant (BoP) components, is an essential condition for the commercialization of SOFC power plants. With no large-scale production of such plants, the lifetime and performance of different system components as well as the SOFC stacks operated at in-system conditions are currently not well established. Furthermore, building large 100 kW to MW range SOFC power systems requires developing large-size SOFC stacks as well as developing the techniques for integrating such stacks with the BoP components. In order to assess the multiple technical challenges related to such SOFC power plants, it is necessary to design, build and experiment on complete SOFC demonstration systems. This paper presents the experimental results of the performance of such a SOFC demonstration unit.

Experimental

The aim of the system design was to realize a grid-connected, single stack SOFC system with a high electrical efficiency while having no external steam or heat supplied to the system. The targeted stack DC-efficiency and system net AC-efficiency at the nominal operating point were 60% and 50%, respectively. The system was designed around a 10 kW planar SOFC stack produced by VPS. An anode recycle loop was included to enable water independent operation for the fuel system. The unit consists of two interconnected modules, the balance of plant (BoP) and the stack module (1). A

power conversion unit converts the stack DC power to AC power and supplies it to the electric grid (2,3). A simplified process flow chart is shown in Figure 1 and a picture of the complete system in Figure 2.

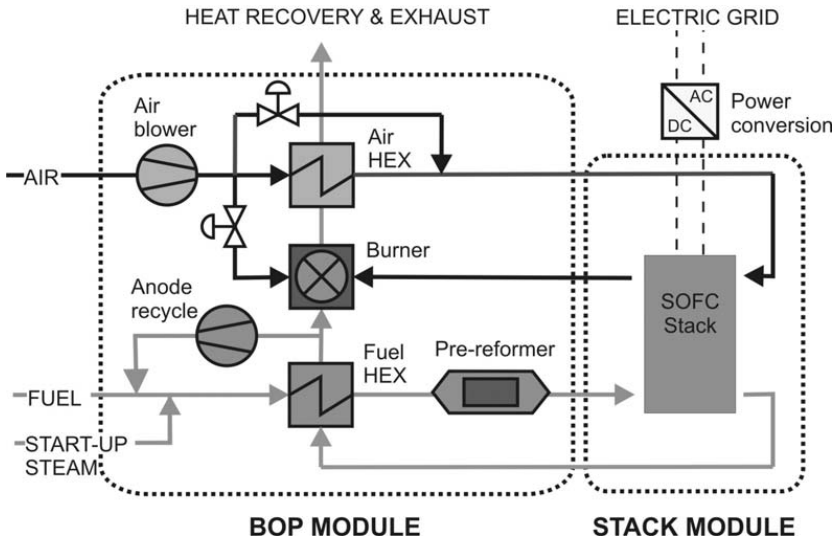

Figure 1. Simplified process flow diagram of the SOFC demonstration unit.

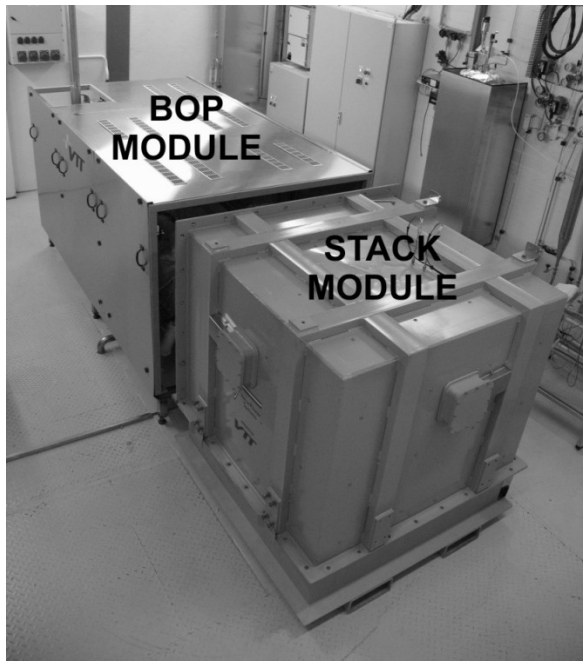

Figure 2. 10 kW SOFC demonstration unit. Physical dimensions are ca. 4 m x 1.5 m x 1.5 m (L x W x H).

The stack module contains the stack and its compression system, thermal insulation, electrical start-up heater and stack-related instrumentation. The stack consists of 64 anode-supported cells each having an active area of 550 cm^2. The internal flow configuration of the stack is cross-flow. The cathode inlet is open to the module internals, and therefore, the inlet air circulates inside the module before entering the stack.

The BoP-module contains the air and fuel processing systems. An air blower draws ambient air into the system and feeds the main flow through a heat exchanger and further into the stack module where it enters the stack cathode. From the cathode, the exhaust air is fed to a catalytic burner which helps in preheating the cathode inlet air. Through a control valve, the air blower also supplies additional cold air to the burner when necessary to prevent it from overheating. Part of the incoming fresh air can also be fed through a heat exchanger by-pass line. This by-pass can be tuned to achieve the desired thermal operating point for the stack. Thermal insulation of the BoP-module is such that all the components and pipelines are independently insulated.

The natural gas fed in to the fuel system is mixed with the recycled anode exhaust gas and heated in the fuel heat exchanger before passing it to the pre-reformer. The pre-reformer is based on a commercial noble metal catalyst. After the pre-reformer, the fuel enters the stack module and reacts in the stack anode. Approximately 12% of the methane present in the fuel is reformed in the pre-reformer. The rest is carried on to the stack, where it is reformed internally. The anode exhaust gas is fed through the heat exchanger to pre-heat the fresh fuel. An anode gas recycle blower draws part of the anode exhaust gas back to the fresh fuel side of the heat exchanger. The rest of the fuel is fed to a catalytic burner to help pre-heat the air.

The unit is designed for unattended operation, and for this purpose a control system has been implemented in an industrial PLC environment. The primary reference variable for the overall system control is the stack DC current, which is set by the system operator. A variety of closed- and open-loop controls are utilized to achieve automated operation and to keep the stack and BoP –components within predefined operating boundaries. Safety logics have been implemented within the control system that monitors the critical process parameters and initiates various levels of shutdown sequences if needed.

Results

Overview of the Test Runs

A successful commissioning test of the demo unit was conducted in April through June 2010 to validate the system design, layout and controls. For this purpose, a previously used stack that had already reached its end-of-life voltage was used. In total, approximately 1000 hours of operation was accumulated during commissioning, and current was drawn from the stack for 720 hours. Thermally self-sustained operation i.e. electric heaters off, as well as water independent operation via anode gas recycle alone i.e. external steam supply off, was accomplished. The control system worked reliably for the entire duration of the commissioning test demonstrating stable and robust operation of the unit. (1)

A long term test with a new stack with beginning-of-life voltage was started in November 2010. The purpose of the long term testing is to optimize the operating conditions to yield maximum electrical efficiency and to study the durability of the SOFC stack and the BoP –components. As of January 4, 2011, the unit has been operated for over 1500 hours. Operation of the unit has been robust with no control disturbances or component failures (Figure 3).

The test run was initiated by heating the system with electric heaters up to operating temperature while flushing the fuel system and stack anode with a hydrogen-nitrogen purge gas mixture. Once the operating temperature was reached the natural gas supply and start-up steam supply were started and the stack current was ramped up to 135 A with 5 A min^{-1}. During the first 500 hours of the test, the unit was operated with varying stack current to measure the part-load operating characteristics of the stack and the BoP-components. The nominal operating point of 200 A stack current, 20% air utilization and 80% system fuel utilization was reached at 505 hours after the test start. At stack currents in excess of 115 A, the unit has relied only on anode gas recycle and no additional steam has been fed to the system. Thermally self-sustained operation with the electric start-up heater switched off was achieved with a stack current of 160 A or higher. With a lower stack current (135-160 A) the start-up heater power ranged from 150 to 400 W.

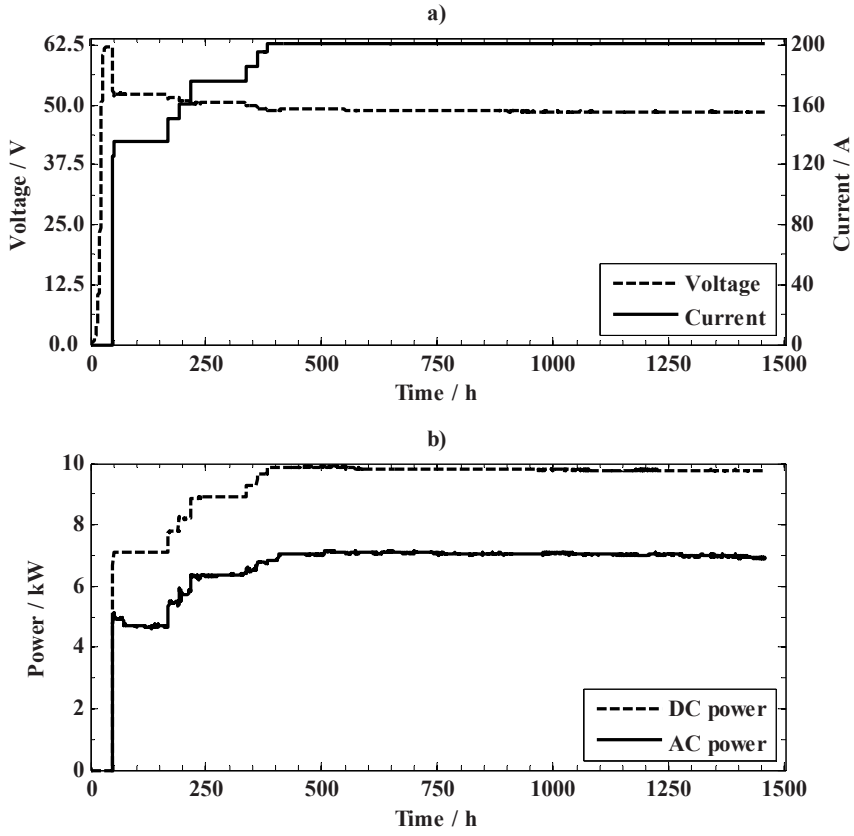

Figure 3. a) DC current and voltage of the SOFC stack and b) the stack DC and unit net AC power output to the grid during the test.

System Performance at Nominal Operating Conditions

At nominal operating conditions, the stack DC efficiency was 60%, based on the lower heating value of natural gas, and DC power output was 9.8 kW. Due to parasitic power consumption of the air and recycle blowers, and the losses in the current collection and DC-AC power conversion, the resulting power output to the electric grid was lower (Figure 4). The net AC efficiency was 43% and the electric power output to the grid was 7.1 kW.

The overall design target of 50% net AC efficiency was not reached due to higher losses than anticipated e.g. in the DC current collection cabling and in the power conversion equipment. However, it is possible to significantly cut down the current collection losses by shortening the current cables and by reducing both bulk resistivity and the contact losses in the hot environment of the stack module as well as the contact losses at several locations in the ambient environment. Furthermore, the power conversion unit (PCU) used for the test run has an overall efficiency of 88%, which is lower than the projected final design value (>90%). By decreasing the current collection losses from 470 W to 150 W, and by increasing the PCU efficiency from 88% to 92%, the net AC efficiency could be improved up to 47%.

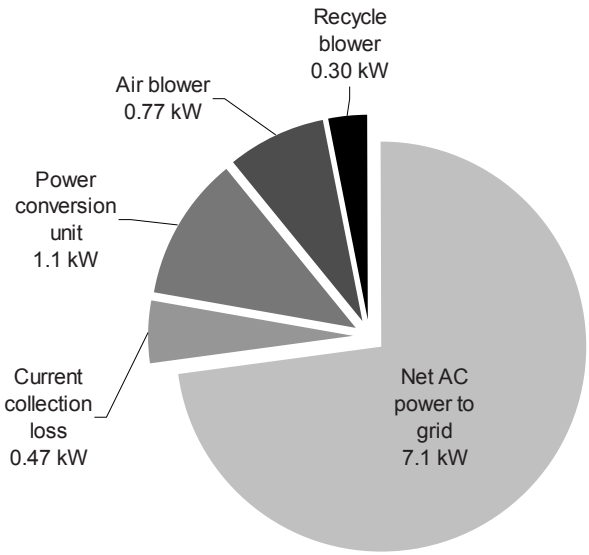

Figure 4. Power conversion and parasitic losses from the stack DC-power (9.8 kW) at nominal operating conditions.

System Performance at Part-load

Operating under partial load generally decreases the system efficiency. Demonstrated part-load operating characteristics and the effect of system controls to the unit and stack efficiency are depicted in Figure 5. It can be seen that though the stack voltage is higher when less current is drawn from the stack (Fig. 5a), the part-load operation results in decreased efficiency of both the stack and the system (Fig. 5b). This is because lower

system fuel utilization rate is used at part load (Fig. 5c) in order to increase the operating temperature of the catalytic burner. Higher burner temperature provides more efficient cathode air pre-heating, and increases the stack module air inlet temperature. (Fig. 5d). At part-load, less heat is generated in the stack proportionally to the heat losses, and higher stack module air inlet temperature is beneficial to maintain thermally self-sustained operation.

Part load efficiency of the system has not yet been optimized, and electrical efficiency could likely be improved by making adjustments to increase system fuel utilization and decrease cathode air flow at part load.

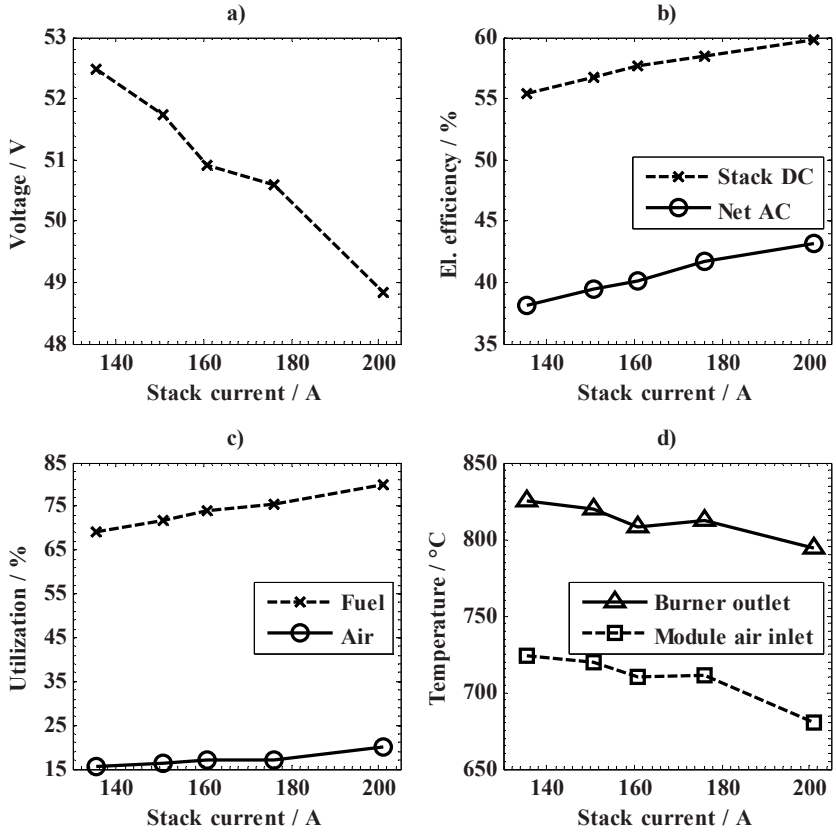

Figure 5. Performance of the unit at part-load. a) Stack voltage, b) DC efficiency of the stack and system net AC efficiency, c) System fuel utilization and air utilization, and d) Stack module air inlet temperature and burner outlet temperature.

Sensitivity to Process Parameters

In order to achieve higher system electrical efficiency, a series of experiments were conducted to investigate the effect of different process control parameters to the power output and electrical efficiency. The control parameters under investigation were the system fuel utilization, recycle ratio and air utilization, where the flow rates of natural gas,

recycle gas and cathode air were varied, respectively. To examine the effect of air utilization, the cathode air flow rate was varied between 1060 and 1250 l_N min^{-1}, corresponding to air utilization rates between of 17% and 20%, respectively. The stack current was kept constant at 200 A and the system fuel utilization rate at 80%. The experiment results are depicted in Figure 6.

Due to back-pressure characteristics of the system components and the operational characteristics of the air blower, the parasitic power consumption of the blower was decreased 1025 W to 790 W by lowering the air flow rate. Concurrently the stack voltage was increased by 0.2 V (~3 mV/cell) with smaller air flow rate, due to slightly increased stack temperature. However, the parasitic power consumption of the blower dominates the overall effect on the power output and efficiency (Figure 6). The net AC power output and the net AC electrical efficiency increased by 270 W and 1.6 %-units, respectively.

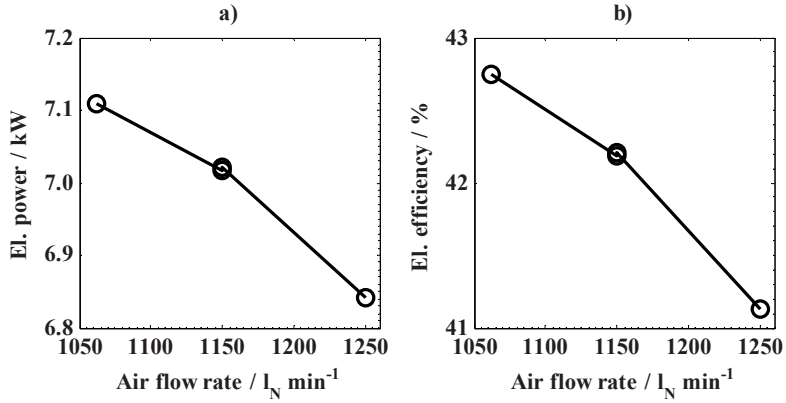

Figure 6. Effect of air flow rate to the a) net AC power output to the grid and b) net AC efficiency. Stack current = 200 A, System fuel utilization = 80%.

Conclusions and Future Work

The SOFC demo unit has been tested successfully at nominal operating conditions as well as under partial load. A DC power output of 9.8 kW with 60% gross DC efficiency was achieved for the SOFC stack. The corresponding values for the unit net AC power and efficiency were 7.1 kW and 43%, respectively. Operation of the unit has been robust for over 1500 hours without any control disturbances or component failures. The effects of several process parameters were investigated to optimize the electrical efficiency and power output of the unit. The experiments have proceeded to long-term testing where the purpose is to study the durability of the SOFC stack and the BoP –components during operation over several thousands of hours.

Acknowledgments

Funding for this study was obtained through the SofcPower project. The Finnish Funding Agency for Technology and Innovation in Finland (TEKES) as well as the

companies participating in the project are gratefully acknowledged for their financial support. Project partners from the Lappeenranta University of Technology (LUT) are acknowledged for the design, manufacturing and testing of the power conversion unit. The Aalto University Department of Engineering Design and Production is acknowledged for their participation in the mechanical design of the BoP-module. Mr. Kari Koskela and Mr. Kai Nurminen from VTT are thanked for their contribution in the construction of the demo unit.

References

1. M. Halinen, J. Saarinen, M. Rautanen, J. Pennanen, J. Kiviaho, M. Pastula, T. Machacek, B. Nuttall and B. Borglum, *Fuel Cell Seminar 2010*, Conference CD, **HRD34-1** (2010).
2. V. Väisänen, J. Hiltunen, T. Riipinen, and P. Silventoinen, *submitted for publication*, (2010).
3. V. Väisänen, T. Riipinen and P. Silventoinen, *IEEE Trans. Pow. Eletrc.* **25**(8), 2033 (2010).

PUBLICATION [P3]

Effect of Anode off-gas Recycling on Reforming of Natural Gas for Solid Oxide Fuel Cell Systems

In: Fuel Cells 12 (5), pp. 754-760

ORIGINAL RESEARCH PAPER

Fuel Cells DOI: 10.1002/fuce.201200047

Effect of Anode off-gas Recycling on Reforming of Natural Gas for Solid Oxide Fuel Cell Systems

M. Halinen[1]*, O. Thomann[1], J. Kiviaho[1]

[1] VTT Technical Research Centre of Finland, P.O. Box 1000, FI-02044 VTT, Espoo, Finland

Received March 26, 2012; accepted June 08, 2012

Abstract

The effect of anode off-gas recycling (AOGR) on the characteristic performance of a natural gas reformer equipped with a precious metal catalyst is investigated experimentally. The reformer is operated both with synthetic AOGR gas and in steam reforming (SR) conditions. The characteristic performance in SR and AOGR mode are compared with equilibrium, and it is found that equilibrium is more readily achieved in AOGR mode. The reformer is used for extended periods of time (100–1,000 h) in conditions where carbon formation is thermodynamically possible to measure any changes in characteristic performance. No significant change in the performance is observed due to carbon formation or catalyst deactivation. The reformer could be successfully implemented in a 10 kW SOFC system with an anode off-gas recycling loop.

Keywords: Anode Off-gas Recycling, Natural Gas, Precious Metal Catalyst, Reforming, Solid Oxide Fuel Cell, Supported Catalyst

1 Introduction

Solid oxide fuel cells (SOFCs) are considered as a very promising technology in the future of energy production due to their high electrical efficiency. Additionally, SOFCs offer fuel flexibility and the fuel processing is simpler compared to fuel cells operating at lower temperature [1–3]. Fuel processing is simplified by the possibility to use hydrogen, carbon monoxide, and methane as a fuel and by the availability of recoverable heat for steam reforming (SR).

It is well known that SR of hydrocarbon fuel, typically natural gas, can be done internally in the SOFC stack [3]. This approach is advantageous due to the highly endothermal reforming reactions with hydrocarbon fuel which reduce the need for stack cooling with excess cathode air, decreases the parasitic loss caused by air blowers and can thus increase the electrical efficiency of the system. However, the temperature gradient caused by internal reforming can lead to excessive thermal stress which is detrimental for the lifetime of the stack components [4]. Moreover, there is a risk of carbon formation at the anode which can lead to a loss of performance and ultimately destruction of the stack [5, 6]. Lastly, internal reforming can decrease locally stack temperature and thus voltage resulting in sub-optimal operation. Therefore, pre-reforming of the hydrocarbon fuels is typically required in SOFC systems to mitigate these effects. The fuel is partially converted to syngas composed of methane, hydrogen, steam, carbon monoxide, and carbon dioxide in a reformer upstream of the stack. The optimum ratio between pre-reforming and internal reforming is dependent on the SOFC stack and system design, and selected operating parameters.

Recycling the hot anode off-gas to the reformer inlet is desirable in SOFC systems to provide steam for fuel reforming, since this can simplify the system design by eliminating the need of external water supply and steam generator during operation [7]. Additionally, recycling unused fuel back to the SOFC inlet can increase the electrical efficiency, since the system inlet fuel flow rate can be decreased and the system fuel utilization increased [8, 9]. Concurrently, the stack fuel utilization remains low, which has been shown to be beneficial for the lifetime of the stack [10].

Sufficient recycling ratio of anode off-gas is required to keep the SOFC, reformer, and other fuel system components free of carbon formation. It is a common engineering practice in SOFC system design to predict the gas composition, temperature, and possibility of carbon formation in a fuel reformer using thermodynamic equilibrium calculation. However, the activity of the reforming catalyst dictates both the charac-

[*] *Corresponding author, matias.halinen@vtt.fi*

teristic performance of the catalyst, and if carbon formation actually occurs to the extent that would threaten the system operation. Therefore, experimental investigation of the catalyst, reformer, and the whole fuel processing system at SOFC system relevant conditions is needed to assess the characteristic performance, measure possible deviations from the equilibrium, and to map the safe operating region without carbon formation.

Anode off-gas recycling (AOGR) has proven to be challenging to implement in actual systems due to various technical challenges, e.g., providing the motive force for recycling gas at high temperature, and identifying the suitable reforming catalyst with reliable and durable performance. Recycling blowers and ejectors suitable for SOFC system use cannot be found off-the-shelf and are still in the development phase [8]. SR of natural gas is traditionally performed with nickel-based catalyst and the effect of AOGR on such a catalyst has been previously reported in the literature. Peters et al. reported that AOGR caused a decrease of activity of a nickel-based catalyst which resulted in a decreased conversion of hydrocarbons [11]. On the other hand, Nummela and Noponen reported that AOGR had no negative effect on the performance of another pre-reformer nickel catalyst [12].

Little experimental data can be found in the literature on the effects of AOGR on a precious metal catalyst using natural gas as a fuel. Precious metal catalysts have been less investigated due to their higher price, despite having potential for higher resistance against sulfur poisoning, carbon formation, and ageing [13]. Powell et al. reported using a precious metal catalyst with natural gas in an SOFC system containing a recycling loop, but the study did not include the evaluation of the reformer performance with different operating conditions [14]. Precious metal catalyst was also used by Dietrich et al. who implemented successfully an anode off-gas recycling loop in an SOFC test setup using propane [8]. The reformer was used at high temperature (>800 °C) and at such high temperatures almost all hydrocarbons are reformed to syngas, and little is left for internal reforming reactions in the SOFC stack. In order to maintain the benefits of internal reforming in an SOFC system, it is relevant to strive for lower operating temperature for the reformer, where the conversion of methane is not complete, i.e., at temperatures between 500 and 700 °C.

This study contributes to the field of fuel processing in SOFC systems by assessing the characteristic performance of a precious metal-based reformer using natural gas in AOGR mode. Performance of the reformer in AOGR conditions is compared against SR conditions at an inlet temperature of 600 °C. Additionally, the effect of varying the recycling ratio is evaluated to determine its effect on the characteristic performance, and to identify the minimum recycling ratio that can be used safely in an SOFC system, i.e., corresponding to carbon formation-free operation. Results of this work led to the successful implementation of an anode off-gas recycling loop in a 10 kW SOFC demonstration unit, where the system is operated at nominal conditions without external water supply, and the motive force for AOGR is achieved by a recycling blower [15].

2 Experimental

2.1 Experiment Setup

The experimental setup includes a natural gas reformer and a gas analysis system. The reformer unit consists of mass flow controllers for natural gas (0–10.0 ± 0.2 L_N min^{-1}), carbon monoxide (0–1.50 ± 0.03 L_N min^{-1}), carbon dioxide (0–10.0 ± 0.2 L_N min^{-1}), hydrogen (0–5.0 ± 0.1 L_N min^{-1}), water (0–10.0 ± 0.1 g min^{-1}), nitrogen (0–10.0 ± 0.2 L_N min^{-1}), and air (0–10.0 ± 0.2 L_N min^{-1}), sulfur removal reactor filled with sulfur adsorbent (Süd-Chemie), water evaporator and mixer (CEM-303, Bronkhorst), superheater, reactor chamber equipped with a commercially available precious metal monolithic catalyst (Süd-Chemie), a particle filter and an heat exchanger (Alfa-Laval) to condensate water in the exhaust gas (Figure 1). Similar reformer catalyst has been used previously at VTT in a 5 kW SOFC demonstration unit [16]. Temperature of the process gas was measured after the evaporator (TI1 in Figure 1), at the reactor inlet (TI2), from the leading surface of the catalyst (TI3), at the center of the catalyst (TI4), from the trailing surface of the catalyst (TI5), at the reactor outlet (TI6), and after the filter (TI7). Pressure was measured before the evaporator unit (PI1), before the reactor (PI2), after the reactor (PI3), and after the particle filter (PI4). Reformer exhaust gas was analyzed with an online gas analyzer (Sick S710 series) and with gas chromatographs (Agilent 6890 N, Agilent 6850, and HP 5890 Series II).

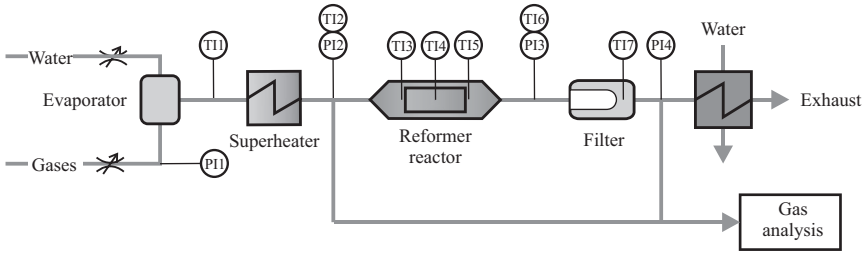

Fig. 1 Principle layout of the test equipment.

The natural gas used in Finland is of Russian origin and contains a high content of methane (ca. 98%) and low amount of higher hydrocarbon (typically 7,000 ppm of ethane, 2,000 ppm of propane, 680 ppm of butane, and trace amounts of pentane and hexane). Carbon monoxide (>99% purity), carbon dioxide (>99.7% purity), and hydrogen (>99.5% purity) were supplied from gas bottles and purified water (Millipore Elix system) was used to create the synthetic recycling gas mixture needed in the experiments.

Electric trace heating elements were used before and after the reactor to prevent cooling of the gas. The heat used in the SR reaction was provided by superheating the inlet gases with electric heaters. In order to achieve operation conditions as close to adiabatic as possible, the reactor was carefully insulated and an electric heater was enclosed around the insulation layer. The reactor and the catalyst were kept close to adiabatic conditions during the experiments, and the heating element around the reactor insulation was used only to minimize the heat losses through the inner insulation layer.

A filter thimble made of micro-quartz was installed in a metallic casing after the reactor. The filter was used to increase the probability to identify carbon formation in the reformer during the experiment. Although carbon can deposit at the surface of the catalyst, part of the carbon containing particles may be carried from the reactor downstream. The particles can be accumulated in the filter thimble gradually obstructing the gas flow. This would result as a measurable pressure increase before the filter and could be used to identify carbon formation in the reformer.

2.2 Experiment Conditions

In order to assess how the use of AOGR affects the performance of the reformer, the reformer was used both in AOGR mode and SR mode with an inlet temperature of 600 °C. The experiments with recycling gas were conducted by supplying a synthetic gas mixture. The AOGR gas mixture corresponds to the composition of a reformer inlet gas, when a varying fraction of the anode exhaust gases are recycled back to the inlet of the reformer and mixed with natural gas. The inlet gas composition and the gas hourly space velocity (GHSV) of the catalyst at different experimental conditions are given in Table 1.

The gas composition given in Table 1 was calculated prior to the experiments on the basis of equilibrated gas with an in-house developed code [9]. Since the results of this study were meant to be used to build a fuel processing unit of an SOFC demonstration unit [15], the experimental conditions given in Table 1 were constrained by a set of pre-defined boundary conditions for that specific system at nominal operating conditions. The reformer inlet temperature was defined to be ca. 600 °C due to heat exchanger present in the fuel system to pre-heat the inlet gas. Constant stack fuel utilization (FU_{SOFC} = 0.6), stack outlet temperature (T = 700 °C) and electric current for the SOFC were used in the calculations.

In an SOFC system, the reformer GHSV should be as high as possible to decrease the size of the reformer reactor, the catalyst and by that the amount of expensive catalytic material. Concurrently, the GHSV should be limited to a value where there is still sufficient catalytic activity to achieve equilibrium for the reformer outlet gas and the pressure drop at the reformer is limited. A GHSV value of ca. 20,000 h^{-1} with recycling ratio of 0.5 was selected as a reference condition for this study. GHSV was allowed to vary according to recycling ratio and other parameters to observe the effect on the reformer performance. The GHSV of the reformer catalyst increases with the recycling ratio which means that the residence time of the gas in the reformer reactor becomes shorter (Figure 2, left). Moreover, since the stack fuel utilization is kept constant in the calculations, less fuel is fed to the reformer when the recycling ratio is increased (Figure 2, right).

Additionally, the atomic oxygen-to-carbon ratio (O/C) of the gas and the conversion of methane at equilibrium are provided in Table 1. In AOGR mode, the O/C increases with the recycling ratio since more oxygen containing species of the anode off-gas are fed back to the reformer inlet. The conversion of methane at equilibrium is calculated for an adiabatic reactor with an inlet temperature of 600 °C. It should be noted that in AOGR mode equilibrium conversion of methane is generally lower compared to SR mode. However,

Table 1 Experimental conditions in SR and AOGR modes.

	Inlet gas composition (vol%)									
	H_2O/C	Recycling ratio	GHSV (h^{-1})	Natural gas	CO	CO_2	H_2	H_2O	O/C	Methane conversion (%)
	2.5	–	21,896	28.6	0.0	0.0	0.0	71.4	2.50	17
SR	2	–	18,781	33.3	0.0	0.0	0.0	66.7	2.00	15
	1.5	–	15,676	40.0	0.0	0.0	0.0	60.0	1.50	13
		0.2	10,209	56.7	5.5	8.8	14.1	14.8	0.53	5
		0.28	12,118	46.0	6.4	11.6	16.5	19.5	0.77	5
		0.36	14,470	37.1	6.9	14.0	17.9	24.0	1.02	6
		0.4	15,760	33.3	6.8	15.3	18.1	26.4	1.15	7
AOGR		0.5	19,974	25.0	6.7	18.3	17.9	32.2	1.51	9
		0.55	22,707	21.5	6.4	19.8	17.4	35.0	1.70	11
		0.6	26,053	18.2	6.0	21.2	16.5	38.0	1.90	13
		0.65	30,286	15.3	5.5	22.7	15.4	41.1	2.12	16
		0.7	35,833	12.5	5.0	24.1	14.1	44.3	2.34	19

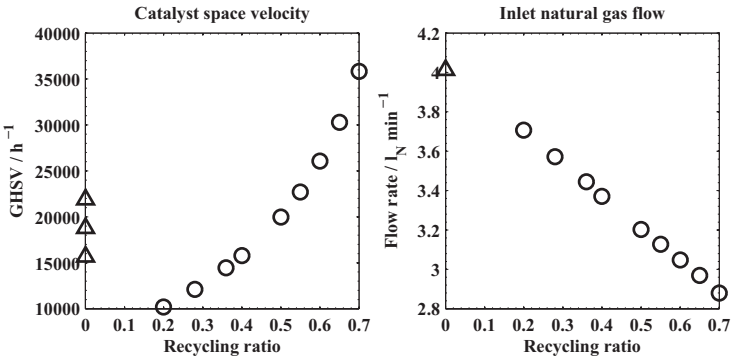

Fig. 2 The gas hourly space velocity (GHSV) of the reformer catalyst and the inlet natural gas flow rate in SR (△) and AOGR (○) modes.

above recycling ratio of ca. 0.30 the amount of methane in the reformer outlet gas becomes lower in AOGR mode than SR mode since the inlet natural gas flow rate decreases with recycling ratio (Figure 2, right). Thus, with recycling ratio above 0.30, less internal reforming would occur in the SOFC stack in AOGR than in SR mode.

The temperature limit of carbon formation in AOGR mode was calculated using HSC 6.1 [17] software to assess which experimental conditions could potentially lead to carbon formation in the reformer. According to the equilibrium calculations, the risk of carbon formation becomes more severe with lower recycling ratios (Figure 3). This is due to the lower oxygen-to-carbon ratio of the inlet gas, *i.e.*, with lower recycling ratios, less steam and other oxygen containing species are recycled back to the system inlet. With recycling ratio below 0.5, the temperature limit of carbon formation is already above the typical operating temperatures of anode supported SOFCs (above 700 °C). On the other hand, reformer can be operated at lower temperatures, e.g., 500–600 °C depending on the system design, and therefore is more prone to carbon formation since thermodynamics predict an increased risk of carbon formation for decreasing temperature.

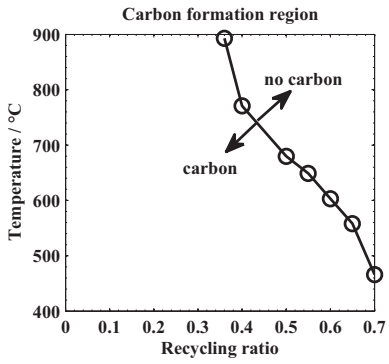

Fig. 3 Calculated temperature limit of carbon formation in AOGR mode.

To assess the characteristic performance of the reformer in AORG and SR modes the experimental results from gas analysis and the temperature measurement at the trailing edge of the catalyst were compared to the thermodynamic equilibrium at corresponding conditions. The equilibrium temperature and the composition of the reformate gas was calculated with Cantera toolbox [18] using GRI-Mech 3.0 reactions developed for natural gas combustion [19]. Equilibrium was solved for an adiabatic system, where the total enthalpy and pressure between reactants and products was kept constant, i.e., the total enthalpy of the inlet gases equals to the total enthalpy of the outlet gases and the sum of reaction enthalpies. Temperature measurement at the reactor inlet and measurements from mass flow controllers were used to define the inlet gas mixture temperature and composition for the calculations.

3 Results and Discussion

3.1 Performance of the Reformer in SR and AOGR Modes

The total duration of the experiment was over 2,500 h. During that time the reformer was used with a set of predefined operating conditions in SR and AOGR modes (Table 1). In order to achieve steady-state results, the reformer was left to stabilize for at least 24 h before each measurement. The measured inlet and outlet temperature, and the calculated reformer outlet temperature at equilibrium with different operating conditions are depicted in Figure 4. It can be seen that higher reformer outlet temperature can be achieved in AOGR mode than in SR mode. The measured and calculated equilibrium temperatures at reformer outlet correspond well in AOGR mode, where the difference between measured and calculated temperature is below 13 °C with every condition. However, in SR mode larger deviation exists between the measured and equilibrium outlet temperature, where the difference is 30–43 °C.

The measured and calculated molar fractions of methane and hydrogen in the reformer outlet gas are presented in Figure 5. The molar fractions are given on dry basis. Similarly to the reformer outlet temperature (Figure 4), there is a larger deviation between the measured and calculated values in SR than in AOGR mode. The difference between the values in SR mode cannot be explained only by the uncertainty related to the gas analysis (ca. 4% of the measured value).

Since both the outlet temperature and mole fraction of methane are higher than corresponding equilibrium values, kinetics are limiting the extent of the SR reaction. This indicates that either the space velocity should be decreased or the inlet temperature should be increased to achieve thermodynamic equilibrium. In AOGR mode and the same reactor inlet

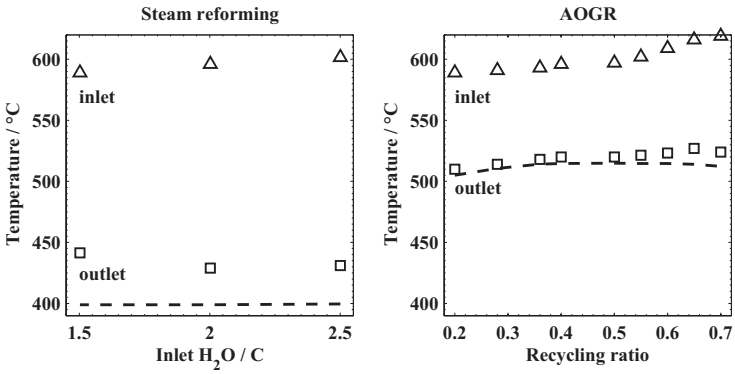

Fig. 4 Inlet and outlet temperature of the reformer in SR and AOGR modes. △: measured inlet temperature, □: measured outlet temperature, dashed line: calculated equilibrium outlet temperature.

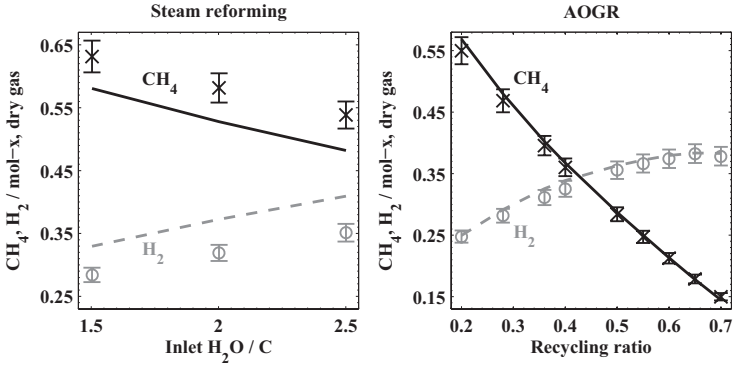

Fig. 5 Molar fraction of methane and hydrogen at reformer outlet with varying SR and AOGR conditions. Measured values are x: methane and ○: hydrogen. Calculated equilibrium values are solid line: methane and dashed line: hydrogen.

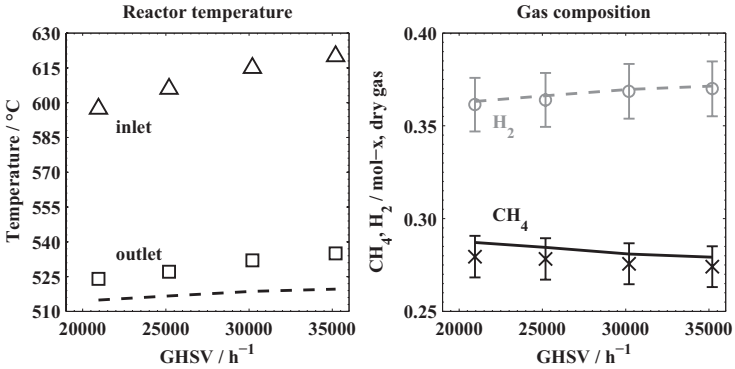

Fig. 6 Inlet and outlet temperature of the reformer operating in AOGR mode (left) and molar fraction of methane and hydrogen at the reformer outlet (right) with varying GHSV at recycling ratio of 0.5. Measured values are △: inlet temperature, □: outlet temperature, x: methane, and ○: hydrogen. Calculated equilibrium values are presented with lines.

temperature at 600 °C, the measured values match well with the calculated values. Equilibrium is reached regardless of the recycling ratio which shows good characteristic performance of the reformer in AOGR mode.

The difference in behavior of the reformer in SR and AOGR mode with respect to achieving equilibrium could be explained by the lower fuel inlet flow rate in recycling condition (e.g., 3.2 L_N min^{-1} of natural gas for a recycling ratio of 0.5) compared to SR condition (4 L_N min^{-1}, see Figure 2). In order to investigate this reason, experiments were conducted in AOGR mode (recycling ratio 0.5) with varying space velocity and thus fuel inlet flow rate. The flow rate of gases was increased to the maximum that was possible with the test equipment. The space velocity and the natural gas flow rate were increased up to 35,000 h^{-1} and 5.4 L_N min^{-1}, respectively. The results depicted in Figure 6 show that there is no increasing deviation between experimental and equilibrium values for temperatures and gas composition. Therefore, it can be concluded that some other rate limiting phenomena are preventing the achievement of equilibrium condition in the SR conditions tested. Additionally, these results show that relatively high space velocity can be achieved using this type of precious metal based catalyst in AOGR mode. As a comparison, nickel-based catalyst have been used at much lower space velocity in the range of 2,000–6,000 h^{-1} [12].

3.2 Performance of the Reformer in Carbon Formation Prone Conditions

Periodically, the reformer was used in certain AOGR conditions for a much longer time to observe any changes in performance of the reformer due to carbon formation and accumulation in the catalyst, or due to other catalyst deactivation processes. The longest hold period used in this study was 1,000 h. In addition to the recycling ratio, the reformer reactor inlet temperature and/or space velocity was varied for selected experiment conditions to see any short term changes in the performance (Table 2). The primary characteristic performance measurements that were monitored during these extended holds were the reformer outlet gas composition, gas temperature, and pressure drop over the catalyst and filter. Additionally, after each extended hold period, the entire test equipment was flushed with nitrogen and air to

Table 2 Operating conditions during extended holds.

Hold no.	Recycling ratio	Inlet temperature (°C)	GHSV (h^{-1})	Hold time (h)
1	0.60	609	26,053	122
2	0.50	597	19,979	121
3	0.50	598	19,965	117
4	0.50	513	19,981	67
5	0.50	600	19,981	1,000
6	0.20	589	10,209	165
7	0.20	646	20,260	165

oxidize possible carbon deposits, and to detect any oxidized carbon as CO and CO_2 with the online gas analysis equipment. It should be noted that carbon formation is thermodynamically possible at the measured reformer reactor outlet temperature with all the conditions given in Table 2 (see Figure 3).

The reactor outlet temperature and fraction of methane at the outlet gas during the periods of extended hold, along with the corresponding equilibrium values, are depicted in Figure 7. It should be noted that no significant changes in the outlet gas composition or gas temperature occurs during the different hold periods. Concurrently, a good correspondence with equilibrium values is maintained over the hold period. Toward the end of the experiments, at low recycling ratio of 0.2, a small increase of methane fraction is observed at higher inlet temperature. However, with this low recycling ratio, carbon can already form readily at the operating temperature of the SOFC and it is very unlikely that an actual system could be operated safely with such a low recycling ratio without additional steam supply.

Similarly to the outlet temperature and methane fraction, the pressure drop over the reformer reactor and filter remained unchanged (measured changes in pressure drop <1 mbar) during the different operating conditions. Additionally, no carbon deposits were detected at the catalyst and downstream with the oxidation procedure performed at the end of each hold period. It is possible that minor carbon deposits were accumulated to the superheater located upstream to the catalyst, but the amount of carbon was very small, only a few milligrams, and did not increase during longer hold periods. These results clearly demonstrate that carbon formation is not occurring in the experimental conditions tested to an extent that would compromise the operation of this reformer in an SOFC system.

4 Conclusion and Future Work

The performance of a natural gas reformer with a precious metal catalyst was experimentally evaluated using a set of operating conditions in SR and AOGR modes. The experiments revealed that thermodynamic equilibrium was achieved in AOGR mode. On the other hand, in SR mode, equilibrium was not achieved; both outlet temperature and methane mole fraction were higher than the values at thermodynamic equilibrium. These results indicate that the SR reactions were kinetically limited and that the space velocities used in the experiments were too high to reach equilibrium.

Therefore, it is clear that equilibrium is more readily achieved in AOGR mode than SR with this precious metal catalyst. When these results are utilized for SOFC system design and operation, it can be concluded that the size of the catalyst and the reformer can be decreased when an anode off-gas recycling loop is used for fuel processing instead of SR.

The reformer unit was used for over 2,000 h with operating conditions where carbon formation is predicted at thermodynamic equilibrium. Recycling ratios as low as 0.2 were used during the experiments, which are already beyond safe operating limits in an actual SOFC system since carbon formation at Ni-YSZ anode would be expected. However, no significant changes in performance were observed based on measurements of outlet gas composition, pressure drop, and temperature. Additionally, the periodic oxidation cycles did not reveal any significant carbon deposits in the reformer. Therefore, no significant carbon formation occurred during the experiment that would change the characteristic perfor-

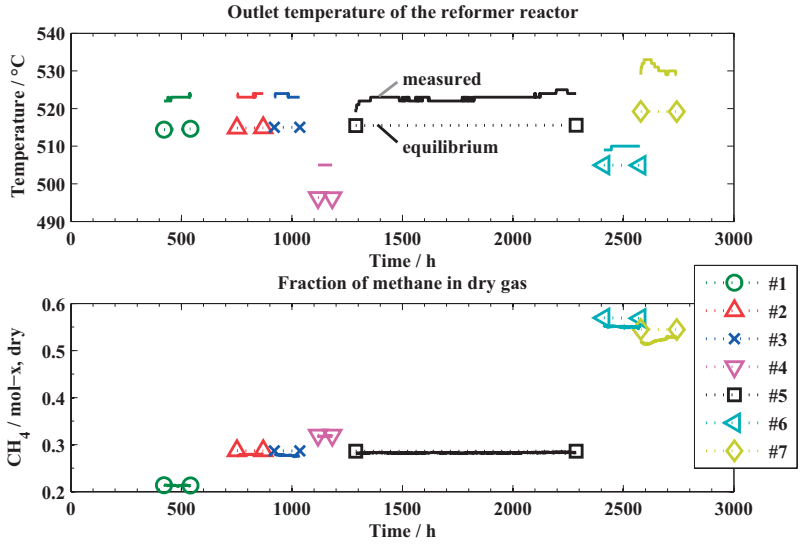

Fig. 7 Temperature (above) and mole fraction of methane (below) at reactor outlet during the experiment. The measured value is presented by a solid line and the calculated equilibrium value by a dashed line with markers at ends. Measured data in other process conditions is excluded to improve the clarity of the figure.

mance of the reformer and compromise operation in SOFC system conditions.

According to the results presented in this study, the reformer unit is suitable to be used in an SOFC fuel processing system which includes an anode off-gas recycling loop. Since good correspondence with equilibrium was always reached when AOGR mode was used, further experiments are needed to assess the operating parameters, e.g., maximum space velocity, where equilibrium is not reached anymore. Furthermore, the natural gas used in the experiments contains less than 1% of higher hydrocarbons than methane. Sufficient conversion of C_{2+} hydrocarbons has to be addressed by conducting future experiments with a fuel gas that contains higher hydrocarbon content.

Acknowledgements

The authors would like to acknowledge Kaisa Lanttola for conducting the GC analysis. Markus Rautanen, Timo Murtonen, and Kai Nurminen are thanked for assisting in the experiments. Anna Kunnas from Wärtsilä Finland Oy is thanked for collaboration and useful discussions. Funding for this study was obtained from SofcPower – project. Finnish Funding Agency for Technology and Innovation, as well as the companies participating in the project are gratefully acknowledged for their financial support.

List of Symbols

$$RR = \frac{\dot{V}^{recycled}}{\dot{V}^{out}_{SOFC}}$$ Recycling ratio

$$GHSV = \frac{\dot{V}^{in}_{reformer}}{V_{reformer}}$$ GHSV of the reformer at NTP, h^{-1}

$$FU_{SOFC} = \frac{I}{F\left(2\dot{n}^{recycled}_{H_2} + 2\dot{n}^{recycled}_{CO} + 8\dot{n}^{recycled}_{CH_4} + z_{NG}\dot{n}_{NG}\right)}$$

Fuel utilization of the SOFC

$$FU_{SYS} = \frac{I}{z_{NG}F\dot{n}_{NG}}$$ Fuel utilization of the whole SOFC system

$$O/C = \frac{\dot{n}_{CO} + 2\dot{n}_{CO_2} + \dot{n}_{H_2O}}{\dot{n}_{CH_4} + \dot{n}_{CO} + \dot{n}_{CO_2}}$$ Oxygen-to-carbon ratio

F Faraday's constant, 96,485 A s mol^{-1}
I Current, A
$\dot{n}$ Molar flow, mol s^{-1}
$V_{reformer}$ Geometrical volume of the reformer
$\dot{V}$ Volume flow in NTP, m^3 s^{-1}
z_{NG} Valence number for natural gas

References

[1] Y. Yi, A. D. Rao, J. Brouwer, G. S. Samuelsen, *J. Power Sources* **2005**, *144*, 67.
[2] S. L. Douvartzides, F. A. Coutelieris, A. K. Demin, P. E. Tsiakaras, *AIChE J.* **2003**, *49*, 248.
[3] D. Mogensen, J.-D. Grunwaldt, P. V. Hendriksen, K. Dam-Johansen, J. U. Nielsen, *J. Power Sources* **2011**, *196*, 25.
[4] R. Peters, R. Dahl, U. Klüttgen, C. Palm, D. Stolten, *J. Power Sources* **2002**, *106*, 238.
[5] N. J. J. Dekker, J. P. Ouweltjes, G. Rietveld, *ECS Trans.* **2007**, *7*, 1465.
[6] H. Timmermann, W. Sawady, D. Campbell, A. Weber, R. Reimert, E. Ivers-Tiffé, *J. Electrochem. Soc.* **2008**, *155*, B356.
[7] E. Riensche, J. Meusinger, U. Stimming, G. Unverzagt, *J. Power Sources* **1998**, *71*, 306.
[8] R.-U. Dietrich, J. Oelze, A. Lindermeir, C. Spitta, M. Steffen, T. Küster, S. Chen, C. Schlitzberger, R. Leithner, *J. Power Sources* **2011**, *196*, 7152.
[9] M. Noponen, M. Halinen, J. Saarinen, J. Kiviaho, *ECS Trans.* **2007**, *5*, 545.
[10] D. Larrain, J. Van herle, D. Favrat, *J. Power Sources* **2006**, *161*, 392.
[11] R. Peters, E. Riensche, P. Cremer, *J. Power Sources* **2000**, *86*, 432.
[12] A. Nummela, M. Noponen, *European Fuel Cell Forum*, Lucerne, Switzerland **2009**, p. B0301.
[13] D. Shekhawat, D. A. Berry, J. J. Spivey, *Fuel Cells: Technologies for Fuel Processing*, Elsevier Ltd., Oxford, UK **2011**, p. 555.
[14] M. Powell, K. Meinhardt, V. Sprenkle, L. Chick, G. McVay, *J. Power Sources* **2012**, *205*, 377.
[15] M. Halinen, M. Rautanen, J. Saarinen, J. Pennanen, A. Pohjoranta, J. Kiviaho, *ECS Trans.* **2011**, *35*, 113–120.
[16] M. Halinen, J. Saarinen, M. Noponen, I. C. Vinke, J. Kiviaho, *Fuel Cells* **2010**, *10*, 440–452.
[17] Outotec. HSC Chemistry 6.1. 2007.
[18] D. G. Goodwin, in *Chemical Vapor Deposition XVI and EUROCVD 14* (Eds. M. Allendorf, F. Maury, F. Teyssandier), PV 2003-08, The Electrochemical Society Proceeding Series, Pennington, NJ, USA **2003**, 155.
[19] G.P. Smith, GRI-MECH 3.0, can be found under http://www.me.berkeley.edu/gri_mech/, accessed **2012**.

PUBLICATION [P4]

Analysis of Leakages in a Solid Oxide Fuel Cell Stack in a System Environment

In: Fuel Cells
Article first published online 16th March 2015

DOI: 10.1002/fuce.201400072

Analysis of Leakages in a Solid Oxide Fuel Cell Stack in a System Environment

M. Halinen[1]*, J. Pennanen[1]

[1] VTT Technical Research Centre of Finland, P.O. Box 1000, FI-02044, VTT, Finland

Received April 25, 2014; accepted November 05, 2014; published online ■■■

Abstract

A solid oxide fuel cell (SOFC) stack can exhibit both anodic and cathodic leakages, i.e. a fuel leak from the anode side and an air leak from the cathode side of the stack, respectively. This study describes the results of an in-situ leakage analysis conducted for a planar SOFC stack during 2000 hours of operation in an actual system environment. The leakages are quantified experimentally at nominal system operating conditions by conducting composition analysis and flow metering of gases for both fuel and air subsystems. Based on the calculated atomic hydrogen-to-carbon ratio of the fuel and air gases, it is found that the fuel leakages are mostly selective by nature: the leaking fuel gas does not have the same composition as the fuel system gas. A simple diffusive leakage model, based on the leakage being driven by concentration differences weighted by diffusion coefficients, is applied to quantify the amount of leakages. The leakage model provides a good correspondence with the experimental results of the gas analysis.

Keywords: Diagnosis, Experimental Results, Fuel Cell System, Leakage, Mass Transport, Solid Oxide Fuel Cell, Stack, Testing

1 Introduction

Solid oxide fuel cells (SOFCs) are electrochemical devices operating at a high temperature. SOFCs have several benefits, such as high efficiency, low emissions, and fuel flexibility, which make them an attractive technology for distributed power generation, auxillary power units (APUs), and various other applications. A planar SOFC stack requires a gas-tight electrolyte as well as high-temperature seals between the different stack components, to prevent harmful mixing of the anode fuel gas (typically reformed gaseous hydrocarbons) and cathode oxidant gas (typically ambient air). Thus, sufficient gas-tightness is required to realize a working and robust SOFC stack, and there are many different techniques and materials developed to achieve this goal [1]. However, experimental work has shown that an SOFC can have both internal leakages between the anode and cathode, e.g. through the electrolyte as well as external leakages between the SOFC and surroundings [2, 3]. Therefore, an SOFC may exhibit a certain characteristic and admissible amount of leakages, which has to be taken into account in the design and operation of SOFC stacks and systems.

In a complete SOFC system, the stack leakages affect the system design, since the leakage can alter the heat production between the different system components. For example, if leakages cause oxidation of a larger amount of the fuel gas already in the stack, then a smaller amount of fuel is fed to the burner downstream of the SOFC stack, thus decreasing the outlet temperature of the burner. Concurrently, there is more heat production in the SOFC stack than is the case without leakages. Moreover, in systems with anode off-gas recycling (AOGR), leakages can create adverse effects during system heat-up and cool-down cycles, and can compromise safe operation of the system [4]. Naturally, leakages mean that less fuel than intended is fed to the anode, thus increasing the fuel utilization of the stack, which can lead to fuel starvation and anode oxidation [5]. Therefore, information on the leakages is relevant and even crucial for various aspects of SOFC system design and operation.

The leakages may be driven by the pressure and concentration differences present between the anode and cathode sides of the stack [2, 5]. A viscous leakage, driven by a pressure difference, has the same composition as the respective bulk gas flowing at the anode or cathode. A diffusive leakage, driven by the concentration difference, does not necessarily have the same composition as the bulk gas, since the composition of such a leak depends on the diffusivity of various substances in the bulk gas. The diffusion mass transport mechanism is relevant especially for fuel gas leakages, since the gas components, such as hydrogen and steam, have large differences in their molecular size. Regardless of the dominating mass transport mechanism, the leakage changes the composition of fuel and air system gases in a similar manner: fuel leaking into an air system combusts to carbon dioxide and steam, while air leaking into a fuel system will oxidize flammable substances of the fuel gas. The nature and quantity of the leakages can be investigated by measuring the changes they make to the com-

[*] *Corresponding author, matias.halinen@gmail.com*

position of the bulk gas, and this approach is used in this study as well.

Online and *in situ* methods to detect or quantify any changes in stack leakages could potentially be used for system fault diagnostics and to evaluate the mechanisms causing stack degradation. Increased stack leakages induce voltage degradation and temperature increases in the stack. Quantification of any changes in the stack leakages during operation would thus be beneficial for distinguishing them from other reasons causing stack voltage degradation, such as an increase in contact resistance, or system faults such as sulphur poisoning or measurement errors. Prior to this study, leakages have been investigated extensively by *ex situ* testing of different materials used as seals for stacks [1], and also by simulations for complete stack aggregates [5], as well as experimentally in single cell test stands [2]. However, to the authors' knowledge, no studies have been published previously on the quantification of leakages for complete stacks operated in an actual system environment.

In this study, a method is presented to: (i) identify the prevailing mass-transport phenomenon causing the anodic leakages; and (ii) quantify the anodic and cathodic leakages. The method is applied for an SOFC stack operated in an actual system environment at nominal operating conditions. The experimental setup and the basis of the analysis method – the use of measurements for both fuel and air systems, together with simple leakage models for diffusive and viscous mass-transport phenomena – are described in Section 2. In Section 3, the composition of the fuel and air systems' gases is determined experimentally, and the prevailing mass-transport mechanism of anodic leakage is identified. Finally, the effects of the leakages on selected characteristics related to the system design and operation are presented and discussed.

2 Experimental

2.1 10 kW SOFC Demonstration Unit

The experiments were conducted with a planar SOFC stack operated in a 10 kW SOFC system at VTT Technical Research Centre of Finland. The 10 kW SOFC system consists of two interconnected modules, the balance of plant (BoP) and the stack module. It utilises an AOGR loop, which enables system operation without an external steam supply when the stack current and single-pass fuel utilization are high enough. Ambient air is fed into the system with a blower and filtered with a particle filter. Other system components include heat exchangers, a catalytic burner, and a reformer to maintain the thermal balance of the system and stack during operation [6].

The SOFC stack was designed, manufactured, and installed in the 10 kW SOFC system by Versa Power Systems (VPS), and it consisted of 64 planar anode supported cells with 550 cm^2 of active area each, and cross-flow geometry for fuel and air gases [7]. The SOFC stack is located inside a thermally insulated and gas-tight module designed by VPS. Inlet air fed to the module flushes the module internal space around the stack before it is forced into cathode inlet air manifolds and through the stack, an arrangement known as air inlet flush (Figure 1). Fuel and cathode outlet gases flow in separate pipes connected to the stack manifold.

The experimental results presented in this study were recorded during a 2,000 h test run, during which the system was operated constantly at the same nominal operating conditions with a stack current of 200 A, an air flow rate of 973 NLPM, a natural gas flow rate of 27.9 NLPM, and a recycle flow rate of 174.7 NLPM. The pressure difference between the anode and cathode of the stack was below 15 hPa at said nominal operating conditions. The pressure was measured from the stack inlet and outlet manifolds.

2.2 Leakage Definitions

As described above, an SOFC stack can exhibit leakages, e.g. through the electrolyte and various interfaces between different parts of the stack assembly. Figure 1 illustrates possible routes for gas leaks taken into account for a planar cross-flow SOFC stack in a gas-tight module with air inlet flush flow configuration. Fuel leakages from the anode side of the stack and from fuel manifolds are called *anodic leakages*, and air leakages from the SOFC cathode side and air manifolds are called *cathodic leakages*. It is evident that there are many possible

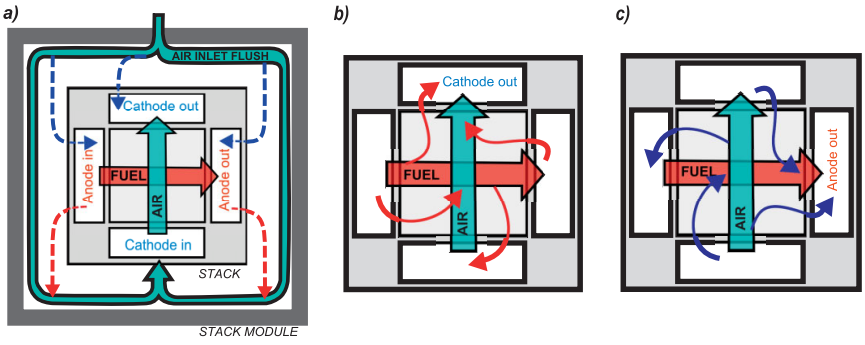

Fig. 1 Valid leakage routes for: a) external anodic (*Aext*) and cathodic (*Cext*) leakages, b) internal anodic (*Aint*) leakages, and c) internal cathodic (*Cint*) leakages.

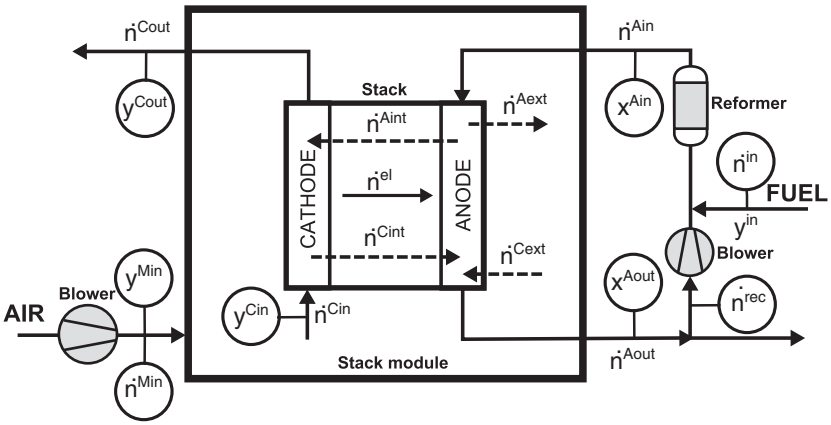

Fig. 2 Experimental setup. Anodic and cathodic leakages are marked with dashed lines. Other system mass flows (air and fuel gas, as well as transport of oxygen) are marked with solid lines. Measured variables are denoted with circles.

interfaces for the leakages to occur, but both the anodic and cathodic leakages can be differentiated from internal and external leakages as follows:

(i) *External leakages* (Figure 1a) occur between the gas manifolds and the module air inlet flush e.g. through manifold seals. Due to the air inlet flush, anodic external leakages are fed into the cathode inlet and, after passing through the stack, end up at the cathode outlet manifold.

(ii) *Internal leakages* (Figure 1b–c) occur inside the stack and between the inlet and outlet manifolds, e.g. through the electrolyte or stack seals. Any anodic internal leakages end up at the cathode outlet manifold (Figure 1b). Similarly, any cathodic internal leakages end up at the anode outlet manifold (Figure 1c).

Due to the many possible leakage paths, the composition of the leakage may not be a single value. The composition depends on the location of the leakage at the various interfaces in the stack, where chemical and electrochemical reactions constantly alter the gas composition according to prevailing conditions (see e.g. [8] for details). However, any leakages depicted in Figure 1a-c mix with a significantly larger amount of bulk gas, fuel, or air, flowing through the anode and cathode and around the stack as air inlet flush. Additionally, due to the high operating temperature and the presence of catalytically active materials, it is expected that reactions occur between the leakages and the bulk gases according to Eqs. (1)–(3). Flammable substances in an anodic leakage react with oxygen and are combusted to CO_2 and H_2O at the cathode side. Similarly, oxygen in a cathodic leakage reacts with fuel gas at the anode side.

$$CH_4 + 2O_2 \rightarrow CO_2 + 2H_2O \quad (1)$$

$$CO + 1/2\ O_2 \rightarrow CO_2 \quad (2)$$

$$H_2 + 1/2\ O_2 \rightarrow H_2O \quad (3)$$

Since the individual leakages mix and react with a larger amount of bulk gas, this study does not try to model or quantify any spatially distributed individual leakages of the stack. Instead of the individual leakage routes illustrated in Figure 1a–c, this study considers the leakages in a form in which the total amounts of the leakages ($\dot{n}^{Atot}$ and $\dot{n}^{Ctot}$) are expressed as flow rates, where:

$\dot{n}^{Atot}$ is the sum of anodic leakages $\dot{n}^{Aext} + \dot{n}^{Aint}$, where

- $\dot{n}^{Aext}$, anodic external leakage, is the total amount of fuel leaking from the anode inlet and outlet manifolds to the air inlet flush, as depicted in Figure 1a.
- $\dot{n}^{Aint}$, anodic internal leakage, is the total amount of fuel leaking from anode to cathode air flow, as depicted in Figure 1b.

$\dot{n}^{Ctot}$ is the sum of cathodic leakages $\dot{n}^{Cext} + \dot{n}^{Cint}$, where

- $\dot{n}^{Cext}$, cathodic external leakage, is the total amount of air leaking from the air inlet flush to the stack fuel manifolds, as depicted in Figure 1a.
- $\dot{n}^{Cint}$, cathodic internal leakage, is the total amount of air leaking from cathode to anode fuel flow, as depicted in Figure 1c.

2.3 Measurements

The experimental setup used in this study to detect and quantify the leakages $\dot{n}^{Ctot}$ or $\dot{n}^{Atot}$ is depicted in Figure 2, and the description of the measured process variables denoted with circles is given in Table 1. In the air subsystem, the fractions of CO_2, H_2O, and O_2 in the cathode air were continuously sampled and measured at module inlet (y^{Min}), cathode inlet (y^{Cin}), and cathode outlet (y^{Cout}). Anodic leakages are detected by observing the changes in the measured gas composition between the sampling locations according to Eqs. (1)–(3). Additionally, measurements with FTIR and GC were conducted for *Cin* and *Cout* gas to ensure that anodic leakage is completely combusted to CO_2 and H_2O. The module inlet air ($\dot{n}^{Cin}$) flow rate was measured with a thermal mass flow meter.

Table 1 The measured variables and their uncertainty.

Measurement	Variable	Uncertainty
Natural gas	$\dot{n}^{in}$	±1% of value
Module inlet air	$\dot{n}^{Min}$	±3% of value
Recycle gas	$\dot{n}^{rec}$	±3% of value
Composition of humid air at *Min*, *Cin*, and *Cout*	y_{H_2O}	±450 ppm
	y_{CO_2}	±(5 ppm + 2% of value)
	y_{O_2}	±(0.2%-units + 2% of value)
Composition of dried fuel gas at *Ain* and *Aout*	x_{CH_4}, x_{CO}, x_{CO_2} x_{H_2}, x_{O_2}, $x_{N_2}x_{C_nC_m}$	±3% of value

A more complex arrangement is required for the fuel subsystem, to detect and quantify the flow rate and composition (y_j) of the gases flowing in the fuel system on a wet basis. Complexity arises because the humid fuel gas was cooled down to 2–3 °C to condensate the water vapour from the gas samples, and the gas analysis was done on a dry basis (x_i). From the dried fuel gas, CH_4, CO, CO_2, H_2, N_2, C_xH_y compounds up to C_5 hydrocarbons, and O_2/Argon were analyzed with GCs. The composition was analysed from periodically extracted gas samples at anode inlet (x^{Ain}) and anode outlet (x^{Aout}). A portion of the anode outlet gas (x^{Aout}) is recycled back into the system inlet, thus the recycling gas (x^{rec}) has the same composition. Composition of the fuel at the system inlet (y^{in}), high-grade natural gas from the Finnish gas grid, used in the experiment was not directly measured due to its stable composition, consisting of more than 98% methane and other hydrocarbons (Table 2). The inlet natural gas ($\dot{n}^{in}$) flow rate was measured with a thermal mass flow meter, and the recycle gas flow ($\dot{n}^{rec}$) with a turbine meter.

2.4 Leakage Analysis

2.4.1 Approach

It is clear that quantification of $\dot{n}^{Ctot}$ or $\dot{n}^{Atot}$, depicted in Figure 2, with any direct physical measurement devices would be extremely challenging to realize in an actual system environment due to, e.g. the high temperature of the gases and various reactions within the SOFC, affecting the composition as well as the molar flow of both the bulk gases and the leakages. Thus, the experimental setup for leakage analysis is based on the fact that leakages will change the flux of the elements, $\dot{n}_e$, $e = C, H, O, N$, between the inlet and the outlet of the anode and cathode of the stack, according to Eqs. (4) and (5), respectively.

Table 2 Average composition of system inlet fuel (natural gas) and uncertainty.

Substance	Variable	Average	Uncertainty
Methane	$y^{in}_{CH_4}$	97.9 mol-%	±1.0 mol-%
Ethane	$y^{in}_{C_2H_6}$	0.8 mol-%	±0.5 mol-%
Propane	$y^{in}_{C_3H_8}$	3,000 ppm	±2,000 ppm
Butane	$y^{in}_{C_4H_{10}}$	1,000 ppm	±600 ppm
Nitrogen	$y^{in}_{N_2}$	1 mol-%	±0.5 mol-%

$$\dot{n}_e^{Aout} = \dot{n}_e^{Ain} - \dot{n}_e^{Atot} + \dot{n}_e^{Ctot} + \dot{n}_O^{el} \quad (4)$$

$$\dot{n}_e^{Cout} = \dot{n}_e^{Min} + \dot{n}_e^{Atot} - \dot{n}_e^{Ctot} - \dot{n}_O^{el} \quad (5)$$

In Eq. (4), $\dot{n}^{Ctot}$ leakage supplies additional O and N to the fuel system gas, which consists mostly of substances containing the elements H and C – the main constituents of the inlet natural gas. Similarly, $\dot{n}^{Atot}$ in Eq. (5) supplies additional H and C to the air system, where any indigenous flux of these elements originates from the inlet ambient air as H_2O and CO_2, respectively. Flux of O through the electrolyte is denoted as $\dot{n}_O^{el}$.

The flux of elements takes place as a flow of the substances in the fuel and air system gases. Thus, the element flux at any process location can be determined based on the molar fractions of each substance containing the given element, and the total flow rate of the gas according to Eqs. (6) and (7).

$$\dot{n}_e = Y_e \dot{n} \quad (6)$$

$$Y_e = \sum_j A_{e,j} y_j \quad (7)$$

For example, for H, Eq. (7) is $Y_H = 4y_{CH4} + 2y_{H2} + 2y_{H2O} + my_{CnHm}$. Now, Eqs. (4) and (5) can be derived using Eqs. (6) and (7) as (8) and (9):

$$\dot{n}^{Aout} Y_e^{Aout} = \dot{n}^{Ain} Y_e^{Ain} - \dot{n}^{Atot} Y_e^{Atot} + \dot{n}^{Ctot} Y_e^{Ctot} + \dot{n}_O^{el} \quad (8)$$

$$\dot{n}^{Cout} Y_e^{Cout} = \dot{n}^{Min} Y_e^{Min} + \dot{n}^{Atot} Y_e^{Atot} - \dot{n}^{Ctot} Y_e^{Ctot} - \dot{n}_O^{el} \quad (9)$$

It should be noted that Eqs. (6)–(9) contain practically measurable process variables, i.e. molar fractions of substances and flow rates at various process locations (see Figure 2), which enable *in situ* leakage analysis of an SOFC stack while operated in an actual system environment. However, it becomes clear when looking into Eqs. (6)–(9) that the composition of the anodic leakage y^{Atot} is required to quantify the leakages. Since y^{Atot} cannot be measured directly, two simple leakage models based on different mass-transport phenomena, viscous and diffusive, are considered in the next chapters, to calculate the composition y^{Atot}.

2.4.2 Viscous Leakage

The composition ($y^{Atot,visc}$) of a viscous leakage, driven by the pressure difference between the anode and cathode sides of the stack, is assumed simply to be identical to the fuel gas composition at the SOFC anode, as in Eq. (10).

$$y_j^{Atot,visc} = y_j^{anode}, \text{ where } y^{anode} = y^{Ain}, y^{Aout} \quad (10)$$

The composition of y^{anode} is approximated with a single value by using either y^{Ain} or y^{Aout}. y^{Ain} and y^{Aout} are selected as representative values for y^{anode} since they represent the two extremes of the gas distribution within the SOFC stack [8], and they are calculated using the fuel system's measurements according to Appendix A.

The total cathodic leakage $\dot{n}^{Ctot}$ is assumed to occur viscously at all times, having an idealised composition of 21 vol-% of O_2 and 79 vol-% of N_2. The simplification is reasonable, since the amount of carbon dioxide and water vapour in $\dot{n}^{Ctot}$ is very small and has a negligible effect on the results.

2.4.3 Diffusive Leakage

The composition $\left(y^{Atot,diff}\right)$ of a diffusive leakage, driven by the difference in concentration between the anode and cathode sides of the stack, is approximated by weighting the molar fraction of substances in the fuel gas at the SOFC anode by their relative binary diffusion coefficients, using Eq. (11).

$$y_j^{Atot,diff} = \frac{D_j^{air}}{\sum_j D_j^{air} y_j^{anode}} \left(y_j^{anode} - y_j^{cathode}\right) \approx \frac{D_j^{air}}{\sum_j D_j^{air} y_j^{anode}} \left(y_j^{anode}\right), \quad \text{where } y^{anode} = y^{Ain}, y^{Aout} \tag{11}$$

D_j^{air} are the binary diffusion coefficients of each substance in air, estimated according to Fuller et al. [9]. The simplification to use only the composition of the fuel gas is reasonable, since $y_j^{anode} \gg y_j^{cathode}$ for CH_4, CO, CO_2, H_2, and H_2O components. Similarly, it is reasoned that no nitrogen or oxygen are leaking diffusively from anode to cathode, since $y_{N_2}^{anode} \ll y_{N_2}^{cathode}$ and $y_{O_2}^{anode} = 0$, respectively.

2.4.4 Distinction between Viscous and Diffusive Leakage

The anodic leakage will introduce an additional flux of C and H-containing substances into the air system. As long as the compounds that contain the elements C and H are oxidized completely, according to Eqs. (1)–(3), these element fluxes can be expressed as Eqs. (12) and (13).

$$\dot{n}_C^{Atot(ox)} = \dot{n}_C^{Cout} - \dot{n}_C^{Min} + \dot{n}_C^{Ctot} \approx \dot{n}^{Cout} y_{CO_2}^{Cout} - \dot{n}^{Min} y_{CO_2}^{Min} \tag{12}$$

$$\dot{n}_H^{Atot(ox)} = \dot{n}_H^{Cout} - \dot{n}_H^{Min} + \dot{n}_H^{Ctot} \approx 2\left(\dot{n}^{Cout} y_{H_2O}^{Cout} - \dot{n}^{Min} y_{H_2O}^{Min}\right) \tag{13}$$

where $\dot{n}_e^{Atot(ox)}$ is the flux of elements due to anodic leakage after complete oxidation of flammable substances. Simplification of Eqs. (12) and (13) is reasonable, as $\dot{n}_C^{Ctot}, \dot{n}_H^{Ctot} \ll \dot{n}_C^{Atot}$, $\dot{n}_H^{Atot}$. The $\dot{n}^{Cout}$ flow rate in Eqs. (12) and (13) is calculated using the nitrogen balance between the module inlet and the cathode outlet, as in:

$$\dot{n}^{Cout} = \frac{\dot{n}^{Min} y_{N2}^{Min} - \dot{n}_{N_2}^{Ctot} + \dot{n}_{N_2}^{Atot}}{y_{N2}^{Cout}} \cong \frac{y_{N2}^{Min}}{y_{N2}^{Cout}} \dot{n}^{Min}, \quad \text{where } y_{N2} = 1 - \sum_j y_j \tag{14}$$

where $j = CO_2, H_2O, O_2$. The simplification of Eq. (14) is reasonable, since $\dot{n}_{N_2}^{Min}, \dot{n}_{N_2}^{Cout} \gg \dot{n}_{N_2}^{Ctot}, \dot{n}_{N_2}^{Atot}$.

The distinction between the viscous and diffusive leakage in the system is done by comparing independently measured HC-ratios of the anodic leakage to each other, according to Eqs. (15) and (16).

$$HC^{Atot,a} = \frac{Y_H^{Atot,a}}{Y_C^{Atot,a}} = \frac{4y_{CH_4}^{Atot,a} + 2y_{H_2}^{Atot,a} + 2y_{H_2O}^{Atot,a}}{y_{CH_4}^{Atot,a} + y_{CO}^{Atot,a} + y_{CO_2}^{Atot,a}}, \quad \text{where } a = diff,\ visc \tag{15}$$

$$HC^{Atot(ox)} = \frac{\dot{n}_H^{Atot(ox)}}{\dot{n}_C^{Atot(ox)}} \tag{16}$$

It should be noted that the HC-ratio in Eq. (15) is obtained with fuel system measurements and the leakage models, while only air system measurements are used for Eq. (16).

2.4.5 Quantification of Leakages

Once the prevailing leakage mechanism has been identified, the anodic leakage is quantified as Eq. (17).

$$\dot{n}^{Atot} = \frac{\dot{n}_C^{Atot}}{Y_C^{Atot,a}} = \frac{\dot{n}_C^{Atot(ox)}}{\left(y_{CH_4}^{Atot,a} + y_{CO}^{Atot,a} + y_{CO_2}^{Atot,a}\right)}, \quad \text{where } a = diff,\ visc \tag{17}$$

Eq. (17) is based on Eq. (6) for the mass balance of carbon.

Quantification of cathodic leakage $\dot{n}^{Ctot}$ is done using Eq. (18).

$$\dot{n}^{Ctot} = \frac{\frac{\dot{n}_C^{Ain} - \dot{n}_C^{Atot}}{Y_C^{Aout}} y_{N_2}^{Aout} - \dot{n}_{N_2}^{Ain} + \dot{n}^{Atot} y_{N_2}^{Atot}}{0.79} \tag{18}$$

where $y_{N_2}^{Atot} = 0$ for diffusive anodic leakage. Eq. (18) is based on Eq. (8) for both nitrogen and carbon balances between *Ain* and *Aout*.

2.5 Uncertainty Analysis

The propagation of the uncertainty of the calculated variables due to the measurements (Table 1) and the inlet natural gas composition (Table 2) is evaluated using Eq. (19):

$$\sigma_y = \sqrt{\sum_{i=1}^{n} \left(\frac{\partial f}{\partial x_i} \sigma_{x_i}\right)^2}, \quad y = f(x_1, \ldots, x_n) \tag{19}$$

where σ_y is the uncertainty of the calculated value y, and σ_{x_i} is the uncertainty of the measured value x_i. Due to large number of measurements (x_i) it is necessary to use symbolic math software to obtain the partial derivates for Eqs. (4)–(18) and calculate their uncertainties numerically. The error bars in all the figures and tables in this manuscript depict either σ_X of a calculated value according to (19), or uncertainty related to the measurement according to Table 1.

3 Results and Discussion

3.1 Air System Measurement Results

Figure 3a–c depicts measured air system gas composition at *Min*, *Cin*, and *Cout* at the time of periodic gas sampling. It is seen that both CO_2 and H_2O fraction at the cathode increases

from the module air inlet to the cathode outlet. These changes can be associated to anodic leakages, since there is no other supply of such substances into the air system. Thus, changes in gas composition between the sampling locations *Min* to *Cin*, *Cin* to *Cout*, and *Min* to *Cout* manifest the effects of the leakages *Aext*, *Aint*, and *Atot*, respectively (see Figure 2), and thus can be used to obtain the HC ratio for any of these leakages, using Eqs. (12)–(14).

The CO_2 and O_2 fractions at *Min* remain nearly constant at approximately 400 ppm and 21.2 vol-%, respectively, while the H_2O fraction varies between 1,000 to 6,000 ppm, according to the prevailing ambient conditions. Compared to *Min*, the measurements at *Cin* show a significant increase for both CO_2 and H_2O, and a much smaller decrease for O_2. The small decrease of O_2 fraction can be associated to the combustion of flammable substances (CH_4, CO, and H_2) of *Aext*, which consume oxygen, and to depletion of air due to *Cext* leakages. However, this small change in the O_2 fraction can be associated to the rather large uncertainty of the O_2 sensor as well.

Similarly, compared to *Min*, even a larger increase for H_2O and CO_2 is evident in *Cout* measurements (Figure 3a–b), due to internal anodic leakages *Aint*, which suggests that *Aint* leakage is of higher magnitude than *Aext*. The O_2 fraction at *Cout* (Figure 3c) is now significantly decreased, mainly due to the utilization of oxygen in the fuel cell reactions.

Generally, due to the high uncertainty associated with the oxygen measurement, quantification of the air leakages cannot be done reliably using air system gas analysis. However, this is not the case for the H_2O and CO_2 measurements – the fuel leakage is significant enough to generate a difference in the measured values that is greater than the sensors' uncertainty, which enables the use of Eqs. (12) and (13) to resolve the element fluxes of the anodic leakage.

3.2 Fuel System Measurement Results

Measured dry fuel gas composition at *Ain* and *Aout* is presented in Figure 4. The total fraction of C_{2+} hydrocarbons was

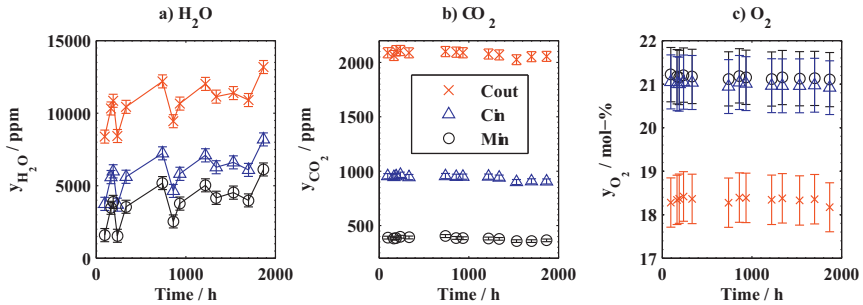

Fig. 3 Measured fraction of a) H_2O, b) CO_2, and c) O_2 in the cathode gas at (○) module inlet *Min*, (△) cathode inlet *Cin* and (×) cathode outlet *Cout*. System at nominal operating conditions with stack current at 200 A.

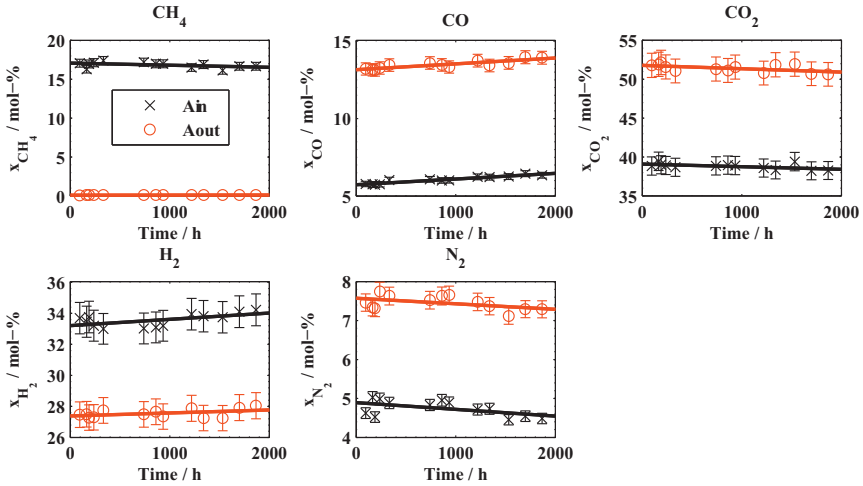

Fig. 4 Measured composition of (×) *Ain* and (○) *Aout* gas on a dry basis. A linear fit is shown as a solid trend line. System at nominal operating conditions with stack current at 200 A.

below 35 ppm for x^{Ain} and below detection limits for x^{Aout}. Figure 4 shows that fuel system gas composition remains relatively stable during the experiment, as the system is operated constantly at nominal operating conditions. According to the first-order linear fit on the measurements, a small trend over time is observed for nearly all gas components. The trend can be related to the temperature increase of the stack during the experiments, which changes gas composition according to the thermodynamic equilibrium.

The wet gas composition at *Ain* and *Aout*, calculated according to Appendix A, is depicted in Figure 5. The wet gas composition is needed to resolve the composition of the anodic leakage in Eqs. (10) and (11), and to quantify the anodic and cathodic leakages according to Eqs. (17) and (18). Similarly to the dry gas composition, the wet gas composition in Figure 5 remains very stable during the experiment. Only a few qualitative observations can be made by inspecting the changes between *Ain* and *Aout*; for example: (i) nearly all methane is reformed in the stack as the y^{Ain}_{CH4} is < 0.1 mol-%; and (ii) cathodic leakages are present in the system, since $y^{Aout}_{N2} > y^{Ain}_{N2}$ and if no cathodic leakages occur then $y^{Aout}_{N2} < y^{Ain}_{N2}$, as all methane is reformed and thus the molar flow at *Aout* is larger than at *Ain*.

3.3 Determination of Prevailing Leakage Mechanism and Quantification of Leakages

The prevailing mass-transport mechanism of the anodic leakage is determined by utilising the independent measurements from the fuel and air subsystems. The leakage models in Eqs. (10) and (11) produce different gas compositions and HC-ratios for the leaking fuel gas. By comparing the HC-ratios obtained (i) with Eq. (16) using air system measurements, and (ii) with Eq. (15) using fuel system measurements and the two leakage models, the leakage mechanism can be determined.

The HC-ratio can be assessed intuitively, even without any analysis results from the fuel system: as the natural gas (mostly CH_4) is the prevailing supply of H and C in the fuel system, then the HC-ratio of the gas in any location of the fuel system should be nearly identical to the inlet natural gas HC ratio of approximately 4. Therefore, if the anodic leakages occur in a viscous manner, a corresponding value of approximately 4 should result for $HC^{Atot(ox)}$ in Eq. (16) as well, regardless of the actual location of the leakage paths within the stack or its manifolds. However, if $HC^{Atot(ox)}$ differs from the inlet natural gas HC-ratio, then the leakage is not occurring viscously, meaning that the composition of the anodic leakage differs from the composition of the fuel gas flowing through the stack.

Figure 6 depicts the HC-ratios obtained by air and fuel system measurements and the two leakage models. The HC-ratios in Figure 6a are calculated with *Ain* gas composition, and in Figure 6b with *Aout* composition, which represent the two extremes in the gas distribution within the stack. It is observed in Figure 6a–b that the HC-ratios given by the viscous leakage model ($HC^{Atot,visc}$) are approximately 4, which are sensible

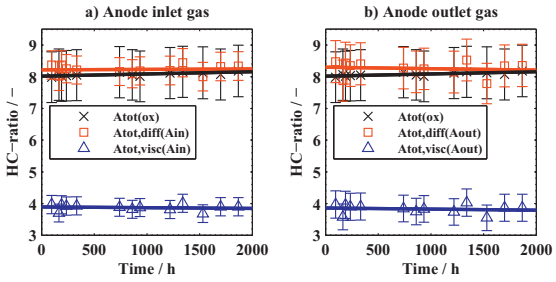

Fig. 6 HC-ratio of the anodic leakage determined by (×) air system measurements, (□) diffusive leakage model, and (△) viscous leakage model, with a) *Ain* and b) *Aout* gas composition. A linear fit is shown as a solid trend line.

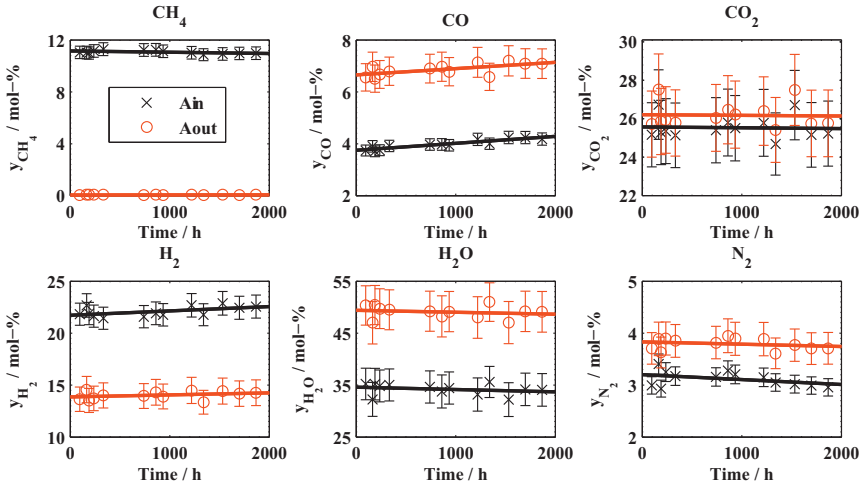

Fig. 5 Composition of the (×) *Ain* and (○) *Aout* gas on a wet basis. A linear fit is shown as a solid trend line.

values that correspond to the properties of the inlet natural gas. However, $HC^{Atot(ox)}$ is approximately 8, which proves that the anodic leakage is not viscous. On the contrary, HC-ratios given by the diffusive leakage model ($HC^{Atot,diff}$) correspond very well to $HC^{Atot(ox)}$. Additionally, within the calculation uncertainty, the HC-ratios for *Aint* and *Aext* leakages are the same as for *Atot* leakage (results omitted for brevity), demonstrating a diffusion-type mass-transfer for both external and internal anodic leakages.

Quantification of the total diffusive anodic and cathodic leakages is now possible using Eqs. (17) and (18), and the results are depicted in Figure 7. Anodic leakages constitute approximately 3% of the anode inlet flow, and it is seen that the leak rate is somewhat higher when y^{Aout} is used as a representative value of the fuel gas composition at the anode. Importantly, it is observed that the leakages of the stack do not increase during the experiment, demonstrating that the gas-tightness characteristics of the stack do not deteriorate, but retain initial performance.

3.4 Complete Combustion of the Anodic Leakage

Calculation of the HC-ratio using Eq. (16) assumes complete combustion of anodic leakage, according to Eqs. (1)–(3), before the gas sample extraction locations in the air system. Incomplete combustion could induce a significant error in the calculated HC-ratio, which can in turn hamper identification of the prevailing mechanism of anodic leakage. Importantly, if any significant amount of unburned CO from anodic leakage was present in the air system, an erroneously high value for the HC-ratio would be obtained.

Table 3 presents the fraction of CH_4, CO, and H_2 at *Cin* and *Cout* gas, measured with GCs and FTIR. The fraction of flammable substances is either below the detection limit or present only as trace amounts, thus their combustion is complete or near-to-complete. In order to emphasize the insignificance of the trace amounts of flammable substances, corresponding values are calculated with 8 NLPM anodic leakage without any combustion taking place.

A comparison of the measured and calculated results clearly reveals that effects of the trace amounts of unburned CH_4, CO, and H_2 on the calculation results are negligible. This is important, since it facilitates the use of simple CO_2 and H_2O sensors to detect anodic leakages, instead of more complex GC and FTIR analysis equipment.

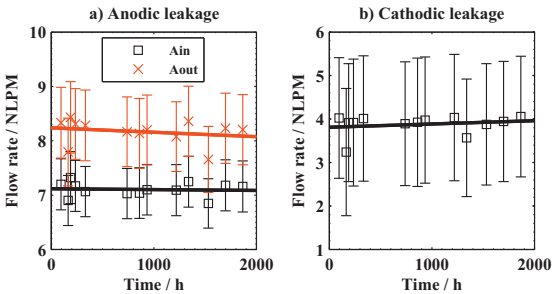

Fig. 7 a) Total anodic leakage calculated using (□) *Ain* and (×) *Aout* gas composition, and b) total cathodic leakage. A linear fit is shown as a solid trend line.

Table 3 Fraction of flammable substances at *Cin* and *Cout*. The measured value and calculated value for an uncombusted anodic leakage are given.

Substance	Unit	Measured		Calculated (uncombusted)	
		Cin	*Cout*	*Cin*	*Cout*
y_{CH_4}	ppm, dry	2	<2	917	893
y_{CO}		2	10	329	321
y_{H_2}		<5	<5	1,828	1,782

3.5 Application of the Analysis Method for System Design and Diagnosis Purposes

The applicability and significance of the developed method for system applications is briefly illustrated next.

3.5.1 System and Stack Design

The presented method can be used to define important operational characteristics for the design of SOFC stacks and systems. To illustrate the applicability of the method, the effects of diffusive anodic leakages on selected important operational characteristics, namely fuel utilization and the additional heat production of the stack, are assessed and discussed. In an ideal case without any leakages, the single-pass fuel utilisation of an SOFC stack in an AOGR system environment can be calculated using Eqs. (20) and (21) [10].

$$FU_{SOFC} = \frac{FU_{SYS}(1-R)}{1-FU_{SYS}R} \tag{20}$$

$$FU_{SYS} = \frac{I}{\sum_j z_j \dot{n}_j^{in} F} \tag{21}$$

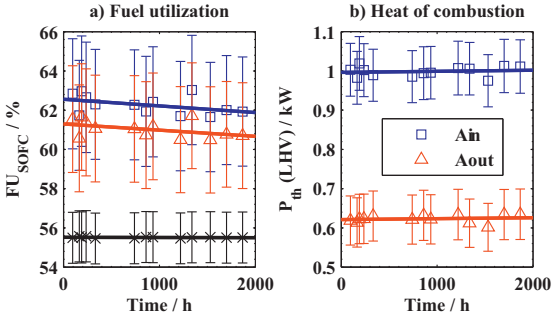

Fig. 8 a) SOFC stack fuel utilisation, and b) heat of combustion due to diffusive anodic leakages with (□) *Ain* and (△) *Aout* gas composition. (×) Ideal fuel utilization without leakages. A linear fit is shown as a solid trend line.

The actual fuel utilization of an SOFC stack, with anodic leakages taken into account, is calculated using Eq. (22). Here, it is assumed the total anodic leakage occurs at the stack inlet manifolds before the anode. Heat produced by complete combustion of the anodic leakages is calculated using Eq. (23).

$$FU_{SOFC}^{leak} = \frac{I}{\left(\sum_j z_j \left(\dot{n}_j^{Ain} - \dot{n}_j^{Atot}\right)\right) F} \tag{22}$$

$$P_{th} = \sum_j \Delta H_j \dot{n}_j^{Atot} \tag{23}$$

Figure 8a depicts both the ideal single-pass fuel utilization of the SOFC stack without leakages (Eq. (20)) and the actual FU with leakages taken into account (Eq. (22)). The results clearly illustrate that the anodic leakages can affect the stack single-pass fuel utilization significantly. The fuel utilization of the stack is increased from approximately 56% up to approximately 62%. It should be noted, however, that Eq. (22) represents the maximum worst-case stack fuel utilization, since all fuel leaks before the anode inlet. In reality, the actual fuel utilization would be lower for the given stack, if leakages are distributed more evenly along the interfaces and occur towards the anode outlet as well. Finally, it is seen that the actual composition of the diffusive anodic leakage will not affect the actual stack fuel utilization significantly, as the difference between the two approximations (i.e. with *Ain* and *Aout* gas compositions) is only approximately 1%-unit.

Combustion of anodic leakages increases the heat production in the stack and its surroundings as depicted in Figure 8b. Here, a diffusive leak approximated by *Ain* gas composition produces more heat, as it contains a higher amount of flammable substances, especially methane. The increased heat production in the stack can be perceived as both a negative and a positive issue with respect to the system operation and design. On the negative side, the increased internal heat production of the stack may require additional cooling - typically accomplished by increasing the cathode air flow rate. Consequently, a penalty to the overall system efficiency is generated as the parasitic power consumption of the air blower increases. On the positive side, leakages may alleviate the need to pre-heat the inlet gas streams using heat exchangers, especially in the case of external anodic leakages, since they will directly heat up the air at the inlet flush. Thus, it may be possible to decrease the size of the air system heat exchangers, which can lower the final cost of the system, provided that the leakages remain the same over the system lifetime.

3.5.2 *Online Diagnosis*

A high enough cross-leakage of hydrogen-containing fuel gas into the air system, for example due to the failure of a seal in an SOFC stack, is detrimental to system reliability and lifetime. The combustion of a leakage concentrated in a specific location is a strong exothermal reaction triggering structural damage, which can in turn increase the leakage and lead to severe equipment failures. Thus, early detection of increased fuel leakages can be beneficial in alleviating the consequences of such failures by using preventive measures such as system shutdown and servicing.

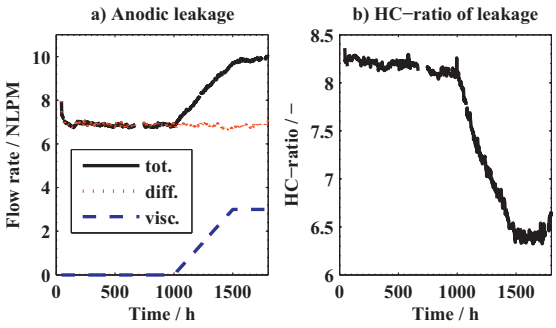

Fig. 9 Simulated case of increasing anodic viscous leakage: a) total anodic (solid line), diffusive (dotted), and viscous (dashed) leakage; b) HC ratio of the total anodic leakage.

The measurement method presented in this study provides means to detect both (i) increases in the absolute amount of leakages, and (ii) changes in the prevailing mass transport mechanism of the leakages. Obviously, any increase of the anodic leakage can be directly detected as an increased flux of carbon and hydrogen in the air system, according to Eqs. (12) and (13). Likewise, the increase of an anodic leakage with a differing mass transport mechanism can be observed as a respective change in the HC-ratio, detectable using the air system measurements, according to Eq. (16). The latter argument is illustrated by a simulated case example, depicted in Figure 9, where a diffusive anodic leakage of approximately 7 NLPM is present in the system, according to the results of this study. A viscous leakage starts to evolve at t = 1,000 h, which can be detected as a progressive decrease of the HC-ratio of the total anodic leakage. Thus, the method presented in this study could be applied, in addition to the general quality assurance for SOFC stacks, for case-specific online fault diagnosis of SOFC systems.

4 Conclusions

In this study, an experimental setup and method is presented to (i) identify the prevailing mass transport mechanism of anodic leakages, and (ii) quantify the anodic and cathodic leakages of an SOFC stack operated in an actual system environment. Identification of the mass transfer phenomenon of anodic leakage cannot be done only by analysing the fuel system's gas composition, but requires measuring the fractions of CO_2, H_2O, and O_2 in the air system, as well as utilization of simple leakage models for diffusive and viscous leakages. Distinction between viscous and diffusive leakages is possible by comparing the HC ratios obtained independently by (i) leakage models and fuel system gas analysis, and (ii) air system gas analysis.

A simple diffusive leakage model provides good correspondence with the HC-ratio calculated directly from the measurement data, and thus it is concluded that the anodic leakages for the given stack occur mainly in a diffusive manner. The effects of diffusive fuel leakages on selected operational characteristics of an SOFC system were studied. Leakages can have negative, but also potentially positive, effects on system design and operation. Importantly, the results of this study demonstrate that the SOFC stack used in the experiments retained its characteristic gas-tightness in a system environment over the whole experiment period, since no changes in either anodic or cathodic leakages were observed.

The experimental method presented in this study was used successfully for *in situ* quantification of leakages during continuous operation of SOFC systems using actual fuel, and without any operational disturbances. Thus, it is possible to utilise the method presented in this study for quality assurance of the SOFC stacks after the manufacturing process, or for fault identification in real-world systems, such as distinguishing a voltage decrease caused by leakages from other degradation mechanisms.

Acknowledgements

Funding for this study was obtained through the projects SofcPower (40074/11) and RealDemo (40076/12). The Finnish Funding Agency for Technology and Innovation (TEKES) and the companies participating in the project are gratefully acknowledged for their financial support. Additionally, M. Halinen would like to thank the following personnel at VTT for their contribution: Kaija Luomanperä and Päivi Jokimies (GC analysis), Hannu Vesala (FTIR analysis), Kari Koskela, Markus Rautanen and Kai Nurminen (help with the experimental setups), and Antti Pohjoranta (manuscript review). Michael Pastula from Versa Power Systems is thanked for his essential contribution related to the stack operability in the 10 kW SOFC system.

Appendix A. Calculation of wet gas composition at anode inlet (y^{Ain}) and anode outlet (y^{Aout})

The solution for y^{Ain} and y^{Aout} is based on the preservation of matter in the elemental flux of the inlet natural gas, recycle, and anode inlet gases (see Figure 2), according to Eq. (A1).

$$\dot{n}_e^{Ain} = \dot{n}_e^{rec} + \dot{n}_e^{in} \tag{A1}$$

We start by defining Eqs. (A2)–(A4), since the fraction of substances in the fuel gas is analyzed from dried fuel gas x^k, for example for H, Eq. (A4) is $X_H^k = 4x_{CH4}^k + 2x_{H2}^k + mx_{CnHm}^k$.

$$\dot{n}^k = \dot{n}_{dry}^k + \dot{n}_{H_2O}^k \tag{A2}$$

$$\dot{n}_{dry}^k = \sum_i \dot{n}_i^k \tag{A3}$$

$$X_e^k = \sum_e A_{e,i} x_i^k \tag{A4}$$

Now, by using Eqs. (A2)–(A4), Eq. (A1) can be written for elements C, O, and H, using separate variables for steam and the remaining substances in the dried gas, as in Eqs. (A5)–(A7).

$$\text{C}: \quad \dot{n}_{dry}^{Ain} X_C^{Ain} = \dot{n}_{dry}^{rec} X_C^{Aout} + \dot{n}_C^{in} \tag{A5}$$

$$\text{O}: \quad \dot{n}_{dry}^{Ain} X_O^{Ain} + \dot{n}_{H_2O}^{Ain} = \dot{n}_{dry}^{rec} X_O^{Aout} + \dot{n}_O^{in} + \dot{n}_{H_2O}^{rec} \tag{A6}$$

$$\text{H}: \quad \dot{n}_{dry}^{Ain} X_H^{Ain} + 2\dot{n}_{H_2O}^{Ain} = \dot{n}_{dry}^{rec} X_H^{Aout} + \dot{n}_H^{in} + 2\dot{n}_{H_2O}^{rec} \tag{A7}$$

Solving (A5)–(A7) for $\dot{n}_{dry}^{rec}$ by eliminating $\dot{n}_{H_2O}^{rec}$ and $\dot{n}_{dry}^{Ain}$, we get Eq. (A8).

$$\dot{n}_{dry}^{rec} = \frac{\dot{n}_C^{in}\left(X_O^{Ain} - 0.5X_H^{Ain}\right) + 0.5\dot{n}_H^{in}\left(X_C^{Ain}\right) + \dot{n}_O^{in}\left(X_C^{Ain}\right)}{X_C^{Ain}\left(X_O^{Aout} - 0.5X_H^{Aout}\right) - X_C^{Aout}\left(X_O^{Ain} - 0.5X_H^{Ain}\right)} \tag{A8}$$

Now, the gas composition on a wet basis at *rec* and *Aout* can be calculated using Eq. (A8), and the measurements for dry gas composition and recycle flow rate using Eqs. (A9)–(A11).

$$\dot{n}_i^{rec} = x_i^{Aout} \dot{n}_{dry}^{rec} \tag{A9}$$

$$\dot{n}_{H_2O}^{rec} = \dot{n}^{rec} - \dot{n}_{dry}^{rec} \tag{A10}$$

$$y_j^{Aout} = y_j^{rec} = \frac{\dot{n}_j^{rec}}{\dot{n}^{rec}} \tag{A11}$$

Similarly, the molar flow rates and gas composition on a wet basis at *Ain* can be calculated using Eqs. (A12)–(A15).

$$\dot{n}_{dry}^{Ain} = \frac{\dot{n}_{dry}^{rec} X_C^{Aout} + \dot{n}_C^{in}}{X_C^{Ain}} \tag{A12}$$

$$\dot{n}_{H_2O}^{Ain} = 0.5\dot{n}_{dry}^{rec} X_H^{Aout} + \dot{n}_{H_2O}^{rec} + 0.5\dot{n}_H^{in} + 0.5\dot{n}_{dry}^{Ain} X_H^{Ain} \tag{A13}$$

$$\dot{n}_i^{Ain} = x_i^{Ain} \dot{n}_{dry}^{Ain} \tag{A14}$$

$$y_j^{Ain} = \frac{\dot{n}_j^{Ain}}{\dot{n}_{dry}^{Ain} + \dot{n}_{H_2O}^{Ain}} \tag{A15}$$

List of symbols

Abbreviations

AOGR	Anode off-gas recycling

Variables and Constants

$\dot{n}$	Flow rate / mol s^{-1} or NLPM
y_j	Fraction of substance j in humid gas / 1
Y_e	Sum of fractions y of element e in humid gas / 1
x_i	Fraction of substance i in dried gas / 1
X_e	Sum of fractions x of element e in dried gas / 1
$A_{e,j}$, $A_{e,i}$	Number of elements e in substance j,i / 1
F	Faraday constant / 96485 C mol^{-1}

FU_{SYS}	System fuel utilization / 1
FU_{SOFC}	SOFC single-pass fuel utilization / 1
R	Recirculation ratio of anode-off gas / 1
z	Number of free electrons in component j / 1
ΔH	Heat of combustion / kJ mol^{-1}

Superscripts

Ain	Anode inlet gas
Aout	Anode outlet gas
rec	Recycle gas
in	System inlet fuel, e.g. natural gas
k	*Ain, Aout, in, rec* process location
Min	Module inlet air
Cin	Cathode inlet air
Cout	Cathode outlet air
Atot	Total anodic leakage
Atot(ox)	Total fully combusted anodic leakage
Atot,visc	Viscous anodic leakage
Atot,diff	Diffusive anodic leakage
Ctot	Total cathodic leakage

Subscripts

e	elements C, H, O, N
j	substances of humid fuel gas C_nH_m, CO, CO_2, H_2, H_2O, O_2, N_2
i	substances of dried fuel gas C_nH_m, CO, CO_2, H_2, O_2, N_2
n	number of carbon atoms in compound
m	number of hydrogen atoms in compound
LHV	lower heating value

Units

NLPM	flow rate in litres per minute at nominal conditions T = 0 °C, p=1013.25 hPa
mol-%	mole fraction as a percentage
ppm	mole fraction as parts per million

6 References

[1] J. W. Fergus, *Journal of Power Sources* **2005**, *147*, 46–47.
[2] J. F. Rasmussen, P. V. Hendriksen, A. Hagen, *Fuel Cells* **2008**, *8 (6)*, 385–393.
[3] M. Powell, K. Meinhardt, V. Sprenkle, L. Chick, G. McVay, *Journal of Power Sources* **2012**, *205*, 377–384.
[4] M. Halinen, O. Thomann, J. Kiviaho, *International Journal of Hydrogen Energy* **2014**, *39*, 552–561.
[5] Z. Wuillemin, N. Autissier, A. Nakajo, M. Luong, J. Van herle, D. Favrat, *Journal of Fuel Cell Science and Technology* **2008**, *5 (011016)*, 1–9.
[6] M. Halinen, M. Rautanen, J. Saarinen, J. Pennanen, A. Pohjoranta, J. Kiviaho, M. Pastula, B. Nuttall, C. Rankin, B. Borglum, *ECS Transactions* **2011**, *35 (1)*, 113–120.
[7] B. Borglum, E. Tang, M. Pastula, *ECS Transactions* **2011**, *35 (1)*, 63–69.
[8] R. J. Kee, E. S. Hetch, G. K. Gupta, H. Zhu, A. M. Dean, L. Maier, O. Deutschmann, *Applied Catalysis A: General* **2005**, *295*, 40–51.
[9] E. N. Fuller, P. D. Schettler, J. C. Giddings, *Industrial and Engineering Chemistry* **1966**, *58 (5)*, 19.
[10] S. Samuelsen, Y. Yaofan, A. D. Rao, C. Brouwer, *Journal of Power Sources* **2005**, *144*, 67–76.

PUBLICATION [P5]

Experimental study of SOFC system heat-up without safety gases

In: International Journal of Hydrogen Energy 39, pp. 552-561

Available online at www.sciencedirect.com

ScienceDirect

journal homepage: www.elsevier.com/locate/he

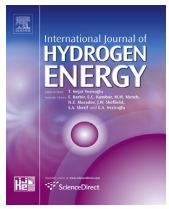

Experimental study of SOFC system heat-up without safety gases

M. Halinen, O. Thomann, J. Kiviaho*

VTT Technical Research Centre of Finland, Espoo, Finland

ARTICLE INFO

Article history:
Received 13 August 2013
Received in revised form
2 October 2013
Accepted 7 October 2013
Available online 8 November 2013

Keywords:
Solid oxide fuel cell
System
Reformer
Heat-up
Start-up
Anode off-gas recycling

ABSTRACT

Premixed safety gas is conventionally used to keep the anode of a solid oxide fuel cell (SOFC) under reducing conditions during heat-up. This article presents the results of an experimental study to heat up a SOFC system and stack without the said premixed safety gases, i.e. by utilizing a natural gas pre-reformer and anode off-gas recycling (AOGR). Firstly, ex-situ experiments were conducted to investigate the operability of a pre-reformer during system heat-up. It was found that any oxygen fed to the reformer hinders the reforming reactions at low temperatures. Secondly, based on the ex-situ findings, series of heat-up cycles were conducted with a complete 10 kW system using AOGR and a planar SOFC stack. In these experiments it was found that the system heat-up is possible with fuel gas and steam only, without the need for premixed reducing safety gases. Use of the fuel gas instead of a premixed safety gas did not result in a significant performance loss in the SOFC stack. Therefore, such a heat-up strategy was developed for SOFC systems that reduces the need of premixed safety gas storage space and thus decreases the system cost.

1. Introduction

Solid oxide fuel cells (SOFCs) enable energy production from different hydrocarbon fuels with high efficiency. SOFCs require high operating temperatures, e.g. 700–800 °C for anode supported cell types. Thus the fuel cell stack and other system components have to be heated up to operating temperature before the electricity production can begin. Lengthy heat-up times of several hours may be required to maintain the temperature gradient and the thermal stresses in the stack at acceptable level [1].

The nickel in the SOFC anode substrate has to remain at reduced state at elevated temperatures. This is accomplished by supplying sufficient amount of fuel or other reducing gas to the stack. If the reducing gas supply is discontinued, then the nickel in the anode substrate will start to re-oxidize, which will first deteriorate the cell performance and eventually destroy the SOFC by cracking the cell [2]. First signs of the oxidation of the nickel cermet anode have been measured as low as 290 °C [3], and it has been shown that the oxidation of the anode substrate proceeds more rapidly as the temperature increases [4]. Permanent damage to the cell may occur in a matter of minutes if there is forced oxygen supply to the anode [5]. Indeed, without the forced oxygen supply and by minimizing the time under oxidizing conditions at elevated temperatures, the redox tolerance of the stack can increase significantly [6]. Ideally, the re-oxidation could be avoided, if no oxygen is transported to anode. However, the anode supported SOFC stack is not a hermetically sealed device, and some air will eventually leak from the cathode side of the stack via the electrolyte or stack seals [7]. Additionally, ambient air can leak to the anode through other fuel system

* *Corresponding author.*
E-mail address: matias.halinen@vtt.fi (M. Halinen).
0360-3199/$ – see front matter
http://dx.doi.org/10.1016/j.ijhydene.2013.10.043

Table 1 – Test gas mixtures used for determining the light-off temperature.

Run		1	2	3	4	5	6	7
Gas flow/NLPM	Natural gas	0.5	0.5	0.5	0.5	0.5	0.5	0.5
	H_2O	10	10	10	10	10	10	10
	N_2	10	10	10	10	10	10	10
	H_2	–	–	0.2	0.05	0.1	0.15	0.4
	Air	–	0.5	0.5	0.5	0.5	0.5	0.5
H_2/O_2			0	2	0.5	1	1.5	4

components (e.g. reformer or heat exchanger) or through connecting piping from the air system. Therefore, it is necessary to feed reducing gas to the stack during the heat-up cycle to displace the oxygen in the fuel system and to protect the stack from re-oxidation. Furthermore, it may be necessary to sustain the flow of reducing gas for several hours during the system heat-up and cool-down, while the stack temperature is still high enough for significant re-oxidation and cell damage.

SOFC system concepts based on the anode off-gas recirculation (AOGR) achieve higher efficiencies and potentially simpler design when compared to systems without AOGR [8]. Therefore, they are considered technically advantageous, and there are studies where the AOGR has been successfully used in SOFC systems [9–11]. However, for a planar stack with cross-over leakage (air is leaking to fuel side and vice versa), utilization of AOGR complicates the heat-up procedure since there is a forced supply of oxygen to the fuel system due to the leakages. Furthermore, prior to starting the SOFC system electricity production, all fuel system components have to be heated up above the dew point before the recirculation of the anode off-gas with high steam content can be initiated. Otherwise, water could condensate to the system components (e.g. reformer catalysts and recirculation blowers), which would have detrimental effects on their operation.

The most straightforward way to provide a reducing gas supply is to utilize gas containers of premixed safety gas e.g. hydrogen–nitrogen mixtures. Indeed, due to its simplicity, this approach has been adopted by the majority of research laboratories that conduct research on solid oxide fuel cells or stacks. For example, the 10 kW demo unit at VTT [9] would consume ca. 5 bottles (50 L, 200 bars) of premixed safety gas with 4 vol-% of hydrogen during a heat-up cycle. In commercial products however, this approach is not desirable, due to large amount of gases needed for heat-up cycles spanning several hours. The gas containers require additional space, and increase the cost of both installation and servicing of the system. Thus it would be beneficial if the reducing gas could be generated with the existing Balance-of-Plant equipment which is fundamental for system operation. The most obvious solution would be to utilize the fuel supply (e.g. natural gas), the pre-reformer and the start-up steam generator to produce hydrogen-containing natural gas reformate.

In this article, the heat-up of a SOFC system and stack without using the premixed safety gases is investigated experimentally. Firstly, ex-situ experiments are conducted in a stand-alone reformer test bench. The experiments were done to realize the restrictions of reforming at low temperature in a system with AOGR and air leakage (i.e. forced oxygen supply to the fuel system). Secondly, series of heat-up cycles were done with a complete 10 kW SOFC system using AOGR and a planar SOFC stack. The results of the ex-situ experiments were applied to devise a safe heat-up procedure that would not damage the stack and removes the need for premixed safety gas. The performance of the stack was investigated after each heat-up to evaluate possible damage to the stack due to these heat-up procedures. There are several studies where the heat-up of a SOFC has been investigated by modelling [1,12–18], but to the authors' knowledge, no experimental work with a complete planar SOFC system utilizing AOGR has been published previously.

2. Experimental

2.1. *Ex-situ reformer experiments*

The ex-situ experiments were conducted in a separate reformer test bench described in detail in Ref. [19]. The aim of the experiment was to assess the activity of the catalyst at low temperature in steam reforming (Eq. (1)) using different inlet gas mixtures. This information is highly relevant to conduct the heat-up experiment on the SOFC system. The light-off temperature was determined by the reformer inlet gas temperature at which the reformer starts to convert methane to hydrogen according to Eq. (1).

$$CH_4 + H_2O \Leftrightarrow CO + 3H_2 \quad (1)$$

The reformer included a commercial precious metal monolithic catalyst (Süd-Chemie). The gas composition at the reformer outlet was monitored continuously with an online gas analysis equipment (IR-based for CH_4, thermal conductivity for H_2 and paramagnetic for O_2, Sick Maihak S700 series). Due to different channels cross-sensitivity, the analyser results should be used to evaluate trends and not as quantitative measurements. The temperature of the inlet gas was ramped up from 200…250–550 °C with a rate of ca. 2 °C min^{-1}. The gas hourly space velocity (GHSV i.e. gas volume flow at NTP divided by catalyst volume) used was ca. 32,000 h^{-1}. The different inlet gas mixtures investigated (Table 1) are relevant to SOFC system operated on natural gas including an anode-off gas recycling (AOGR) loop during first stages of the heat-up, where the fuel and steam supply have just been initiated. At that time, the temperature of both the pre-reformer and the stack are low and little or no reforming activity is expected to occur. Without reforming reactions, the gas

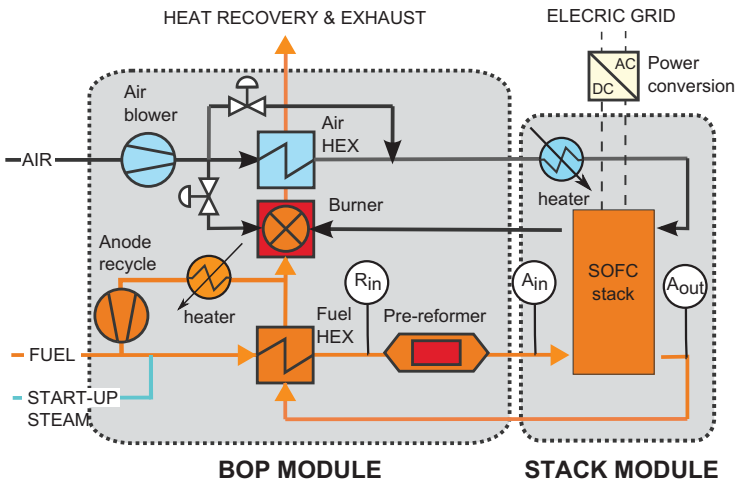

Fig. 1 – VTT 10 kW demo unit layout with fuel system gas sampling locations. Reproduced and adapted from Ref. [9]. Copyright 2011, The Electrochemical Society.

recirculating in the fuel system consists of the inlet flows i.e. fuel gas and steam as well as air originating from stack leakages. The test gas in run 1 consisted of natural gas (ca. 98% methane [19]), steam and nitrogen. A small fraction of air was introduced in the run 2–7 to simulate the effect of the presence of oxygen originating from air leakage to the fuel system and into the recycled gas. In the other test gases (run 3–7), hydrogen was added with varying H_2/O_2 ratio from 0 to 4 according to the Eq. (2).

$$O_2 + 2H_2 \Leftrightarrow 2H_2O \quad (2)$$

2.2. System heat-up experiments

The heat-up experiments were conducted on VTT's 10 kW SOFC demo unit [9]. The VTT demo unit consists of two interconnected modules, the balance of plant (BoP) module and the stack module, containing a planar SOFC stack (Fig. 1). The fuel system utilizes an AOGR loop, which enables operation without external steam supply when the stack current and single-pass fuel utilization are high enough. Ambient air is fed to the air system with a blower and filtered with a particle filter. Other system components include e.g. heat exchangers, catalytic burner and reformer which are necessary to maintain the thermal balance of the system and stack during operation. The SOFC stack was designed, manufactured and installed into the demo unit by Versa Power Systems (VPS), and it consisted of 64 planar anode supported cells with 550 cm^2 of active area [20]. The SOFC stack is located inside a thermally insulated and gas-tight module designed by VPS. Internal temperature of the stack is measured with thermocouples inserted at various locations inside the stack. Voltage is measured from each cell.

Fuel system gases were analysed at reformer inlet (R_{in}), anode inlet (A_{in}) and anode outlet (A_{out}) (Fig. 1). Anode outlet gas is recycled back to system inlet thus the recycling gas has

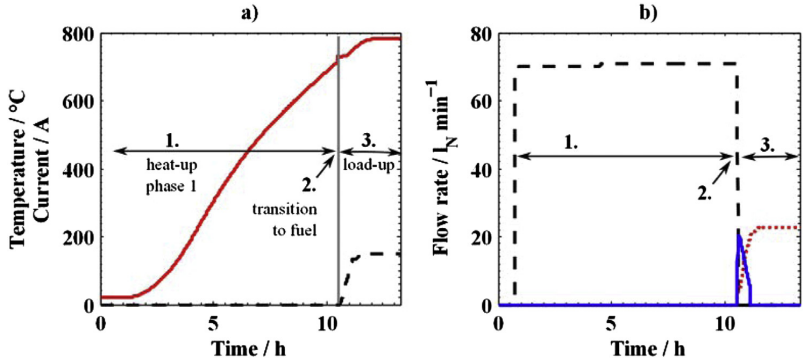

Fig. 2 – Standard start-up (a) Stack temperature (solid line) and current (dashed line) (b) Flow rate of premixed safety gas (dashed line), fuel (dotted line) and steam (solid line).

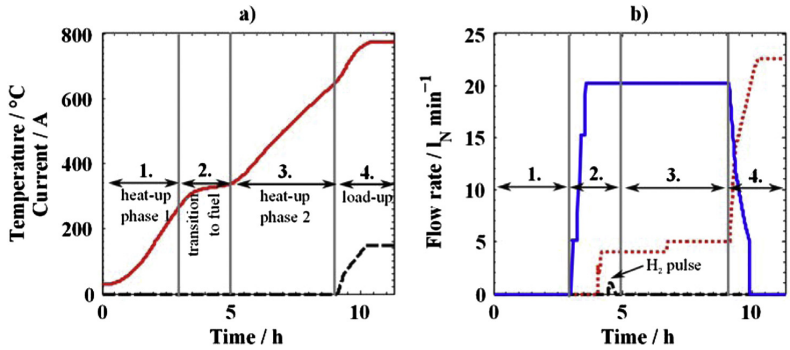

Fig. 3 – Experimental start-up (a) Stack temperature (solid line) and current (dashed line) (b) Flow rate of hydrogen pulse gas (dashed line), fuel (dotted line) and steam (solid line).

the same composition. Continuous gas analysis for CH_4, CO, CO_2, H_2 and O_2 is done with online gas analysis equipment.

The heat-up of the stack and the system was accomplished primarily with the electric heater of the stack module, which heated up the inlet stack air as well as the stack and the surroundings close to the operating temperature (Fig. 1). Secondarily, the heat-up was assisted by a smaller electric heater present in the AOGR loop. The reformer did not have an electric heater thus necessitating the need of temporary hydrogen pulse to start the reforming reactions in the pre-reformer and the stack, which is described in more detail in the following chapters. The rate of temperature change of the stack was below 3 °C min^{-1} during all heat-up cycles.

A standard laboratory style heat-up and start-up cycle has been previously established for this particular SOFC system (Fig. 2). The standard start-up consists of three different phases.

1. Heat-up phase. Premixed safety gas of 4 vol-% hydrogen and 96 vol-% of nitrogen (70 NLPM) is supplied to the fuel system, and air is supplied to air system with a blower (500 NLPM). AOGR is used continuously with an AOGR flow rate above 90 NLPM at all times.
2. Transition to fuel. After the heat-up phase, once the stack temperature is ca. 700 °C, a gradual transition from the premixed safety gas to fuel and steam supply is initiated. Once the transition is completed, premixed safety gas supply is stopped whereas 5 NLPM of natural gas and 20 NLPM of steam are supplied to fuel system.
3. Load-up phase. After transition to fuel gas, a load-up phase is commenced, where the stack current is first ramped up to 150 A, and later to 200 A which is the nominal operating current. During the load-up phase, the natural gas, steam and AOGR flow rates are changed proportionally to the stack current. The external steam supply is stopped at 115 A, once sufficient stack fuel utilization and concurrent transport of oxygen via the cell electrolyte are established. At higher currents, the fuel flow rate is increased, and the fuel system and the stack are kept free of carbon formation by AOGR alone.

In the experimental heat-up cycles devised for this study, the standard heat-up procedure was altered by dividing the heat-up into two distinct phases (Fig. 3).

1. Heat-up phase 1. Firstly, the stack is heated above 200 °C and all other components in the fuel system, e.g. reformer, AOGR blower and heat exchangers, to at least 100 °C (Fig. 3(a)). Similarly to the standard heat-up, AOGR is in operation and cathode air is fed with a blower.
2. Transition to fuel. Firstly, the steam supply is started once the minimum stack temperature is above 200 °C (Fig. 3). For safety reasons, the supply of hydrocarbon fuel was initiated only once the minimum measured in-stack temperature has reached 300 °C. This approach was chosen to eliminate the risk of accidental formation of toxic nickel carbonyl compounds in the SOFC stack. Reformer light-off was accomplished by a short-term hydrogen pulse.

Table 2 – Summary of different system heat-up cycles (HUs).

	Standard	HU1	HU2	HU3
HU phase 1 gas supply	Safety gas	Safety gas	None	None
Stack max. temperature at transition to fuel	700 °C	320 °C	350 °C	400 °C
HU phase 2 gas supply	–	Fuel & steam	Fuel & steam	Fuel & steam

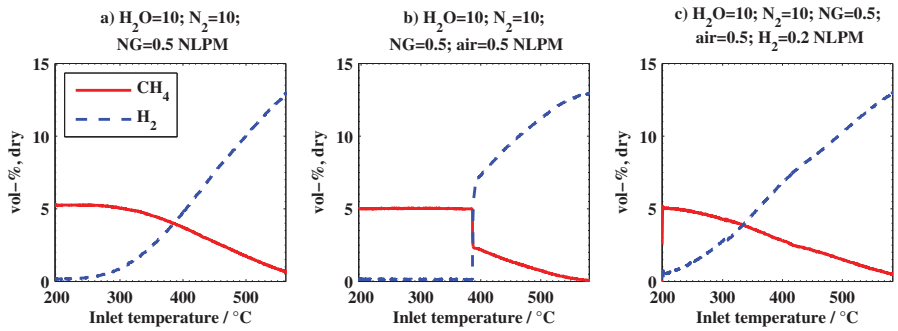

Fig. 4 – Reformer dry outlet gas composition against reformer inlet gas temperature. (a) fuel and steam (run 1), (b) addition of air (run 2) and (c) addition of air and hydrogen at stoichiometric ratio (run 3).

3. Heat-up phase 2. The system is heated up close to stack operating temperature with fuel reformate used as reducing safety gas.
4. Load-up. The load-up procedure remains similar for both standard and experimental heat-up cycles.

In order to assess the feasibility to heat-up a system without premixed safety gases, the demo unit and the SOFC stack were subjected to three different experimental heat-up cycles (HUs). The operational conditions were changed successively to more severe with respect to the possibility of re-oxidizing the stack (Table 2) i.e. higher stack maximum temperature was allowed before the transition to reducing fuel gas was done. Another important distinction between different heat-up cycles should be emphasized. Premixed safety gas (70 NLPM) was supplied during phase 1 only in HU1 (see Table 2). For HU2-3 there was no premixed safety gas supplied at all (see Table 2 and Fig. 3(b)). Instead, the gas during phase 1, circulating in the fuel system by the AOGR blower, was originating from whatever gas was leaking into the fuel system, through the stack or from other sources.

3. Results and discussion

3.1. *Ex-situ reformer experiments*

Fig. 4 illustrates the different qualitative results obtained in the ex-situ experiments. In Fig. 4(a), it can be seen that the catalyst exhibits some activity in steam reforming at temperature as low as 235 °C with test gas of run 1. The conversion of methane increases gradually with the inlet temperature. The inlet temperature at which the methane conversion by steam reforming starts is further referred to as the reformer light-off temperature. In Fig. 4(b), air is added to the test gas, simulating the effect of air leakage to fuel system. The catalyst behaviour is qualitatively very different compared to test gas of run 1, as no methane is reformed before ca. 390 °C. At ca. 390 °C, methane conversion starts abruptly, in other words, reformer light-off occurs.

Apparently, the presence of oxygen in air has an inhibitive effect on the steam reforming reactions at low temperature on this catalyst. In Fig. 4(c), hydrogen is added to the gas stream at stoichiometric ratio with oxygen. In this case, the catalyst exhibits some activity already at 200 °C and the conversion of methane increases gradually with the inlet temperature. This behaviour is qualitatively similar as the one obtained with the test gas of run 1 (Fig. 4(a)), performed with only natural gas and steam and in the absence of oxygen. It appears that the combustion reaction of hydrogen (Eq. (2)) takes place already at 200 °C. As a consequence, molecular oxygen and its inhibiting effect on steam reforming are removed by the reaction (Eq. (2)). Therefore, this enables methane conversion at reformer inlet temperature as low as 200 °C.

Fig. 5 illustrates the effect of the H_2/O_2 ratio on the light-off temperature. The light-off temperature is approximately 390 °C when H_2/O_2 ratio is zero and it decreases with increasing H_2/O_2 ratio to fall below 200 °C at H_2/O_2 ratio of two (corresponding to the stoichiometric ratio of H_2 and O_2).

The results show that methane conversion can be triggered by two ways in the reformer during the heat-up of a SOFC system. Firstly, if no hydrogen is supplied, the reformer inlet gas temperature has to be ca. 400 °C because of the inhibitive effect of oxygen originating from air leakages and recycled by the AOGR loop. Alternatively, the light-off temperature can be decreased by supplying a relatively small amount of hydrogen. Thus the hydrogen production can start already at

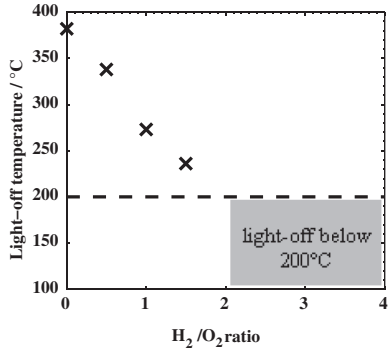

Fig. 5 – The effect of the H_2/O_2 ratio on the light-off temperature of the reformer, results from run 2–7.

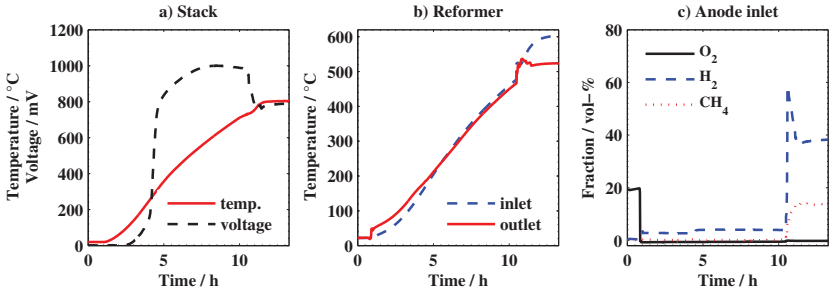

Fig. 6 – Standard heat-up cycle with premixed safety gas (a) stack temperature and average cell voltage, (b) inlet and outlet temperature of the reformer (c) fraction of methane, hydrogen and oxygen in the anode inlet gas on dry basis.

temperature as low as 200 °C. These results suggest that during the heat-up of a SOFC system, a small amount of hydrogen can be supplied to the reformer inlet to trigger the activity of the reformer at low temperature and accomplish the light-off. This is advantageous because the hydrogen produced in the reformer protects the SOFC anode from the damaging effects of re-oxidation. These results are further exploited to design the experiments on system level presented in the next Section 3.2.

3.2. *System heat-up experiments*

3.2.1. *Standard heat-up*

A more detailed planning of the heat-up (HU) cycles was done based on results of the ex-situ experimental results presented in Chapter 3.1. At the time of the experiments, there was no possibility to pre-heat the reformer inlet gas to 400 °C in the 10 kW demo unit, since the pre-heating of the reformer inlet gas was realized only with the fuel system heat exchanger (see Fig. 1). Therefore, it was decided to accomplish the reformer light-off in HUs 2–3 with short-term hydrogen pulse of ca. 1 NLPM during the heat-up cycle.

Firstly, the characteristics of the stack and the reformer during a standard heat-up cycle are depicted in Fig. 6. Before the heat-up is commenced, the hydrogen-containing reducing safety gas supply and AOGR are activated. This is evident at test time ca. 1 h in Fig. 6(c), where the fraction of oxygen is decreased from 21 vol-% to zero and replaced by hydrogen (and nitrogen). Interestingly, the introduction of hydrogen containing safety gas can be observed also by an increase of the reformer T_{outlet} (Fig. 6(b)). This can be explained by the high activity of the precious-metal catalyst used in the pre-reformer. The reaction (Eq. (2)) between the oxygen, leaking into the fuel system (through stack or otherwise), and hydrogen in the safety gas is occurring already at room temperature. Thus the pre-reformer is disposing all oxygen from the anode inlet gas (Fig. 6(c)).

In a standard heat-up, the voltage of the stack starts to increase already at ca. 150 °C stack T_{max} (Fig. 6(a), $t = 3$ h). Significant and faster increase in the stack voltage is present between 250 and 300 °C stack T_{max} (Fig. 6(a), $t = 4–5$ h). The increase of the stack voltage can be interpreted as the start and progression of the reduction process. Additionally, the difference between the reformer outlet and inlet temperature diminishes to zero once the stack temperature reaches 400 °C (Fig. 6(b), $t = 5$ h), and no oxygen is detected anymore in the anode outlet gas, which indicates that oxygen is reacting with hydrogen already in the stack.

After the heat-up, the transition from safety gas to fuel gas and the load-up procedure are observed as an increase of both hydrogen and methane fractions at the anode inlet (Fig. 6(c), $t = 10$ h), and as a decrease in stack voltage (Fig. 6(a)).

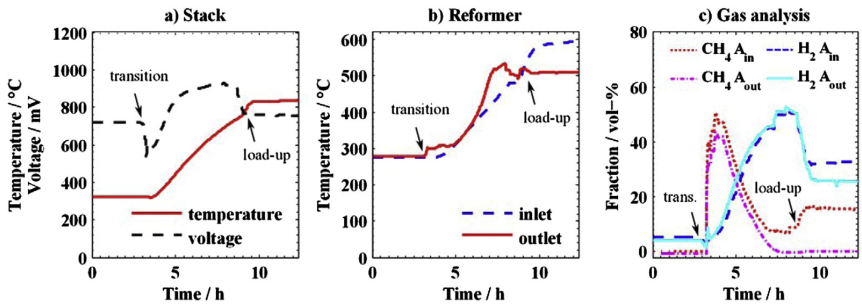

Fig. 7 – Heat-up cycle 1 (a) stack temperature and average cell voltage, (b) inlet and outlet temperature of the reformer (c) fraction of methane and hydrogen in the anode inlet/outlet gas on dry basis.

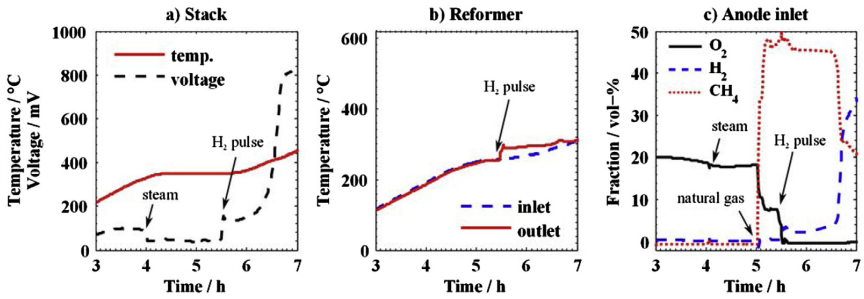

Fig. 8 – Fuel transition of heat-up cycle 2 with no premixed safety gas (a) stack temperature and average cell voltage, (b) inlet and outlet temperature of the reformer (c) fraction of methane, hydrogen and oxygen at the anode inlet on dry basis.

Concurrently, the endothermic steam reforming reactions cause that the T_{outlet} of the pre-reformer decreases ca. 80 °C below the T_{inlet} (Fig. 6(b)).

3.2.2. *Heat-up experiment 1*

The experimental heat-up cycle 1 (HU1) is depicted in Fig. 7. In HU1 the premixed safety gas was still used during heat-up phase 1 (see Table 2) and transition to fuel was done with the stack T_{max} of 320 °C by decreasing the premixed safety gas flow from 70 NLPM to zero and increasing the natural gas and steam flow rates to 5 and 20 NLPM, respectively. The transition to fuel is evident as a drop in the stack voltage (Fig. 7(a), $t = 3$ h), increase in reformer T_{outlet} (Fig. 7(b), $t = 3$ h) and increase in the CH_4 fraction of the fuel system gases (Fig. 7(c), $t = 3$ h). Lower voltage in HU1 compared to standard heat-up can be explained by the higher amount of steam in the fuel gas which decreases the Nernst potential of the cell. The stack voltage increases with the stack temperature as the H_2 fraction of the fuel gas increases ($t = 3$–5 h).

It should be noted that the steam reforming reactions and therefore the majority of the hydrogen production occurs in the SOFC stack throughout the heat-up cycle, since the temperature of the pre-reformer remains lower than the stack. Nearly all methane is converted to hydrogen in the stack once the stack T_{max} reaches 650 °C (Fig. 7(c), $t = 7$ h) and the resulting hydrogen-rich gas is fed back to reformer inlet with AOGR. Concurrently, the reformer inlet temperature is still at ca. 400 °C at that time (Fig. 7(b), $t = 7$ h). The combination of hydrogen-rich inlet gas and low temperature causes that exothermic methanation reaction (reverse to Eq. (1)) takes place in the pre-reformer instead of steam reforming. This can be observed (Fig. 7(b), $t = 6$–9 h) as a second increase of the reformer T_{outlet} above T_{inlet} before the load-up ($t = 8.5$ h) after the first increase caused by oxidation of hydrogen in the reformer (Fig. 7(b), $t = 3$–5 h).

Similarly to the standard heat-up, steam reforming in the pre-reformer starts during the load-up, once more fuel is supplied to the system, and the reformer T_{inlet} increases above 500 °C (Fig. 7(b)). Even though the Ni-cermet of the SOFC stack makes it a very efficient steam reformer during the heat-up process, the amount of hydrogen remains relatively low, below 10 vol-% (dry basis) at the beginning of the heat-up cycle. Marked increase of hydrogen starts to occurs only at higher temperatures, when the stack T_{max} is above 400 °C (Fig. 7(c), $t = 4$ h). Since the pre-reformer has the capability for steam reforming as well, it would be beneficial to operate the reformer at higher temperature during that time i.e. when relatively little methane is reformed in the stack. Therefore, when the fuel supply is started, the reformer T_{inlet} should preferably be above 550 °C to accomplish both reformer light-off and immediate production of H_2-rich gas. However, a pre-reformer is required and very useful also when it is used at lower temperature than the stack, since it removes any oxygen from the anode inlet gas.

3.2.3. *Heat-up experiments 2 and 3*

The experimental heat-up cycle 2 (HU2) is depicted in Fig. 8. It was observed that the system characteristics were similar to HU1 soon after the transition to fuel was done, thus the measurements depicted in Fig. 8 are shown only for this transition phase. In HU2, the stack T_{max} was ca. 350 °C when the transition to fuel gas was done ($t = 4$–5.5 h) and, additionally, no premixed safety gas was supplied to system at all. The reformer light-off was accomplished by a 10 min duration H_2 pulse. The transition to fuel was initiated by starting the steam supply at $t = 4$ h. At $t = 5$ h natural gas supply was started, and at $t = 5.5$ h the hydrogen pulse was done (see Fig. 8 for annotations).

During the phase 1 of the HU2, prior to fuel transition, the oxygen fraction in the fuel system gas is measured to be ca. 21 vol-%, which clearly shows that air is circulating in the fuel system and through the stack (Fig. 8(c), $t = 3$ h). The oxygen concentration is observed to decrease by ca. 1 vol-% before fuel transition at stack $T_{max} > 200$ °C ($t = 3$–4 h), which indicates that oxidation of the Ni-cermet starts to occur. Additionally, the cell voltage decreases once steam supply of 20 NLPM is started (Fig. 8(a), $t = 4$ h). The O_2 fraction decreases significantly, from 18 to 7.5 vol-%, upon introduction of 4 NLPM of natural gas (Fig. 8(c), $t = 5$ h) and the CH_4 fraction in the fuel system gas increases to nearly 50 vol-%, a sign that the flow rate of the air leaking into the fuel system is of the same magnitude i.e. 4 NLPM.

Similarly to the ex-situ reformer experiments no light-off occurred in the pre-reformer even at 250 °C reformer T_{inlet} due to oxygen present in the fuel system (Fig. 8(b), $t = 3$–5.5 h). The reformer light-off and production of H_2 is commenced

only after the H_2 pulse at $t = 5.5$ h, where a simultaneous decrease of O_2 fraction accompanied with a step-wise increase in the stack voltage, reformer T_{outlet} and H_2 fraction is observed. Interestingly, after turning off the H_2 pulse, the H_2 fraction at the anode outlet and inlet, as well as stack voltage show little or no further increase in nearly 1 h. After $t = 6.5$ h, a drastic increase in the stack voltage is observed which is explained by faster progressive reduction of the Ni-cermet. Concurrently, the fraction of CH_4 decreases and the H_2 increases suddenly at anode inlet and outlet gas, which is a sure indication of the activation of steam reforming reactions in the SOFC stack.

The experimental heat-up cycle 3 (HU3) was otherwise similar to HU2, but the duration of the H_2 pulse was longer, nearly 1 h, and the stack T_{max} was allowed to increase to 400 °C before starting the natural gas supply into the system. The results with respect to the behaviour of the reformer are alike to HU2 (Fig. 8). Therefore, detailed presentation of the measurements during HU3 is omitted to avoid repetition of the discussion. Instead, the difference of HU3 compared to other heat-up cycles is discussed next in Chapters 3.2.4 and 3.3.

3.2.4. *Reduction and reforming activity of the anode during heat-up*

There are specific differences between the HU1 (safety gas used) and HU2-3 (no safety gas used) with respect to (i) reduction/oxidation behaviour of the stack and (ii) the activity of the Ni-cermet to catalyse steam reforming reactions. This phenomenon is illustrated with Fig. 9, where the flow of fuel and hydrogen, as well as the average cell voltage and the H_2 fraction at anode outlet, are presented for HU1-3. The measurements are plotted as a function of stack T_{max}, a common denominator for the phenomenon under discussion. It should be noted that the stack T_{max} is relative to test time as well, since heating of the stack occurred at relatively steady rate of ca. 2 °C min^{-1} from 300 to 500 °C.

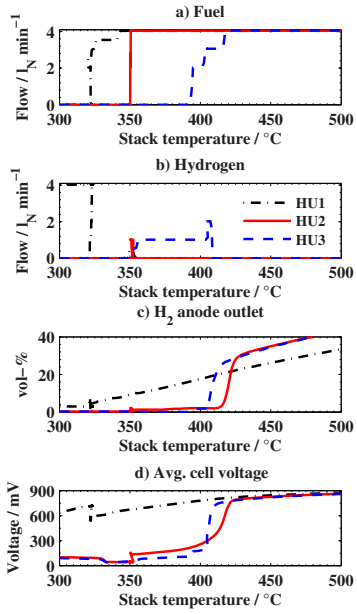

Fig. 9 – Reduction and reforming in the stack for HU1-3 (a) fuel flow (b) hydrogen flow, (c) fraction of H_2 in anode outlet gas and (d) average cell voltage.

Qualitatively, it is evident that in HU1 the stack is already more reduced (stack voltage is higher) and also catalytically active with respect to steam reforming. In HU1, the H_2 fraction at the anode outlet as well as voltage increases steadily with the stack temperature (Fig. 9(c–d)), occurring immediately when the H_2 supply is stopped and fuel supply started (Fig. 9(a–b)). Moreover, the results show that the steam reforming reactions and H_2 production in the stack can start already at 300–350 °C.

In HU2, the short-term H_2 pulse of 10 min duration is triggering both reduction and reforming activity in the stack, observed as a stepwise transition for both H_2 and stack voltage (Fig. 9(c–d)). However, the stack has to heat up ca. 70 °C more to 420 °C (in 1 h, see also Fig. 8) until the reduction of the stack has proceeded to a level where a notable recovery of the stack voltage, as well as in increased reforming activity is observed.

In HU3, however, the recovery of stack voltage as well as reforming activity is occurring nearly simultaneously with the introduction of the natural gas. Faster recovery can be related to longer duration of the H_2 pulse. The H_2 flow is started once the stack temperature reached 350 °C, and the reduction process of the stack can proceed while the stack heats up to 400 °C (Fig. 9(b)). Thus the reduction is completed faster in HU3 once the natural gas supply is initiated. However, the 1 NLPM of H_2 in HU3 is insufficient to reduce the entire active cell area since no H_2 is detected in the anode outlet gas at first. The H_2 is present in anode outlet gas only after transition to fuel is complete.

Based on the results it is clear that in HU2-3 both the electrochemical, as well as steam reforming activity, are first inhibited by the oxidation of the Ni-cermet already at lower temperature than 350 °C for stack T_{max}. Additionally, to realize the reduction of the Ni-cermet after oxidation has occurred at low temperature, all oxygen has be removed from the anode inlet gas (see Fig. 8) and replaced with high enough amount of hydrogen, so that there is hydrogen present at the anode outlet gas as well. Otherwise, it appears that the Ni-cermet of the stack will remain in oxidized state and will not start the steam reforming reactions, and the accompanied production of reducing hydrogen gas.

3.3. *Effect of the heat-up experiments on the SOFC performance*

Voltage characteristics of the SOFC stack is commonly used as a performance indicator. Thus the effects of the different heat-up cycles on the SOFC can be assessed by observing changes in the stack or individual cell voltages [6]. If the experiments cause permanent damage to the cells e.g. due to re-oxidation, it would be recorded as a stack voltage decrease.

Voltage characteristics of the SOFC stack were investigated by conducting a load-up cycle to 150 A (0.273 A cm^{-2}) after each heat-up experiment and allowing the system to stabilize for 20 h (Fig. 10(a–c)). After the stabilization, the individual

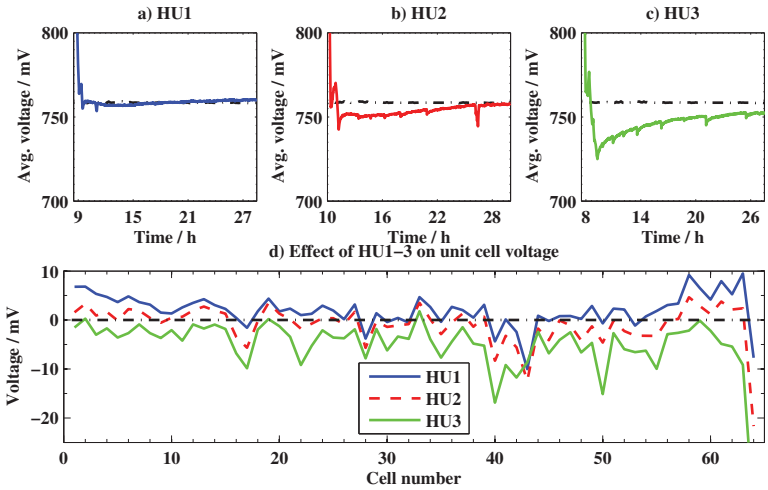

Fig. 10 – Effect of HU1-3 on stack performance. (a–c) average cell voltage after load-up for HU1-3 (solid line) and prior to experiments (dashed line) (d) difference in unit cell voltages after each heat-up cycle.

voltage measurements from all 64 cells of the stack were averaged for a period of 1 h. Then, a difference was calculated to the measurements at 150 A prior to performing any of the experiments HU1-3 (Fig. 10(d)). The average cell voltage prior to HU1-3 is also shown in Fig. 10(a–c).

The majority of the cells in the stack do not show any performance deterioration after the HU1-2 compared to the values recorded at 150 A prior to experiments (Fig. 10(a),(b) and (d)). However, after the HU3 the average cell voltage is ca. 6 mV lower at the end of the stabilization period (Fig. 10(c)), and nearly all cells exhibit voltage decrease (Fig. 10(d)). In the HU3 the stack maximum temperature was allowed to increase up to 400 °C before the supply of fuel gas was started. Thus it is possible that the higher temperatures used in HU3 may have caused too severe oxidation of the anode, thus damaging the stack.

However, the differences of the cell voltages compared to prior measurements in Fig. 10(d) are small and within 10 mV for the majority of the cells. Moreover, some of the cells exhibit increased voltage compared to prior measurement. This indicates that the resulting differences in the voltage between the heat-up cycles can be partly explained by other effects as well e.g. by the variation of the in-stack temperature distribution due to small hysteresis of the plant controllers. Additionally, deep thermal cycling of a SOFC stack down to room temperature can cause damage and performance loss of the stack even with premixed reducing gas, and this phenomena can also contribute to the apparent lower cell voltage with increased number of heat-up cycles.

Therefore, this comparison of the cell voltage distribution with respect to the effect of the heat-up cycles should be treated as indicative rather than conclusive since there are other mechanisms which can affect the performance of cells. However, the results show that the stack can withstand a heat-up cycle with fuel reformate and AOGR without any significant performance deterioration. Moreover, stack temperatures below 350 °C appears to be a more beneficial region to introduce the fuel gas and trigger the reforming reactions to produce hydrogen-rich reducing gas because (i) performance loss was measured after HU3 when the stack was heated up to 400 °C before starting the fuel supply and (ii) the Ni-cermet is oxidized already below 350 °C which prevents steam reforming reactions.

4. Conclusions

The results of this study clearly show that it is essential to investigate the characteristic operation of the system pre-reformer to accomplish a safe heat-up cycle. Furthermore, the interactions with other system components e.g. air leakages and the choice for system layout, such as the use of AOGR, will affect the feasibility of any heat-up strategy and have to be taken into account.

The light-off temperature, i.e. start of the reforming reactions in a pre-reformer, is significantly affected by the use of AOGR and any leakages of air to the fuel system, through stack or otherwise. The light-off temperature is increased by ca. 200 °C when oxygen is present in the reformer inlet gas. However, it is possible to accomplish lower reformer light-off temperatures by adding hydrogen to the reformer inlet.

SOFC stack is an efficient steam reformer due to high amount of catalytically active nickel in the anode cermet, and thus is an obvious solution to produce the hydrogen-rich reducing gas from the fuel during system heat-up. It is observed, that the SOFC stack can start sufficient steam reforming and production of hydrogen-rich reducing gas at temperatures above 400 °C. However, oxidation of the anode Ni-cermet in system conditions can proceed already below 350 °C, which inhibits the reforming activity of the anode. Thus, the usage of a pre-reformer to remove trace oxygen from the anode inlet gas is required with AOGR, since any air

leakages to fuel system will retain the anode in oxidized state. Moreover, some performance loss was measured when the stack was heated to 400 °C before fuel supply was started. Therefore, it is recommended that the supply of hydrogen-rich reducing gas is started already below 350 °C, or as low temperature as possible, to prevent oxidation of the Ni-cermet.

During the system experiments it was noted that sufficient temperatures for pre-reformer light-off were not possible by relying only on the heat recuperated from the fuel system heat exchanger. Thus electrically or otherwise assisted heating of the pre-reformer (i) to 400 °C enables reformer light-off without the short-term hydrogen pulse, thus simplifying the system layout even further and (ii) above 500 °C shifts the hydrogen production from the stack to pre-reformer, which increases the amount of hydrogen when the reforming activity of the stack is still low and thus enhances the quality of the reducing gas. Additionally, if the pre-reformer would be mainly responsible of the hydrogen production, the stack temperature can potentially be lower than 300 °C when the fuel is introduced to the system. This would significantly decrease the risk of oxidizing the Ni-cermet anode.

The results show that a heat-up from room temperature to the operating temperature of SOFC stack is possible without premixed gas and without significant loss of stack performance. This finding allows reducing the premixed gas storage capacity in a SOFC system and thus the physical size of the system as well capital and servicing costs.

Acknowledgements

Funding for this study was obtained through the projects SofcPower and RealDemo. The Finnish Funding Agency for Technology and Innovation (TEKES) as well as the companies participating in the project are gratefully acknowledged for their financial support. M. Halinen would like to thank T. Hottinen from Wärtsilä Finland and M. Pastula from Versa Power Systems for the helpful discussions related to the system experiments. M. Rautanen from VTT is acknowledged for his essential assistance in the experiments.

REFERENCES

[1] Selimovic A, Kemm M, Torisson T, Assadi M. Steady state and transient thermal stress analysis in planar solid oxide fuel cells. J Power Sources 2005;145:463–9.
[2] Ettler M, Timmermann H, Malzbender J, Weber A, Menzler NH. Durability of Ni anodes during reoxidation cycles. J Power Sources 2010;195:5452–67.
[3] Jeangros Q, Faes A, Wagner JB, Hansen TW, Aschauer U, Van herle J, et al. In situ redox cycle of a nickel–YSZ fuel cell anode in an environmental transmission electron microscope. Acta Mater 2010;58(14):4578–89.
[4] Pihlatie M, Kaiser A, Mogensen M. Redox stability of SOFC: thermal analysis of Ni–YSZ composites. Solid State Ionics 2009;180:1100–12.
[5] Laurencin J, Roche V, Jaboutian C, Kieffer I, Mougin J, Steil MC. Ni-8YSZ cermet re-oxidation of anode supported solid oxide fuel cell: from kinetics measurements to mechanical damage prediction. Int J Hydrogen Energy 2012;37:12557–73.
[6] Brabandt J, Fang Q, Schimanke D, Heinrich M, Mai BE, Wunderlich C. System relevant redox cycling in SOFC stacks. ECS Trans 2011;35(1):243–9.
[7] Rasmussen JFB, Hendriksen PV, Hagen A. Study of internal and external leaks in tests of anode-supported SOFCs. Fuel Cells 2008;8(6):385–93.
[8] Peters R, Deja R, Blum L, Pennanen P, Kiviaho J, Hakala T. Analysis of solid oxide fuel cell system concepts with anode recycling. Int J Hydrogen Energy 2013;38(16):6809–20.
[9] Halinen M, Rautanen M, Saarinen J, Pennanen J, Pohjoranta A, Kiviaho J, et al. Performance of a 10 kW SOFC demonstration unit. ECS Trans 2011;35(1):113–20.
[10] Dietrich RU, Oelze J, Lindermeir A, Spitta C, Steffen M, Küster T, et al. Efficiency gain of solid oxide fuel cell systems by using anode offgas recycle – results for a small scale propane driven unit. J Power Sources 2011;196(17):7152–60.
[11] Powell M, Meinhardt K, Sprenkle V, Chick L, McVay G. Demonstration of a highly efficient solid oxide fuel cell power system using adiabatic steam reforming and anode gas recirculation. J Power Sources 2012;205:377–84.
[12] Rancruel D, von Spakovsky M. Investigation of the start-up strategy for a solid oxide fuel cell based auxiliary power unit under transient conditions. Int J Thermodyn 2005;8(2):103–13.
[13] Apfel H, Rzepka M, Tu H, Stimming U. Thermal start-up behaviour and thermal management of SOFC's. J Power Sources 2006;154:370–8.
[14] Ki J, Kim D. Computational model to predict thermal dynamics of planar solid oxide fuel cell. J Power Sources 2010;195:3186–200.
[15] Jiang W, Fang RF, Khan J, Dougal R. Control strategies for start-up and part-load operation of solid oxide fuel Cell/Gas turbine hybrid system. J Fuel Cell Sci Technol 2010;7:0110161–9.
[16] Damm LD, Fedorov AG. Reduced-order transient thermal modeling for SOFC heating and cooling. J Power Sources 2006;159:956–67.
[17] Chen MH, Jiang TL. The analyses of the start-up process of a planar, anode-supported solid oxide fuel cell using three different start-up procedures. J Power Sources 2012;220:331–41.
[18] Petruzzi L, Cocchi S, Fineschi F. A global thermo-electrochemical model for SOFC systems design and engineering. J Power Sources 2003;118:96–107.
[19] Halinen M, Thomann O, Kiviaho J. Effect of anode off-gas recycling on reforming of natural gas for solid oxide fuel cell systems. Fuel Cells 2012;12(5):754–60.
[20] Borglum B, Tang E, Pastula M. Development of solid oxide fuel cells at versa power systems. ECS Trans 2011;35(1):63–9.

PUBLICATION [P6]

Stack Temperature Estimation in System Environment by Utilizing the Design of Experiments Methodology

In: ECS Transactions 57 (1), pp. 205-214

ECS Transactions, 57 (1) 205-214 (2013)
10.1149/05701.0205ecst ©The Electrochemical Society

Stack Temperature Estimation in System Environment by Utilizing the Design of Experiments Methodology

M. Halinen, A. Pohjoranta, J. Pennanen, and J. Kiviaho

VTT Technical Research Centre of Finland, Espoo, Finland

The behavior of the maximum temperature measured inside a SOFC stack with respect to three independent input variables (stack current, air flow and air inlet temperature) is examined by using a full factorial screening experiment, following the design of experiments methodology. The experiments were carried out with a complete 10 kW_e SOFC system. Multivariate regression models are developed to estimate said temperature and a statistical analysis is carried out on the model parameters.

Introduction

The temperature of and inside a planar solid oxide fuel cell (SOFC) stack is a property of interest for several reasons; the stack temperature affects the stack performance as well as its degradation rate (1,2). Moreover, the stack characteristics do not remain identical over its lifetime due to voltage degradation – with constant system inputs the stack temperature will increase as the stack degrades. Therefore, it is highly desirable to monitor the internal stack temperature for control and diagnosis purposes. The temperature inside an SOFC stack can be measured directly by installing measurement probes inside the stack. However, in commercial systems direct measurement of the temperature can be difficult and costly, and can also decrease the stacks' durability due to the increased complexity. Therefore, estimating the stack temperature indirectly, from other process measurements, is well-motivated. In reality, the stack temperature is certainly not a single temperature value, but an infinite number of temperature values distributed continuously over the stack. For practical purposes, however, a single representative value is chosen, and this is the approach taken in this paper as well.

This paper reports a systematic effort carried out to create a simple numerical estimator for the maximum temperature measured inside a SOFC stack. Furthermore, the test protocol utilized in this work was also used to evaluate which system inputs are most effective for controlling the said temperature.

Multivariable Regression Modeling and the Design of Experiments

Multivariable linear regression (MLR) models are functions of the form

$$\hat{y} = \beta_0 + \beta_1 x_1 + \cdots + \beta_{p-1} x_{p-1} = \mathbf{X}\boldsymbol{\beta}, \text{ where } \mathbf{X} = [x_1 \quad x_2 \quad \cdots \quad x_{p-1}]. \qquad [1]$$

x_i and $\hat{y}$ are (column) vectors of the measured input and estimated output values, respectively. The parameter vector $\boldsymbol{\beta} = [\beta_1 \quad \beta_2 \quad \cdots \quad \beta_{p-1}]^T$ is calculated so to produce

an estimate which is optimal in the least squared error sense. See e.g. (3) for details on MLR modelling.

MLR models can be evaluated based on several criteria, but in this work mostly the adjusted-R^2 [2] and the root-mean-squared-error [3] were utilized – the former for its scalability with a varying number of model parameters and the latter for its ease of interpretation. Their values were computed as follows:

$$R^2_{adj} = 1 - \frac{(N-1)\sum_{i=1}^{N}(\hat{y}-y)^2}{(N-p)\sum_{i=1}^{N}(\bar{y}-y)^2} \quad [2]$$

$$RMSE = \sqrt{\frac{\sum_{i=1}^{N}(\hat{y}-y)^2}{(N-p)}} \quad [3]$$

In [2]-[3] N is the number of data points used, y the measured property value and $\bar{y}$ is the mean of y. p is the number of parameters in the regression model. The closer R^2_{adj} is to 1 or the smaller $RMSE$ is the better is the model considered to be.

Obtaining rich data that sufficiently covers the domain of interest is the most important step in creating regression models. To this end, a series of experiments were designed by following the design of experiments (DoE) methodology. The DoE methodology is especially suitable to be applied hand-in-hand with multivariable regression modeling. Good coverage of the DoE methodology is found in several text-books, e.g. (3) and therefore DoE is not discussed here in detail.

Experimental

A full factorial experiment design, with three factors (input variables), each of them obtaining two levels (the minimum and the maximum) and a nominal level, was carried out. The system response, i.e. the maximum temperature of the stack, was obtained by recording the values of several temperature measurements placed inside a SOFC stack and then using the maximum of the measured values. The test plan, i.e. the factors, their levels and the experimental conditions' execution order is given in Table I. The test plan was designed so that the execution time of all experiment conditions (relative to start time of the designed experiments) was fixed in advance. Then, a D-optimal test plan considering the three factors plus time as the model input was calculated by varying the experiment conditions' order. The aim was to maximize the information obtained with the experiment design, also with respect to the stack performance degradation, which increases with time.

A minimum stabilization period of 24 hours was reserved per condition. A longer interval between conditions 4 and 5 is due to the weekend falling amidst the test run and the system was brought to the nominal operating condition (NOC) for this period, enabling thus also the repetition of the NOC.

The experiments were carried out according to the test plan with a complete 10 kW_e SOFC demonstration unit (4). The demo unit was equipped with a planar SOFC stack by

Versa Power Systems (5). The stack had 64 cells with ca. 550 cm^2 of active area. The designed experiments were started at 145 hours into the test run. Before this, the system was brought to NOC for stabilization after the start-up. All-together the test run lasted for 470 hours, of which the designed experiments (including the first and last NOC) took ca. 300 hours.

TABLE I. Test Plan of the Full Factorial Experiment and Description of Additional Experiment Conditions. The experiment condition numbers refer to figure 2(b).

Data short desc.	Exp. cond. #	Current (x_1) A	Air flow (x_2) l_N/min	Air inlet temperature (x_3) °C	Time from test start (t) h
Nominal	3, 4, 5, 10, 11, 12, 17	200	1063	695	-
DoE	6	205	962	705	145
	7	195	1162	685	169
	8	205	1162	685	193
	9	195	962	705	217
	13	195	1162	705	313
	14	205	962	685	337
	15	195	962	685	361
	16	205	1162	705	385
Part-load	1, 2	150	960	705-695	25-50

A graphical representation of the 2^3 full factorial experiment design is given in Figure 1.

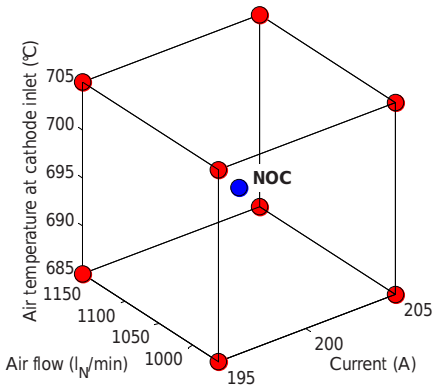

Figure 1. The input variables' domain of variation in the experiment design.

Data Analysis and MLR Modeling

Figure 2 shows the input variables' time-series during the experiment, with the steady-state experiment conditions marked with red circles. The completed experiment provided data from altogether 17 conditions (points 1-17 in Fig. 2(b)): 8 non-nominal experiment conditions (pts. 6-9, 13-16), 7 repetitions of NOC at different time instants (with a minimum of 24 hours between the instants, pts. 3-5, 10-12, 17), and 2 extra

conditions measured during system start-up when the system was operating at part-load (with stack current of 150A, pts. 1-2). The 7 repeated measurements at NOC were carried out to capture system degradation effects and the part-load conditions were used for exploratory purposes, described further below. In Figure 2, the period of the designed experiments is indicated with the dashed vertical lines.

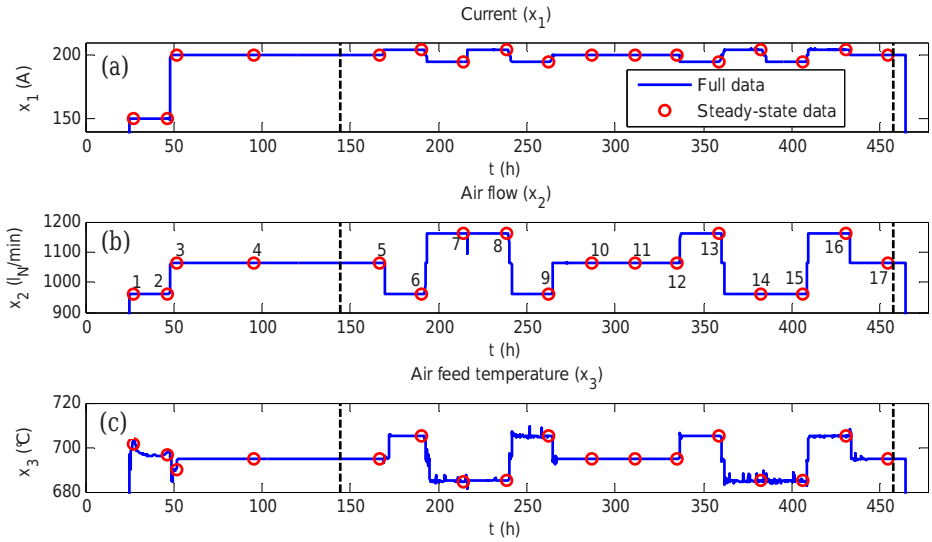

Figure 2. The input variables during the test run. Steady-state conditions are denoted with circles and indexed with a running number in subfigure (b).

Data Analysis

One aim of the data analysis was to resolve the significant input variables (and significant input interactions) with respect to the measured stack temperature. For the purpose of the input variables' significance analysis, the inputs were all scaled to the range [-1, 1] by using equation [4]. The input interactions were then calculated after scaling the inputs. Only the 13 data points from the period of designed experiments (8 non-nominal conditions + 5 repetitions in NOC) were used in this analysis.

$$x_{i,sc} = 2\frac{x_i - \min(x_i)}{\max(x_i) - \min(x_i)} - 1 \qquad [4]$$

For further analysis, the linear regression models [5] and [6], based on all (scaled) input variables and their interactions, as well as on only the input variables were fit to the data. Figure 3 shows the model coefficients of the models per input and input interaction, and the corresponding coefficients' 95 % confidence intervals (CIs). If the confidence interval of a coefficient includes zero, the respective term in the regression model can be concluded insignificant.

$$\hat{y} = \beta_0 + \beta_1 x_1 + \beta_2 x_2 + \beta_3 x_3 + \beta_{12} x_1 x_2 + \beta_{13} x_1 x_3 + \beta_{23} x_2 x_3 + \beta_{123} x_1 x_2 x_3 \qquad [5]$$

$$\hat{y} = \beta_0 + \beta_1 x_1 + \beta_2 x_2 + \beta_3 x_3 \qquad [6]$$

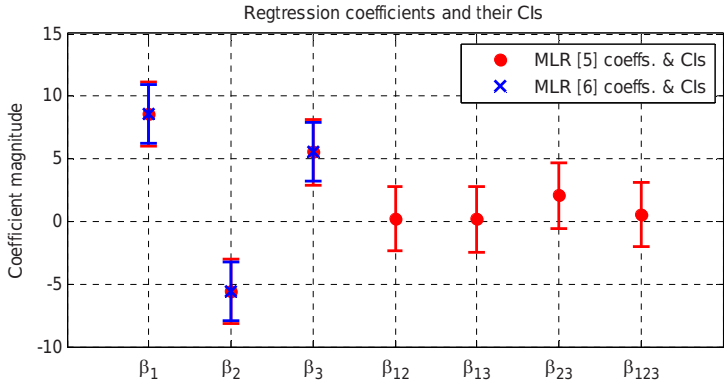

Figure 3. Regression coefficients of the MLR models [5] and [6].

Judging by the confidence intervals of model [5], all of the inputs (x_1, x_2, x_1) clearly have a significant (mean) effect on the output. Notably, the interaction of air inlet temperature and air volumetric flow (x_2x_3) seems like the only interaction term to have some significance. This would be reasonable as that term (more typically denoted $\dot{V}_{gas}T_{gas}$) is directly related to the heat transferred convectively by a gas flow.

The coefficients of model [6] enable assessing the relative significance of the inputs with respect to the output. Notably, $\beta_{1\ldots3}$ of [5] and [6] nearly coincide due to the insignificant impact of the interactions. Clearly, current (x_1) has the strongest relative effect on the output (β_1=8.57), whereas air flow (x_2) and the air inlet temperature (x_3) have a close to equal, but opposite-signed relative mean effect (β_2=–5.59, β_3=5.54). Thus, if considering control of the stack temperature within the examined operating domain, either air inlet temperature or the air flow may be used equally effectively. The air inlet temperature, however, can be manipulated without affecting the parasitic losses of the system and is thus preferable.

Preliminary MLR Modeling

With the data analysis as background, an initial MLR estimate [7] for the stack temperature was created using all three inputs as regressors. Again, only the 13 data points (8 DoE + 5 NOC) described above were used. The R^2_{adj} and $RMSE$ values for the fitting data are 0.913 and 2.90 °C, respectively. Figure 4 and Figure 5 illustrate the obtained estimate accuracy for both the utilized steady-state data and the full data time-series, respectively. Most of the steady-state estimates lie within the point-wise confidence intervals (Figure 4a) and the estimation error has a zero mean (Figure 4b). However, when looking at the time-series data in Figure 5, problems with the estimator become obvious. The estimate is stationary and differs significantly from the measurement during set-point changes. Also, the estimator fails to capture the measurement trend, due to the stack degradation. Both of these problems are consequences of the MLR model structure.

$$\hat{y} = 141 + 1.71x_1 - 0.0559x_2 + 0.542x_3 \qquad [7]$$

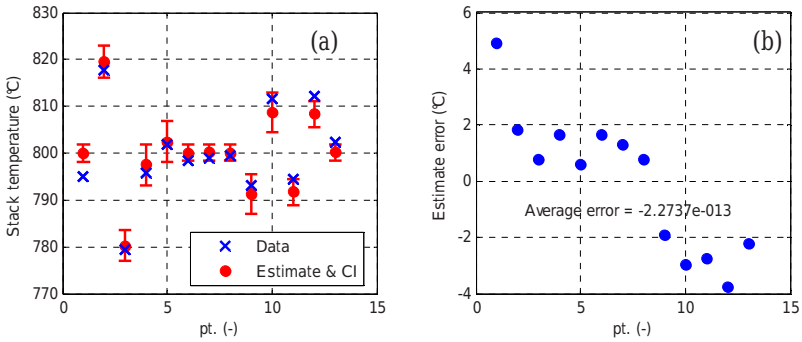

Figure 4. The steady-state data and the corresponding estimate of model [7] compared (a). The estimation error (b).

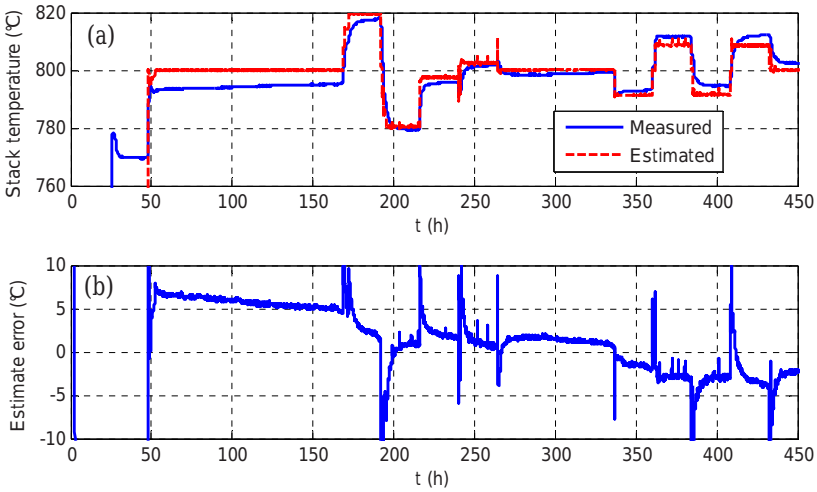

Figure 5. The time-series data and the corresponding estimate of model [7] compared (a). The estimation error (b).

Improved MLR Models

In order to improve the MLR model estimation accuracy on behalf of both the accuracy at stationary points, as well as during transients, two means were found especially useful:

1) Including the cathode outlet flow temperature measurement as regressor both (i) improves the estimation accuracy by capturing the measurement trend and (ii) provides a "dynamic input" to the MLR estimator, thus improving the estimate accuracy during transient phases
2) Expanding the model fitting data series to include part-load data improves the model accuracy as well as expands its feasible application area.

Cathode Outlet Flow Temperature as Regressor

An MLR model [8] with the cathode outlet flow temperature (x_4) as a regressor variable was created to enable better estimation accuracy during both transient operation as well as in steady-state. The model R^2_{adj} and $RMSE$ values for the fitting data are 0.991 and 0.946 °C, respectively.

$$\hat{y} = -75.5 - 0.0877x_1 - 0.0265x_2 - 0.290x_3 + 1.51x_4 \quad [8]$$

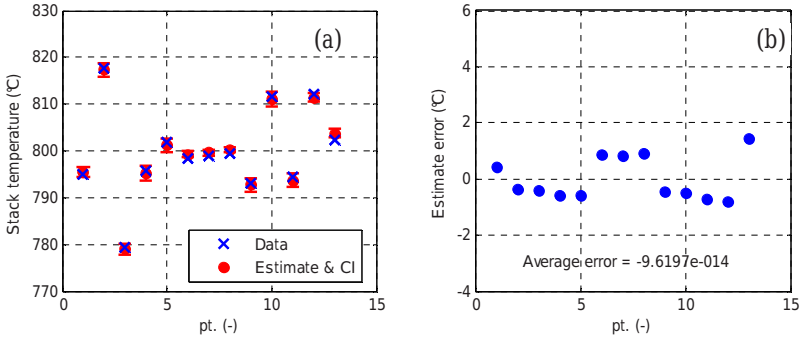

Figure 6. The steady-state data and the corresponding estimate of model [8] compared (a). The estimation error (b).

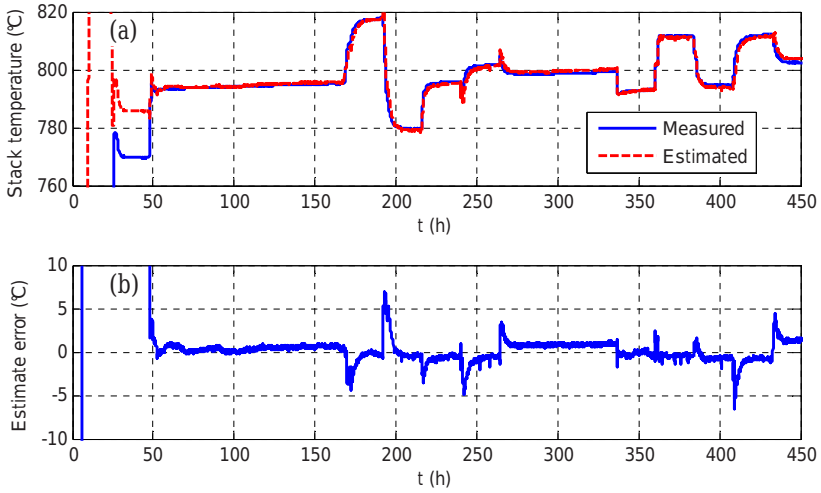

Figure 7. The time-series data and the corresponding estimate of model [8] compared (a). The estimation error (b).

When comparing Figure 4a and 6a, it is clear how introducing x_4 as regressor narrows the estimate confidence intervals (for the fitting data). Also the reduction in the estimation error from Figure 4b to 6b is evident. The most significant improvement in the

estimation accuracy is, however, noticeable in the time-series data, Figure 7a-b. Since x_4 is a stack output variable, it changes according to the stack dynamics and thus provides the MLR estimate with information of the stack dynamics. The downside of including x_4 as a regressor is that the MLR model coefficients lose their physical interpretability (because the regressors are no longer independent of each other).

Although the estimator [8] already provides good estimation accuracy when operating around the nominal operating conditions, the accuracy is poor outside this operating domain. To correct this, the MLR model parameter fitting data was expanded to include part-load operation data, although this data was not a part of the original test plan.

Adding Part-load Data to Regression Coefficient Calculation

The system was operated at part-load (150 A) during 25-50h into the test run and, as seen in e.g. Figure 7a, the stack temperature is significantly lower there than at NOC. Two measurements from this operating period were included in the MLR model parameter calculation data, yielding model [9], with R^2_{adj} and $RMSE$ for the fitting data 0.994 and 1.06 °C, respectively. The estimation results for model [9] are shown in Figures 8-9.

$$\hat{y} = -33.8 + 0.353x_1 - 0.0327x_2 - 0.110x_3 + 1.17x_4 \qquad [9]$$

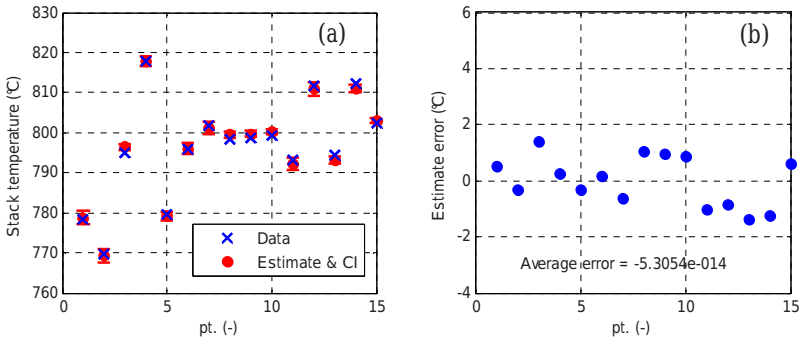

Figure 8. The steady-state data and the corresponding estimate of model [9] compared (a). The estimation error (b).

As is seen in Figure 8 and 9, the model estimation accuracy is still good, though the $RMSE$ value for the fitting data increased compared to [7] and also the error in Figure 9b is visibly greater than in Figure 7b. With the slight sacrifice of estimation accuracy at NOC, the estimator can be seen to have significantly improved over the part-load operating period (25-50h) in the data time-series, Figures 7a and 9a. The confidence intervals of the fitting data estimates still remain narrow, also for the added data points (pts. 1-2).

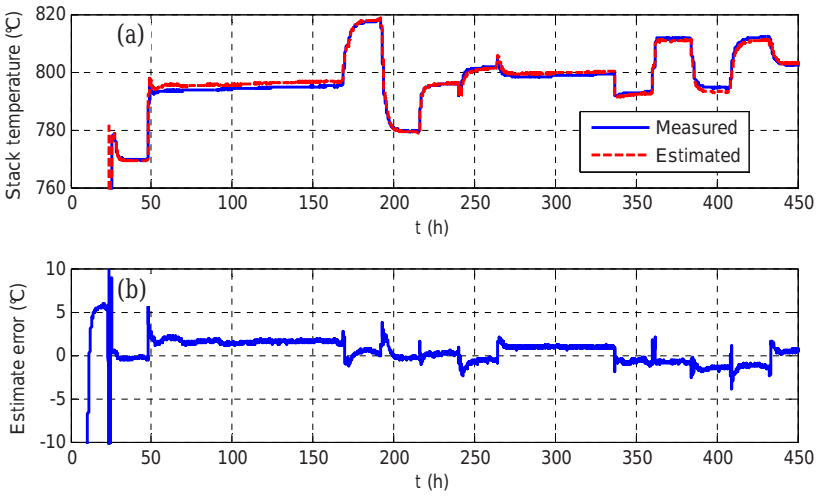

Figure 9. The time-series data and the corresponding estimate of model [9] compared (a). The estimation error (b).

Conclusions

A series of multi-variable linear regression models were created based on experimental data from a complete 10kW SOFC system to estimate the maximum internal temperature measured from a SOFC stack. The data was obtained with a full factorial experimental design, where three input variables (stack current, air flow and air inlet temperature) were manipulated.

The benefits of a systematic, designed, experimental procedure were found to manifest as straightforward regression modelling and in the accuracy of the consequent models. Furthermore, the full factorial experimental design enabled clearly quantifying the significance of the inputs with respect to their impact on the monitored output value. This information is valuable when developing a control strategy for the system.

Because the MLR model itself is only a static mapping of a series of regressor variables to the estimated output it was found beneficial, from a practical viewpoint, to include such variables to the regressors which convey the dynamics of the estimated property. In this case the cathode outlet flow temperature was used as regressor to include the dynamics of the stack temperature. Furthermore, as the designed experiments may cover only a part of the system operating domain, it is beneficial to include data from outside the domain of the designed experiments. In this case, part-load data was used to expand the applicable area of the MLR model.

Acknowledgments

Funding for this study was obtained through the project RealDemo. The Finnish Funding Agency for Technology and Innovation (TEKES) as well as the companies participating in the project are gratefully acknowledged for their financial support. Additionally, A. Pohjoranta would like to thank the gentlemen Fabio Postiglione from the University of Salerno and Angelo Esposito from the European Institute for Energy Research for the many helpful discussions related to the design of experiments and data analysis. M. Pastula from Versa Power Systems is acknowledged for good collaboration and helpful comments. M. Rautanen and M. Kotisaari from VTT are thanked for assisting in the experiments.

References

1. R. Knibbe, A. Hauch, J. Hjelm, S. Ebbesen and M. Mogensen, *Green*, **1**, 141 (2011)
2. A. Nakajo, Z. Wuillemin, J. Van herle and D. Favrat, *J. Power Sources*, **193**, 203 (2009)
3. D.C. Montgomery, *Design and Analysis of Experiments*, 8th ed., John Wiley & Sons, Singapore (2009)
4. M. Halinen, M. Rautanen, J. Saarinen, J. Pennanen, A. Pohjoranta, J. Kiviaho, M. Pastula, B. Nuttall, C. Rankin, B. Borglum, *ECS Trans.*, **35**(1), 113 (2011)
5. B. Borglum, E. Tang, M. Pastula, *ECS Trans.*, **35**(1), 63 (2011)

PUBLICATION [P7]

Application of Multivariable Regression Model for SOFC Stack Temperature Estimation in System Environment

In: Proceedings of 11th European SOFC & SOE Forum,
Chapter 15, pp. 183-191

A1306

Application of Multivariable Regression Model for SOFC Stack Temperature Estimation in System Environment

Matias Halinen, Antti Pohjoranta, Jari Pennanen and Jari Kiviaho
Technical Research Centre of Finland VTT, Fuel cells
Biologinkuja 5
P.O.Box 1000, FI-02044 VTT / Finland
Tel.: +358-20-722-6590
Fax: +358-20-722-7048
firstname.lastname@vtt.fi

Abstract

The applicability of multivariable linear regression (MLR) models to estimate the maximum temperature inside a SOFC stack is investigated experimentally. The experiments were carried out with a complete 10 kW SOFC system using an 80-cell stack by Versa Power Systems. The behavior of the maximum temperature measured inside a SOFC stack with respect to four independent input variables (stack current, air flow, air inlet temperature and fuel flow) is examined following the design of experiments methodology, and MLR models are created based on the retrieved data.

The practical feasibility of the MLR estimate is investigated experimentally with the 10 kW system by evaluating the accuracy of the estimate in two test cases: (i) a system load change where the stack temperature is regulated by a closed-loop controller using the MLR estimate (Figure 1) and (ii) during operator-imposed disturbances in the fuel system (a variation in the methane conversion in the fuel pre-reformer). Finally, the performance of the MLR estimate is evaluated with another, 64-cell stack operated at higher current density. This work continues previous research reported in [1-2].

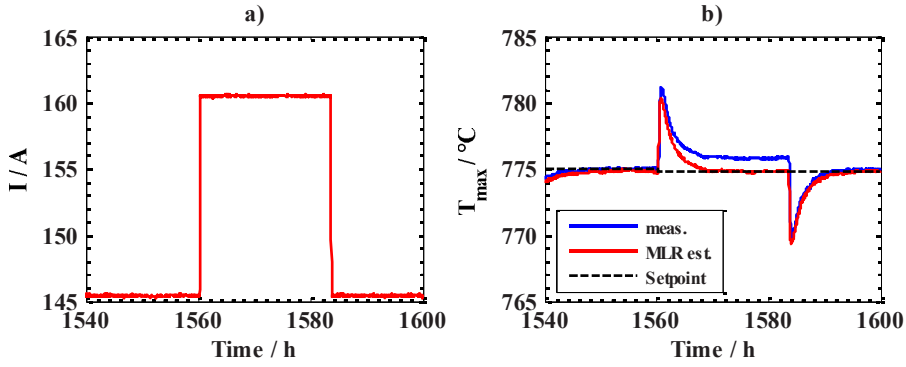

Figure 1 – Closed loop-control of stack temperature during a load change a) stack current and b) measured, estimated and setpoint value for T_{max}.

Introduction

The internal temperature of a solid oxide fuel cell (SOFC) stack can affect both the performance and the lifetime of the stack. Thus accurate and reliable monitoring, as well as regulation, of the stack temperature is beneficial to prevent sub-optimal performance or excessive degradation. Direct physical measurement of the temperature inside the stack is possible, but can be costly and complex to realize in real-world systems due to the high number of temperature probes required to map the temperature profile with a high-enough resolution. Therefore the estimation of the stack temperature with other, more practically feasible measurements, such as inlet gas flow rates and temperatures or stack current, is well-motivated.

1. Approach

This study is a direct continuation of systematic efforts [1-2] carried out to create a simple numerical estimator for the maximum temperature measured inside a SOFC stack over its lifetime in system environment. The numerical estimator is based on multivariable linear regression (MLR) model, which are functions of the form

$$\hat{y} = \beta_0 + \beta_1 x_1 + \cdots + \beta_{p-1} x_{p-1} = \mathbf{X}\boldsymbol{\beta}, \text{ where } \mathbf{X} = [1 \quad x_1 \quad x_2 \quad \dots \quad x_{p-1}], \qquad (1)$$

where x_i and $\hat{y}$ are (column) vectors of the measured input and estimated output values, respectively. The parameter vector $\boldsymbol{\beta} = [\beta_0 \quad \beta_1 \quad \beta_2 \quad \dots \quad \beta_{p-1}]^T$ is calculated so to produce an estimate which is optimal in the least squared error sense. The data to create the MLR model can be obtained by following the Design of Experiments (DoE) methodology. See e.g. [3] for details on MLR modelling and DoE.

Firstly, formal experiments are conducted according to the DoE methodology to obtain rich-enough data to calculate the parameters for the MLR model, and to assess the feasibility of the obtained MLR model to estimate the stack temperature. The experiments are conducted in a similar fashion as in the previous work reported in [1-2]. However, in this study an 80-cell stack is used with a current of 160 A at system nominal operating conditions (NOC). In [1-2], a 64-cell stack was used with 200 A current at system NOC.

Secondly, the practical feasibility of the obtained MLR model is investigated experimentally by evaluating the accuracy of the estimate in two test cases:

1) a system load change and
2) during operator-imposed disturbance in the fuel system where the methane conversion in the fuel pre-reformer is changing.

In both test cases the stack temperature is regulated by a closed-loop PI-controller, where the MLR-estimate is used as a feedback value for the controller.

Thirdly, the general feasibility of the studied approach is investigated by calculating a common MLR model for both 80-cell and 64-cell stacks and assessing its estimation accuracy at system NOC. The motivation for this exercise is to evaluate whether or not a MLR model derived with operational data of one stack can be utilized for the temperature estimation of another stack.

2. Experiments

The experiments were carried out with a complete 10 kW SOFC system [4] at VTT, Finland. The system incorporated an 80-cell SOFC stack provided by Versa Power Systems [5] and the stack contained altogether 23 temperature measurement probes inside the stack. Four independent system inputs, given in Table 1, were manipulated according to a so-called fractional factorial experiment design (see e.g. [3] for details). The fractional design was adopted as previous work [1-2] proved that interactions of the previously investigated inputs ($x_1 - x_3$) is insignificant and thus the number of experimental conditions could be decreased. The fractional test plan was designed for two individual nominal levels i.e. for NOC1 and NOC2 at 160 A and 145 A stack current, respectively, and in both cases, each input is varied between two levels (minimum and maximum). Two individual nominal levels were used to enlarge the operational area of the derived MLR model.

Table 1 – The experiment design: manipulated input variables ($x_1 - x_4$), two nominal levels (NOC1 & NOC2) and the variation of the inputs.

	Input			NOC1	NOC2	DoE variation
x_1	Current	I	A	160	145	±5
x_2	Air flow	$\dot{V}_{Air}$	NLPM	1062	1023	±50
x_3	Air inlet temp.	T_{Air}	°C	735	745	±10
x_4	Natural gas flow	$\dot{V}_{NG}$	NLPM	27.9	25.8	±0.5

The stack maximum temperature (T_{max}) and the cathode outlet temperature (T_{out}) were measured as responses once the system had reached steady-state conditions after changing the inputs. (The maximum temperature was taken as the maximum of the temperature measurements inside the stack, on one, representative cell.) The system was brought periodically to NOC1 or NOC2 in order to observe stack degradation. Altogether the designed experiments lasted for ca. 1300 hours, during which time a total of 16 DoE, 9 NOC1 and 4 NOC2 conditions were measured at steady-state. Additionally, 9 other steady-state conditions, e.g. at part-load were recorded to be used for model development.

The practical feasibility of the created MLR model was investigated experimentally with a closed-loop PI-controller set to regulate the stack temperature. Instead of using the in-stack thermocouples for measured feedback, the feedback signal for the PI-controller was calculated by the MLR model. The PI-controller regulates the stack temperature by adjusting the module inlet air temperature (T_{Air}) by manipulating a by-pass valve of the air system heat exchanger.

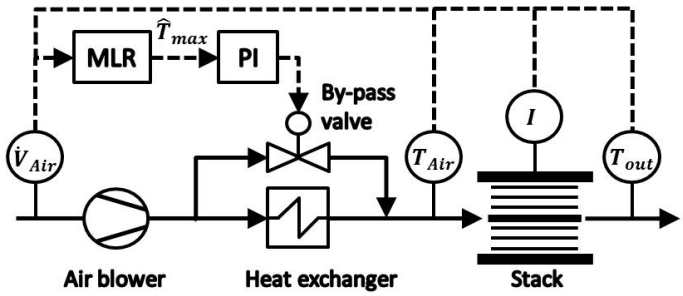

Figure 2 – Closed-loop controller to regulate stack temperature using the MLR-estimate.

3. Results

3.1 Temperature estimation with the MLR model

The MLR model (2) to estimate the stack temperature was created with similar methodology as presented in [1-2] by using all 4 inputs and the measurement of the cathode outlet gas temperature as regressors. All previously mentioned 38 steady-state operating conditions were used to calculate the coefficients of the MLR model in order to (i) fully utilize the conducted experiments and (ii) to maximize the accuracy and the operational envelope for the MLR estimate.

$$\hat{T}_{max} = 12.16 + 0.49\, I - 0.0248\, \dot{V}_{air} + 0.0102\, T_{Air} - 1.30\, \dot{V}_{NG} + 1.00\, T_{out} \qquad (2)$$

Figure 3 illustrates the accuracy of the obtained MLR estimate for both the utilized steady-state fitting data and the full time-series data. The MLR model (2) fits the measurement data very well, which can be observed by high estimation accuracy with respect to both steady-state fitting data (Figure 3b) as well as the full time-series data (Figure 3a). The average estimation error $RMSE$ and the adjusted degree of variance explanation power R^2_{adj} of the fitting data are 0.93°C and 0.99, respectively (Figure 3c). (See e.g. [1] for a detailed description of R^2_{adj} and $RMSE$ for MLR model evaluation.)

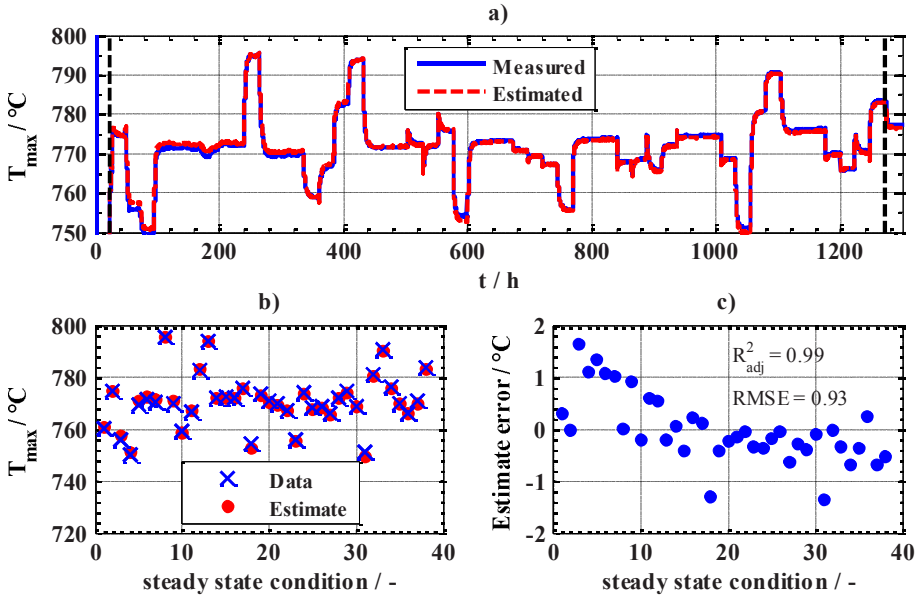

Figure 3 – Measured and estimated stack maximum temperature for a) time-series data b) steady-state data and c) error of the estimate.

3.2 Load transient experiment

The feasibility of the MLR model (2) for stack temperature regulation was investigated by performing a load transient from 145 A to 160 A and back, accompanied by a 24-hour stabilization period between transitions (Figure 4a). The T_{max} setpoint was set to 775°C for this experiment. During a load transient, all input variables of the MLR model are changing, since $\dot{V}_{air}$ and $\dot{V}_{NG}$ are controlled as a function of the current, T_{Air} is adjusted by the PI-controller and T_{out} changes according to the temperature characteristics of the stack.

It is observed that the MLR model provides good estimation accuracy during the load transients as the estimate remains within 2°C of measured T_{max}throughout the transient (Figure 4b). Morever, it is observed that the dynamic response of the estimated and measured value is similar during the experiment, which is largely due to the utilization of cathode outlet temperature measurement (T_{out}) as an input for the MLR model. The results depicted in Figure 4b show that using T_{out}enables application of the as-such static MLR estimate for dynamic control purposes.

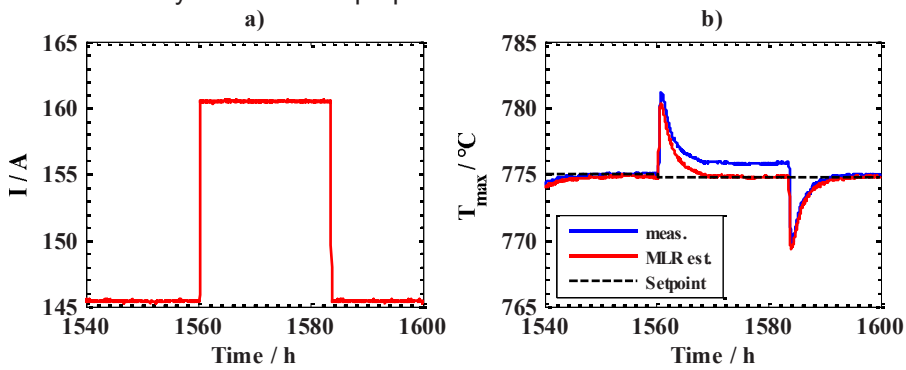

Figure 4 – Load transient experiment a) stack current and b) measured, estimated and setpoint value for T_{max}.

3.3 Process disturbance experiment

The feasibility of the MLR model (2) for stack temperature regulation was further investigated by imposing such a disturbance to the fuel system that the stack temperature is also affected. During the experiment the system was operated at NOC1 with 160 A current and T_{max} setpoint of 775°C. The process disturbance was created by changing the inlet temperature of the fuel pre-reformer by ±50°C from the nominal value of 625°C (Figure 5a). A change in the inlet temperature alters the conversion of methane and thus the reformer outlet (and stack inlet) methane flow rate (Figure 5b). In turn, the stack inlet methane flow rate will affect the stack temperature due to endothermic steam reforming reactions. During the experiment, the methane outlet flow and conversion of methane varied from 25.6 to 21.2 NLPM, and from 10 to 23 %, respectively. It should be noted that all independent inputs ($x_1 - x_4$) of the MLR model - which are concurrently the primary control variables of the 10 kW SOFC system - were kept constant during the experiment. Of the MLR model inputs, only the cathode outlet temperature (T_{out}) changes due to the experiment.

In Figure 5 it is seen that the MLR model provides good estimation characteristics also during the process disturbance. The accuracy of the estimate remains within 3°C of the measured T_{max} throughout the experiment (Figure 5b). Additionally, the dynamic response of the estimated and measured value is similar as well. Again, the effects of the process disturbance on stack temperature are picked up by T_{out}., enabling the good estimation characteristics for the MLR model.

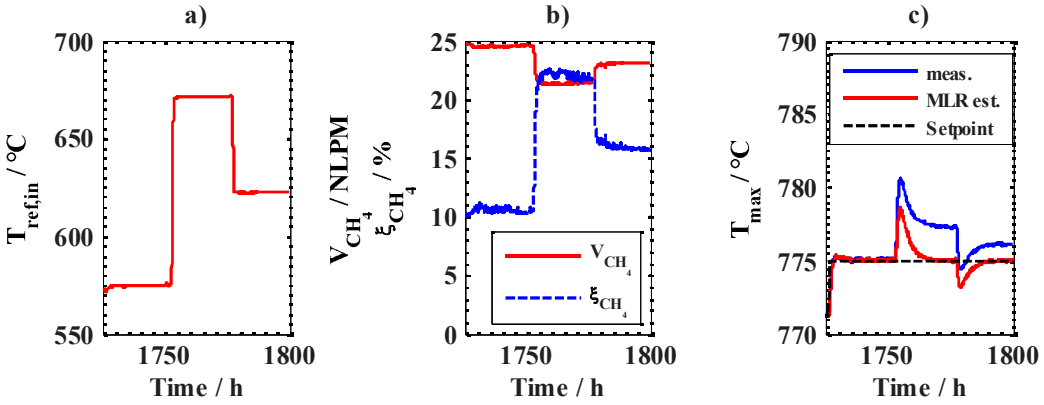

Figure 5 – Process disturbance experiment a) reformer inlet temperature and b) flow rate and conversion of methane and c) measured, estimated and setpoint value for T_{max}.

3.3 A common MLR model for two different stacks

Finally, the general feasibility of the studied approach, i.e. utilization of a common MLR – model to estimate the internal stack temperature, is investigated by utilizing the experimental results of previous work [1-2] for a 64-cell stack and the data of the current work. A common MLR model is created based on the 80-cell stack data and its estimation accuracy is assessed for both the 80-cell and the 64-cell stacks.

The 64-cell stack was operated at a current of 200 A at system NOC, but with same gas flow rates as the 80-cell stack at 160A current, resulting as same NOC air and fuel utilization. (The total Faradic current of the stack at NOC remains the same.) A simple trial reveals that the MLR model (2), created upon the 80-cell stack experiments, does not provide a good estimate for the T_{max} of the 64-cell stack.

Since the estimate given by (2) is biased significantly when applied to a different stack, another MLR model was created by using an alternative definition for the inputs of the model. Instead of using only the independent system inputs as such, e.g. air or fuel flow rates, the feasibility of proportional operational variables for SOFC stacks, such as fuel and air utilization rates, was evaluated.

An exhaustive search was conducted over different combinations of the proportional operational variables as well as selected temperature measurements to find proper inputs for the common MLR model. All evaluated models were ranked according to R^2_{adj} and $RMSE$ for the fitting data, and a MLR model with nine inputs was found to provide the best T_{max} estimate for both 64- and 80-cell stack (Table 2).

Table 2 – Input variables and coefficients for the common MLR model

MLR model input, x_i	Unit	Coefficient β_i*
Current	A	-0.000825
Module inlet air temperature	°C	-0.025604
Cathode outlet gas temp.	°C	0.272114
Stack voltage	V	-0.678215
System fuel utilization	%	0.394374
Stack air utilization	%	0.5714224
Stack fuel utilization	%	0.3351744
Anode inlet gas temp.	°C	-0.4159904
Anode outlet gas temp.	°C	1.2430144
		*β_0=-52.292776

The measured T_{max} and the estimate for the time-series data of the two stacks given by the common MLR model is depicted in Figure 6. The common MLR model provides an accurate estimate for the 80-cell stack (Figure 6a) throughout the experiment, which can be expected, since the coefficients presented in Table 2 are calculated with the corresponding steady-state data. More interestingly, the common MLR model can estimate the T_{max} also for the 64-cell stack (Figure 6b) with high accuracy, even though no data from this experiment is used to calculate the coefficients of the model. Moreover, the common MLR model provides an accurate estimate for the 64-cell stack albeit it was operated at higher current and higher stack internal temperature. An interesting detail is that the MLR retains its accuracy as the both stacks are subjected to a number of full thermal cycles down to room temperature.

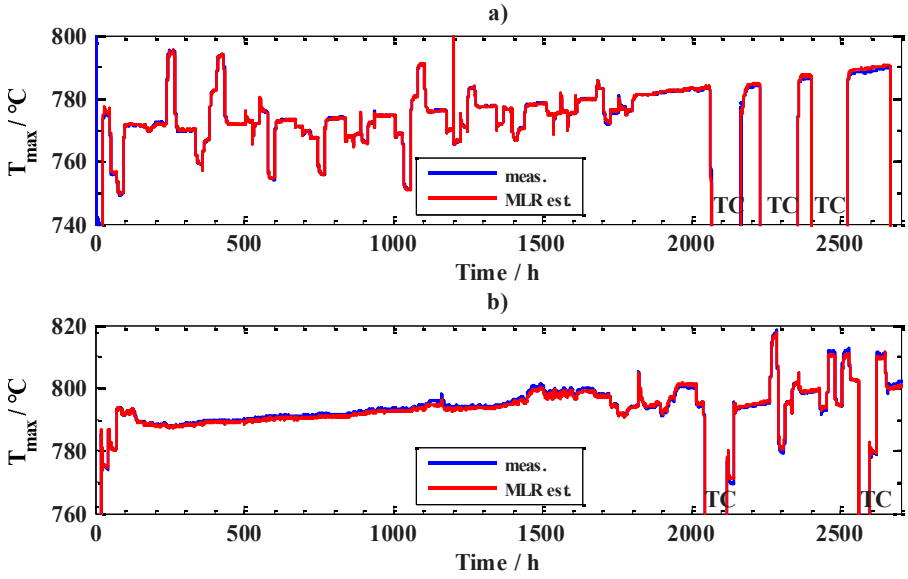

Figure 6 – Common MLR model estimate and measurement of T_{max} for a) 80-cell and b) 64-cell stack. TC denotes a full system thermocycle.

4. Conclusions

The practical applicability of multivariable linear regression models for the estimation of the SOFC stack maximum temperature was evaluated experimentally. Designed experiments on a complete 10 kW SOFC system were utilized in the work. An MLR model was applied to produce the feedback for a closed-loop PI controller for the regulation of the stack maximum temperature under two test cases: a load change and a process disturbance. The estimate and subsequently also the controller performed well. Finally, a universal approach for developing MLR models for the estimation of the maximum temperature of different SOFC stacks was studied based on experimental data obtained with two different stacks. A common MLR model using proportional operational variables as model inputs can provide an accurate estimate of the T_{max} for both stacks.

Acknowledgements

This work was carried out under the project RealDemo, funded by the Finnish Agency for Technology and Innovation TEKES, whose financial support is gratefully acknowledged. Michael Pastula, Ben Nuttall and Oliver Grande from VPS are acknowledged for successful stack installations and collaboration during the experiments. Mikko Kotisaari, Timo Lehtinen and Markus Rautanen from VTT are thanked for assisting in the experiments.

References

[1] M. Halinen, A. Pohjoranta, J. Pennanen, J. Kiviaho, Stack temperature estimation in system environment by utilizing the design of experiments methodology, ECS Trans., 57 (1), 205-214, 2013

[2] A. Pohjoranta, M. Halinen, J. Pennanen, J. Kiviaho, Multivariable linear regression for SOFC stack temperature estimation under degradation effects, J. Electrochemical Soc., 161, F425-F433, 2014

[3] D.C. Montgomery, Design and Analysis of Experiments, 8th ed., John Wiley & Sons, 2009

[4] M. Halinen, M. Rautanen, J. Saarinen, J. Pennanen, A. Pohjoranta, J. Kiviaho, M. Pastula, B. Nuttall, C. Rankin and B. Borglum, Performance of a 10 kW SOFC Demonstration Unit Stacks and Systems, ECS Trans., 35 (1), 113-120, 2011

[5] B. Borglum, H. Ghezel-Ayagh, Development of solid oxide fuel cells at Versa Power Systems and FuelCell Energy , ECS Trans., 57 (1) 61-66 (2013)

Series title and number

VTT Science 82

Title	**Improving the performance of solid oxide fuel cell systems**
Author(s)	Matias Halinen
Abstract	Solid oxide fuel cell (SOFC) systems can provide power production at a high electrical efficiency and with very low emissions. Furthermore, they retain their high electrical efficiency over a wide range of output power and offer good fuel flexibility, which makes them well suited for a range of applications. Currently SOFC systems are under investigation by researchers as well as being developed by industrial manufacturers. The first commercial SOFC systems have been on the market for some years now, with the help of government subsidies. However, the performance, cost and durability of SOFC systems must be improved in order for them to be competitive in the open market. For this purpose, it is important to evaluate the technical feasibility and performance of possible SOFC system designs and the balance of plant components. Furthermore, the operating environment of the costly SOFC stack must be controlled rigorously in order to attain both high efficiency and long lifetime. The instrumentation and the peripheral equipment of SOFC systems must be simplified in order to decrease system costs, although without sacrificing the system's operational reliability. This thesis focuses on the design and operational aspects of SOFC systems. The top-level targets for the research work were (i) to identify a feasible system design and a set of components which would enable utilization of the high electrical efficiency potential, above 45%, of SOFC technology and (ii) to find solutions which would improve and simplify the operation of SOFC systems. This work presents a novel SOFC system design capable of reaching an electrical efficiency of 45%. The design utilizes the so-called anode off-gas recycling concept, which improves the system's self-sufficiency by eliminating the need for an external water supply during normal operation. The technical feasibility of the system design was validated by constructing a proof-of-concept prototype and performing long-term experiments with it. The proof-of-concept prototype was further used to investigate several specific operational challenges of the systems, including (i) prevention of carbon formation in the fuel system, (ii) quantification of the effects of stack leakages, (iii) protection of the anode from damage during system start-up cycles and (iv) control of the SOFC stack temperature. The solutions found for these challenges are readily implementable and could promote commercialization of SOFC systems by simplifying system design and improving their operational capabilities.
ISBN, ISSN	ISBN 978-951-38-8237-2 (Soft back ed.) ISBN 978-951-38-8238-9 (URL: http://www.vtt.fi/publications/index.jsp) ISSN-L 2242-119X ISSN 2242-119X (Print) ISSN 2242-1203 (Online)
Date	March 2015
Language	English, Finnish abstract
Pages	72 p. + app. 85 p.
Name of the project	
Commissioned by	
Keywords	Solid oxide fuel cell, system, anode off-gas recycling, carbon formation, leakage, anode protection, temperature control
Publisher	VTT Technical Research Centre of Finland Ltd P.O. Box 1000, FI-02044 VTT, Finland, Tel. 020 722 111

Julkaisun sarja ja numero

VTT Science 82

Nimeke	**Kiinteäoksidipolttokennojärjestelmien suorituskyvyn parantaminen**
Tekijä(t)	Matias Halinen
Tiivistelmä	Kiinteäoksidipolttokennojärjestelmät (solid oxide fuel cell, SOFC) mahdollistavat sähköntuotannon hyvällä hyötysuhteella ja pienillä päästöillä. SOFC-järjestelmät soveltuvat monille erilaisille polttoaineille ja eri teholuokkiin, joten niitä voidaan käyttää laajasti erityyppisissä sovelluskohteissa. Tällä hetkellä ensimmäiset SOFC-järjestelmät ovat jo markkinoilla, joskin erilaisten taloudellisten tukijärjestelmien avustamina. Järjestelmien suorituskyky, hinta ja elinikä eivät ole vielä kilpailukykyisiä perinteisiin sähköntuotantomenetelmiin verrattuna, vaan vaativat yhä kehitystyötä. SOFC-järjestelmä voidaan toteuttaa monin eri tavoin, ja siksi on tarpeellista tutkia järjestelmien rakennetta ja rakentamiseen käytettävien komponenttien suorituskykyä sekä teknistä soveltuvuutta kokonaisuutena. Lisäksi järjestelmän pääkomponentin, SOFC-kennoston, toimintaolosuhteet vaativat tarkkaa hallintaa korkean hyötysuhteen ja pitkän käyttöiän turvaamiseksi. Järjestelmien vaatimien mitta- ja oheislaitteiden vähentäminen on tarpeen järjestelmän hinnan pienentämiseksi. Tämä väitöskirja käsittelee SOFC-järjestelmien rakennetta, komponentteja ja operointia. Väitöskirjatyön tavoitteina oli (i) löytää SOFC-järjestelmälle toteuttamiskelpoinen rakenne, jolla voidaan saavuttaa korkea, yli 45 %:n sähköhyötysuhde, ja (ii) kehittää ratkaisuja, jotka parantavat ja yksinkertaistavat järjestelmien operointia. Väitöskirjassa esitetään uudenlainen järjestelmärakenne, jolla työlle asetettu hyötysuhdetavoite on mahdollista saavuttaa. Järjestelmässä käytetään ns. anodikaasun takaisinkierrätystä, joka parantaa järjestelmän omavaraisuutta poistamalla ulkoisen vedensyötön tarpeen. Järjestelmärakenteen toteutettavuus osoitetaan kokeellisesti rakentamalla prototyyppi järjestelmästä ja suorittamalla sillä pitkäaikaiskokeita. Prototyyppiä käyttäen selvitetään SOFC-järjestelmien rakenteessa ja operoinnissa esiintyviä ongelmia, jotka liittyvät (i) hiilenmuodostumisen estämiseen polttoainejärjestelmässä, (ii) kennoston vuotojen ja niiden vaikutusten määrittämiseen, (iii) kennoston anodin suojaamisen vaurioilta järjestelmän käynnistyksen aikana ja (iv) kennoston lämpötilan hallintaan. Kyseisille ongelmille esitetään toteuttamiskelpoiset ratkaisut, jotka parantavat ja yksinkertaistavat SOFC-järjestelmien rakennetta ja operointia ja voivat osaltaan helpottaa niiden kaupallistumista.
ISBN, ISSN	ISBN 978-951-38-8237-2 (nid.) ISBN 978-951-38-8238-9 (URL: http://www.vtt.fi/publications/index.jsp) ISSN-L 2242-119X ISSN 2242-119X (Painettu) ISSN 2242-1203 (Verkkojulkaisu)
Julkaisuaika	Maaliskuu 2015
Kieli	Englanti, suomenkielinen tiivistelmä
Sivumäärä	72 s. + liitt. 85 s.
Projektin nimi	
Rahoittajat	
Avainsanat	Solid oxide fuel cell, system, anode off-gas recycling, carbon formation, leakage, anode protection, temperature control
Julkaisija	Teknologian tutkimuskeskus VTT Oy PL 1000, 02044 VTT, puh. 020 722 111

Improving the performance of solid oxide fuel cell systems

Solid oxide fuel cell (SOFC) systems can provide power production at a high electrical efficiency and with very low emissions. Currently SOFC systems are under investigation by researchers as well as being developed by industrial manufacturers. The performance, cost and durability of SOFC systems must be improved in order for them to be competitive in the open market.

This thesis focuses on the design and operational aspects of SOFC systems. It presents a novel SOFC system design capable of reaching an electrical efficiency of 45%. Moreover, the thesis investigates several specific operational challenges related to SOFC systems by using actual system hardware. The presented solutions are readily implementable and can alleviate the challenges of commercialization of SOFC systems by simplifying system design and improving their operational capabilities.

ISBN 978-951-38-8237-2 (Soft back ed.)
ISBN 978-951-38-8238-9 (URL: http://www.vtt.fi/publications/index.jsp)
ISSN-L 2242-119X
ISSN 2242-119X (Print)
ISSN 2242-1203 (Online)